Universidade do Minho
Escola de Ciências

João Pedro Lourenço de Castro

Design of fluorescent probes for the detection of ions and models of drugs of abuse in urine: synthesis, sensing studies and chemometric analysis

December 2021

João Pedro Lourenço de Castro

Design of fluorescent probes for the detection of ions and models of drugs of abuse in urine: synthesis, sensing studies and chemometric analysis

Master's dissertation
Master in Chemical Analysis and Characterization Techniques

Under the supervision of
Professor Susana Costa
and
Doctor Diogo Barros Gonçalves

December 2021

DIREITOS DE AUTOR E CONDIÇÕES DE UTILIZAÇÃO DO TRABALHO POR TERCEIROS

Este é um trabalho académico que pode ser utilizado por terceiros desde que respeitadas as regras e boas práticas internacionalmente aceites, no que concerne aos direitos de autor e direitos conexos.

Assim, o presente trabalho pode ser utilizado nos termos previstos na licença abaixo indicada.

Caso o utilizador necessite de permissão para poder fazer um uso do trabalho em condições não previstas no licenciamento indicado, deverá contactar o autor, através do RepositóriUM da Universidade do Minho.

Declaration of integrity

I declare to have acted with integrity in the preparation of this academic work and I confirm that I have not resorted to plagiarism or any form of misuse or falsification of information or results in any of the steps leading to its elaboration. I further declare that I know and have complied with the Code of Ethical Conduct of the University of Minho.

Resumo

Design de sondas fluorescentes para a deteção de iões e modelos de fármacos de abuso na urina: síntese, estudos de deteção e análise quimiométrica

Atualmente, existem muitos sensores químicos óticos baseados em moléculas orgânicas, porém os derivados de 4,4-difluoro-4-bora-3a,4a-diaza-*s*-indaceno, comummente conhecidos como BODIPYs, e os derivados de dicianovinilo representam duas classes de fluoróforos que têm ganhado considerável interesse em uma ampla variedade de aplicações. As propriedades fotofísicas e versatilidade química destes compostos explicam o seu exponencial crescimento, destacando a sua aplicação como sensores óticos para o reconhecimento e deteção de espécies químicas iónicas e neutras.

A aplicação de métodos quimiométricos a dados espetrais é cada vez mais utilizada como uma grande ferramenta para desenvolver modelos de quantificação para diferentes tipos de analitos com grande capacidade preditiva.

O objetivo deste trabalho foi o *design*, síntese e caracterização de novos derivados de BODIPY, funcionalizados com diferentes grupos substituintes nas posições 2 e 4'' do núcleo de BODIPY e do substituinte *meso*, e a caracterização de derivados dicianovinilo com diferentes unidades aromáticas, visando diversificar as propriedades fotofísicas e as propriedades sensoras dos compostos face a diversos analitos. Numa segunda fase, foi realizado o estudo da capacidade dos derivados de BODIPY e de dicianovinilos como sensores óticos de iões, com relevância em áreas como a saúde e o ambiente, e aminas e álcoois, como modelos de fármacos de abuso como a codeína e o fentanyl.

Na sequência do estudo preliminar que revelou a seletividade/sensibilidade a certos iões, foram realizadas titulações espetrofotométricas e espetrofluorimétricas na presença de F^-, CN^-, Cu^{2+} e Fe^{3+}. O comportamento como sensor do tipo quimiodosímetro dos derivados dicianovinílicos foi verificado por meio de uma titulação de RMN de ^1H com o ião cianeto.

No caso dos álcoois e aminas modelo, o teste preliminar revelou seletividade de alguns dos compostos testados para álcoois e aminas, complementada com a avaliação dos efeitos dos meios, pH e sais utilizados.

Em termos da análise quimiométrica, foram aplicados modelos SLR, PLS e PCR apresentando os melhores resultados para quantificação de CN^- e Fe^{3+}, com coeficiente de determinação superior a 95%.

Palavras-chave: BODIPY; sensor ótico; fluorescência; *machine learning*; modelos de quantificação.

Abstract

Design of fluorescent probes for the detection of ions and models of drugs of abuse in urine: synthesis, sensing studies and chemometric analysis

Currently, there are many optical chemical sensors based on organic molecules, however 4,4-difluoro-4-bora-3a,4a-diaza-*s*-indacene derivatives, commonly known as BODIPYs, and dicyanovinyl derivatives represent two classes of fluorophores which have been gaining considerable interest in a wide variety of applications. The photophysical properties and chemical versatility of these compounds explain their exponential growth, highlighting their application as optical sensors for the recognition and detection of ionic and neutral chemical species.

The application of chemometric methods to spectral data has been a great tool to develop quantification models for different types of analytes with great predictive capacity.

The aim of this work was the design, synthesis and characterization of new BODIPY derivatives functionalized with different substituent groups at position 2 and 4'' of the BODIPY core and the *meso* substitute, and the characterization of dicyanovinyl derivatives with different aromatic moieties, intending to diversify these compounds' photophysical and sensing properties for varied analytes. In a second stage, the study on the ability of BODIPY and dicyanovinyl derivatives as optical sensors for ions with medical and environmental relevance, and amines and alcohols, as models for drugs of abuse such as codeine and fentanyl.

As a result of the preliminary study which revealed the selectivity/sensitivity towards certain ions, spectrophotometric and spectrofluorimetric titrations were carried out in the presence of F^-, CN^-, Cu^{2+} and Fe^{3+}. The behaviour as a chemodosimeter of dicyanovinyl derivatives was verified through a ^1H NMR titration with the cyanide ion.

In the case of the model amines and alcohols, the preliminary test revealed selectivity of some of the testes compounds towards alcohols and amines, complemented with the evaluation of the effect of media, pH and salts.

In terms of chemometric analysis, LR, PLS and PCR models were applied showing the best results for quantification of CN^- and Fe^{3+}, with coefficient of determination superior to 95 %.

Keywords: BODIPY; optical sensor; fluorescence; machine learning; quantification models.

Index

Symbols, Acronyms and Abbreviations

abs	Absorbance
Ac	Acetyl group
ACN	Acetonitrile
ACN-d_3	Trideuteroacetonitrile
AIE	Aggregation induced emission
AI	Artificial intelligence
A_{comp}	Absorbance of the compound solution at maximum absorption wavelength
A_{stand}	Absorbance of the fluorescence standard solution at maximum absorption wavelength
AN	Aniline
Ar	Aromatic
BODIPY	4,4-Difluoro-4-bora-3a,4a-diaza-s-indacene
Bz	Benzyl group
CRT	Creatinine
CHEF	Chelation-induced enhancement of fluorescence
2D-GC/MS	Two-dimensional gas chromatography - mass spectroscopy
d	Duplet
DCHA	Dicyclohexylamine
dd	Double duplet
DCM	Dicloromethane
DMF	Dimethylformamide
DEA	Diethylamine
DDQ	2,3-Dichloro-5,6-dicyano-1,4-benzoquinone
DEPT	Distortionless enhancement by polarization transfer
DOE	Design of experiments
DPA	9,10-Diphenylanthracene
Φ_{comp}	Compound relative fluorescence quantum yield
Φ_F	Relative fluorescence quantum yield
Φ_{stand}	Standard fluorescence quantum yield
δ	Chemical shift in nuclear magnetic resonance
ε	Coefficient of molar absorptivity

equiv	Equivalents
ESI	Electrospray ionization
F_{comp}	Area under the fluorescence curve for the compounds
F_{stand}	Ares under the fluorescence curve for the fluorescence standard
ν	Frequency
GC	Gas-cromatography
GPCR	G-protein-coupled receptor
HA	Hexylamine
HMBC	Heteronuclear multiple bond correlation
HMQC	Heteronuclear multiple quantum correlation
HPLC/MS	High performance liquid chromatography - mass spectrometry
HOMO	Highest occupied molecular orbital
I	Intensity
IC	Internal conversion
ICT	Intramolecular charge transfer
ID	Illicit drugs
IR	Infrared
ISC	Intersystem crossing
J	Coupling constant
λ_{abs}	Wavelength of maximum absorption
λ_{eml}	Wavelength of maximum emission
λ_{exc}	Wavelength of excitation
LC/MS	Liquid chromatography - mass spectrometry
LUMO	Lowest unoccupied molecular orbital
LRMS	Low resolution mass spectrometry
M	Concentration in molarity (mol/dm^3)
m	Multiplet
M^+	Molecular ion
MA	Multivariate analysis
Me	Methyl group
ML	Machine Learning
MLR	Multiple linear regression

MS	Mass spectrometry
m/z	Mass to charge ratio
N	Sample size
n_{comp}	Refractive index value of the solvent of the compound solution
n_{stand}	refractive index value of the solvent of fluorescence standard solution
NIR	Near-infrared
NMR	Nuclear magnetic resonance
PBS	Phosphate-buffered saline
PC	Principal component
PCA	Principal component analysis
PCR	Principal componente regression
PET	Photoinduced electron transfer
R^2	Coefficient of determination
RMSE	Root mean square error
s	Singlet
S_0	Fundamental state
S_1	First singlet excited state
SLR	Simple linear regression
PLS	Partial least square regression
T_1	First excited triplet state
TBT^+	Tributyl tin
TEA	Triethylamine
TFA	Trifluoroacetic acid
THC	Δ^9-Tetrahydrocannabinol
TLC	Thin layer chromatography
U	Urea
a.u.	Arbitrary units
UV-vis	Ultraviolet-visible
WHO	World Health Organization
y_i	Obtained data
$\hat{y}_i$	Predicted results
$\overline{y}_i$	Average value of the obtained data

1P	1-pentanol
2B	2-butanol
4MP	4-methoxyphenol

Index of Figures

Index of Schemes

Index of Tables

Scientific Communications

Part of the work developed during this dissertation gave rise to a poster communication in an international symposium and to a publication in a book of proceedings of an international congress:

Poster communication at an international symposium

Castro, J. P.; Raposo, M. M. M.; Costa, S. P. G.; Spectroscopic characterization and optical chemosensing of ions with *meso*-triphenylamine-BODIPY derivatives, 3rd Iberian Symposium of Young Photochemists, 18-22 October 2021.

Publication in international conference proceedings book

Castro, J. P.; Raposo, M. M. M.; Costa, S. P. G.; A thiophene-based dicyanovinyl as an anion chemosensor. Proceedings of the 25th Int. Electron. Conf. on Synth. Org. Chem., 15–30 November 2021, MDPI: Basel, Switzerland. doi:10.3390/ecsoc-25-11769

https://sciforum.net/manuscripts/11769/manuscript.pdf

Chapter 1

Introduction

1. Introduction

1.1. Document structure

The work presented in this dissertation deals with different aspects of organic and analytical chemistry and machine learning, focusing on the synthesis and characterization of organic compounds, supramolecular chemistry and development of machine learning models to quantify analytes based on spectroscopic data.

This thesis is divided in five chapters. The first chapter presents an overview of the most important aspects of this work, serving as a basis for understanding it.

Chapter 2 presents the technical descriptions of the work developed, both with regard to organic, analytical chemistry and data mining, followed by chapter 3 where a detailed discussion of the obtained results and their meaning before and after the application of machine learning is presented.

In chapter 4, the conclusions encompassing the perspectives of the various areas present in the work are presented. The bibliography of this work is found in chapter 5. Supplementary data is presented as appendix.

1.2. Supramolecular approach on molecular recognition

Supramolecular chemistry definitions include "chemistry beyond the molecule", "chemistry of molecular assemblies and the intermolecular bond", and "non-molecular chemistry". Its main objective is the design and development of novel functional systems by joining multiple chemical components, mainly through non-covalent interactions[1]. This kind of system is generated through non-covalent interactions between a host molecule that has binding sites (such as donor atoms), sites for the formation of hydrogen bonds and/or sizable cavity, and an analyte. The analyte, named guest, has divergent binding sites such as hydrogen bond acceptor atoms[1].

Supramolecular interactions refer to intermolecular non-covalent interactions, for example, hydrogen bonds, salt bridges, π–π stacking, van der Waals forces, and hydrophobic interactions. Many textbooks and authors also list metal coordination as a type of supramolecular interaction since the coordination bond could be electrostatic or covalent, depending on the electron distribution[2].

The concept of a chemical sensor is related to supramolecular systems, since the recognition is associated with the detection process due to changes in the physical-chemical properties of these molecular receptors induced by the formation of complexes with the analyte[3].

1.2.1. Optical chemosensors

Various analytical techniques are used for detection and quantification of analytes, such as gas chromatography (GC) or high-resolution liquid chromatography (HPLC)[4]. However, most of these techniques are costly, time-consuming especially during sample preparation, and may exhibit low sensitivity for certain analytes. Optical sensors have appeared to overcome the previously mentioned limitations of these techniques[5]. From the early '90s, numerous researchers have worked in supramolecular chemistry combining the concepts of host-guest complex and fluorescence optical sensing. Fluorescence detection and imaging techniques concerning chemical sensors are essential tools in many fields of science and technology[6,7]

A chemosensor is a sensor that measures the change in a chemical property, often the concentration or activity of a specific chemical species. Similarly, optical sensors are based on reagents that alter their optical properties in the interaction with the analyte of interest and employ optical transduction mechanisms[8,9]. The commonly measured optical properties are absorption, fluorescence intensity and decay time, but in addition, reflectance, index refraction, light scattering and light polarization have also been used as analytical parameters allowing the optical detection of certain analytes[8.] Optical chemosensors are usually constituted by two parts: the signaling unit, that signals the recognition event through an optical change, and the recognition unit with the capability to identify the analyte. The signaling unit is normally a chromophore or a fluorophore and the sensor configuration can be chromophore/fluorophore–spacer–receptor, where the spacer connects both units, or simply the chromophore/fluorophore directly connected to the receptor[10].

1.2.2. Fluorimetric sensors

Fluorescence spectroscopy is a recurrent analytical technique in many research areas. This technique, based on fluorescence emission, has advantages when compared to other analysis techniques, for example higher sensitivity, which allows reaching lower analytic limits for quantifying analytes in biological and environmental samples[11].

As said before, a fluorimetric sensor is a sensor that changes its optical properties in the interaction with the analyte producing differences in fluorescence[8]. Fluorescence emission is easily explained with a Jablonski diagram. To detect a molecule based on fluorescence, the molecule must be excited from the ground level to a higher energy level through absorption of radiation. This transition must have a high probability of occurring.

After absorption, relaxation occurs, where the molecule releases the previously absorbed energy.

In a detailed way, relaxation may occur in two ways: by emitting a photon (radiative process, fluorescence or phosphorescence emission) or by dissipation of energy through vibrations and collisions between molecules (non-radiative process)[12]. Other relaxation processes include intersystem crossing (ISC) and internal conversion (IC). These processes are shown in a simplified Jablonski diagram in **figure 1**[13]. Internal conversion is characterized as a non-radiative process of relaxation between a higher excited singlet state to the lower energy excited state of the same spin[14], whereas intersystem crossing is characterized by energy transfer via orbital spin coupling between an excited singlet state and a near-energy triplet vibrational state. It is characteristic for shortening the fluorescence lifetime. The consequent relaxation occurs through the radiative process of phosphorescence or through vibrational relaxation[15].
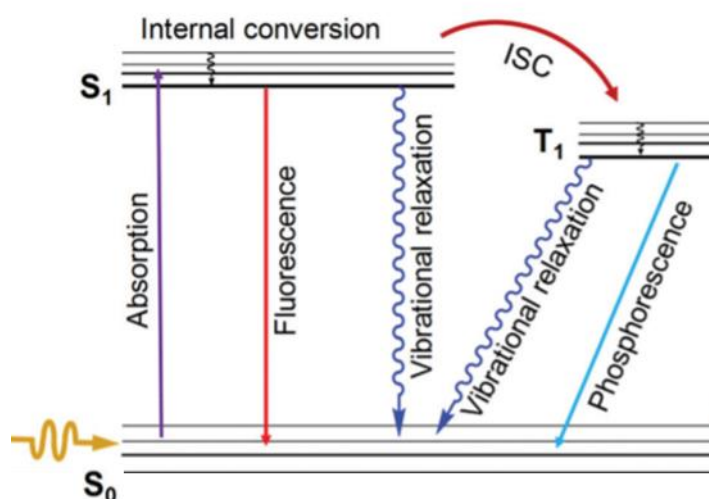
Figure 1- Simplified Jablonski diagram. S_0 is the ground state, S_1 is the first excited singlet state and T_1 is the first excited triplet state. The arrows associated with fluorescence and phosphorescence represent radiative relaxation pathways and the arrow associated with vibrational relaxation represents the non-radiative pathway[13].

1.2.3. Signaling mechanisms on fluorimetric sensors

The detection process by a fluorimetric sensor is usually achieved with photophysical mechanisms as chelation-induced enhanced fluorescence (CHEF), intramolecular charge transfer (ICT), photoinduced electron transfer (PET), aggregation-induced emission (AIE), among others.

A sensor that functions with ICT mechanism is normally composed of two moieties, one which is rich in electrons and other which lacks electrons. This mechanism occurs in excited molecules after the absorption of light. After being excited, electrons can move through π-bounds causing differences on the molecule's charge distribution, compared to the ground state. When the molecule relaxes, it is possible to see the emission related to this process[16].

3

A sensor that functions with PET mechanism in its 'off' state, when the fluorophore unit is excited, it produces an electron transfer from the receptor HOMO to the fluorophore HOMO, which prevents the occurrence of fluorescence (**scheme 1a**).

In its 'on' state when the fluorophore is excited, fluorescence occurs because the PET process is arrested by the interaction between the receptor and the analyte, lowering the energy of the HOMO orbital of the receptor. In the fluorophore-receptor-analyte complex, there is a transition of an electron from the LUMO orbital of the fluorophore to the respective HOMO orbital, and fluorescence occurs (**scheme 1b**).

This is easily comprehended by considering a proton as the analyte. H^+ electrostatically attracts the electron which causes an increase in the oxidation potential of the analyte-bound receptor to the point that the thermodynamics for PET is no longer favorable causing the fluorescence[17,18].
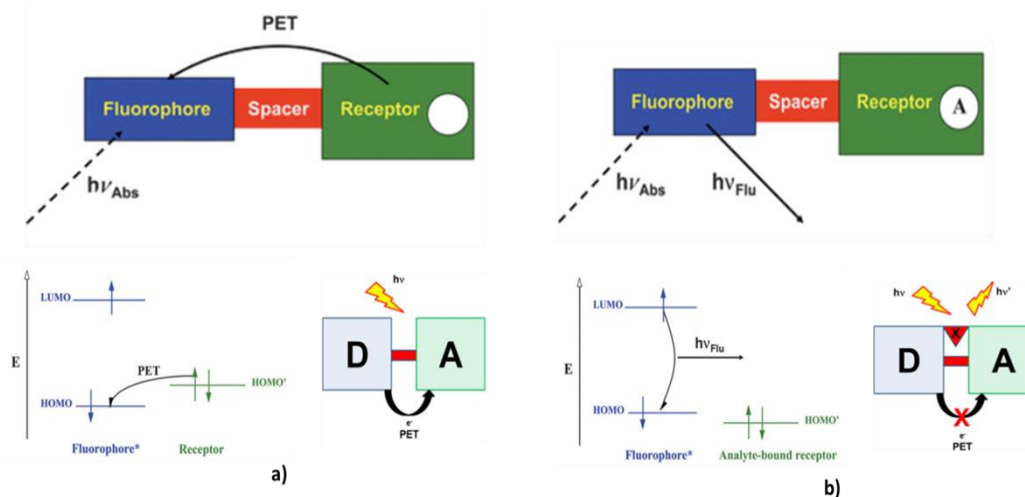
Scheme 1- PET mechanism. (a) 'Off' state of the sensor caused by an electron transfer from the analyte-free receptor HOMO to the photo-excited fluorophore HOMO. (b) 'On' state of the sensor, fluorescence is displayed because the electron transfer from the analyte-receptor complex is blocked[17,18]
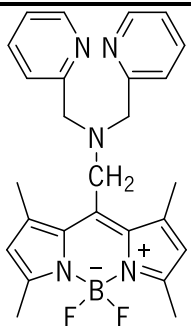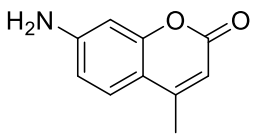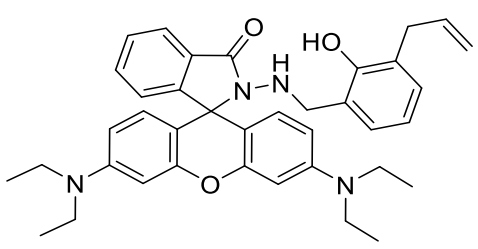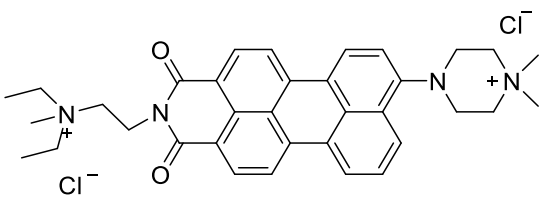
1.2.4. Chemodosimeter sensors

A sensor is described as a chemodosimeter when it shows irreversible interaction with a guest with high selectivity. These sensors are usually composed of two units: the reaction site and the signaling unite which provides a spectroscopic signal according to the irreversible interaction between the sensor and the guest. The spectroscopic changes are also irreversible, in principle[19,20]. These compounds are usually colorimetric or fluorimetric "turn on" or "turn of" probes, revealing fluorescence/color or quenching after the interaction[20,21].

1.3. Brief over view of heterocyclic probes used on recognition systems

Nowadays, the wide use of fluorometric probes is common to identify different types of analytes in different contexts, whether for disease diagnosis or prevention, monitoring of environmental parameters, among others. There is a large literary repertoire regarding heterocyclic probes for recognition proposes and these probes are used for detection of metal ions and anions, drugs of abuse, toxic pollutants and bioimaging of metabolic processes, among many others[22–27]. In **table 1** are given some examples of heterocyclic probes used for different applications, although there is a wide variety of other types of heterocyclic probes widely studied and reported.

Table 1-Examples of heterocyclic fluorescent probes applied to the recognition of different analytes.

Probe	Analyte	Structure example
4,4-difluoro-4-bora-3a,4a-diaza-*s*-indacene (BODIPYs)[22]	Hg^{2+}	 **1**
Coumarins[27]	$H_2PO_4^-$ and HPO_4^{2-}	 **2**
Rhodamines [23,25]	Heavy and transition metals (Cu^{2+}, Al^{3+}, Hg^{2+}, Au^{3+},)	 **3**
Perylene dyes[26]	Drugs (cocaine and angel dust)	 **4**

1.4. BODIPY derivatives

It has been reported that BODIPYs have facile synthesis and structural versatility, excellent spectroscopic properties, high molar extinction coefficients, moderate redox potentials, negligible triplet-state formation and negligible sensitivity to solvent polarity, excellent photostability, and high solubility in commonly used organic solvents[28,29]. Due to these properties, BODIPY dyes are used in many areas as laser dyes, fluorescent stains, labels in fluorescence imaging, and as indicator dyes in sensor applications. It can be used as a signaling unit as a constituent of a colorimetric or fluorimetric sensor and then functionalized with a recognition unit that changes its optical properties.

In **scheme 2** is presented the first synthesis reaction reported for the BODIPY derivative core. It is a multicomponent reaction, involving a Lewis acid catalyzed condensation with acetylation of the β-positions to form the first known BODIPY dye[30].
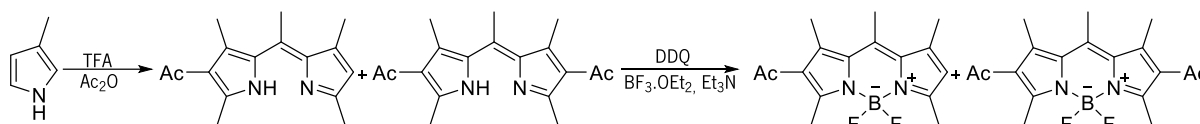
Scheme 2- Treibs and Kreuzer's simplified BODIPY synthesis reaction[30].

Although BODIPYs' structure **(figure 2)** is quasi-aromatic, since the boron atom does not participate in the electronic delocalization, their properties are broadly similar to aromatic π-systems since the coordination of the boron atom holds the dipyrromethene ligand in a rigid and planar conformation[28].
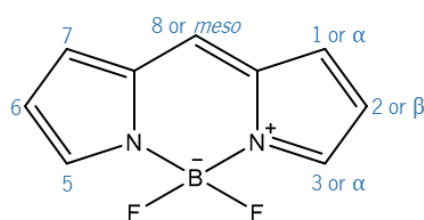
Figure 2- BODIPY chemical structure and numbering[28].

The simplest BODIPY with hydrogens in the dipyrrin core shows sharp and strong absorption and fluorescence bands in the green-yellow zone (500–510 nm) of the visible spectrum corresponding to the highest occupied molecular orbital (HOMO) to lowest unoccupied molecular orbital (LUMO) transition[31].

Besides this, the planar conformation of the π-system leads to high quantum yields (Φ_f) and a very low rate of nonradiative decay. If the BODIPY core is structurally modified, with an increase degree

of conformational flexibility, the fluorescence quantum yield tends to lower values[28].

In terms of water solubility, BODIPYs have limited utility since for biological applications or biological samples analysis, good water solubility and resistance to the formation of nonfluorescent dimer and higher aggregates is necessary. This solubility problem is usually improved by introducing ionizable hydrophilic groups within the core structure. Niu S. *et al.* reported novel water-soluble BODIPY derivatives by introducing one or two sulfonate groups onto the hydrophobic BODIPY core obtaining good yields in the synthesis and without great changes on photophysical properties. Another recent approach to improve BODIPYs water solubility was reported by Isik M. *et al.* and consisted of introducing ethylene glycolic entities bounded on phenolic hydroxyl groups and applied into the BODIPY core (**figure 3**)[32,33].
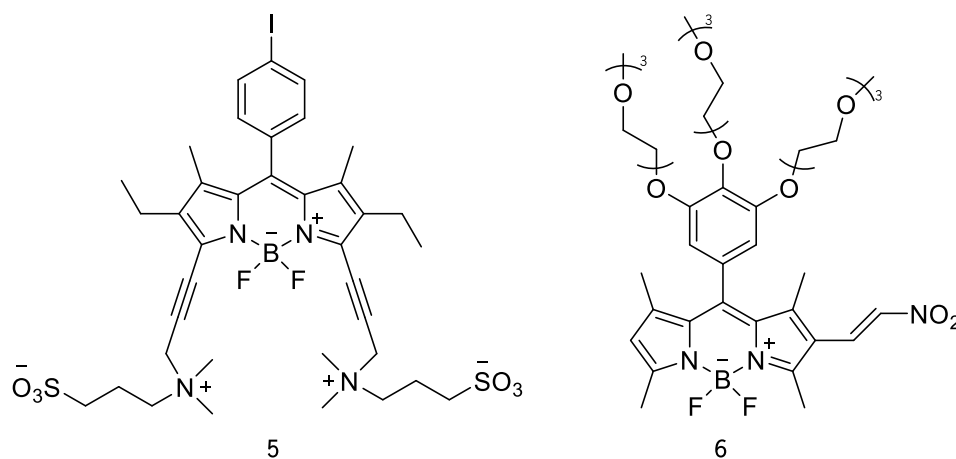
Figure 3- Examples of two BODIPY derivatives soluble in water with sulfonate groups (**5**) and hydroxyl groups (**6**)[32,33].

1.4.1. BODIPYs general design strategies

The use of organic probes with fluorescence on the red and NIR (near infrared) part of the electromagnetic spectrum has advantages from the current simple fluorescence probes, gaining a lot of importance nowadays. This kind of sensors work on the 650–1000 nm window, where autofluorescence, and scattering are minimized, and there is less light scattering, avoiding those problems[28].

Until recently, cyanine dyes have been the principal choice for NIR probes design, but issues related to their poor photostability and low Φ_F values are often seen. Also, rotation and photoisomerization of their flexible structures results in nonradiative fluorescent pathways[28].

BODIPYs have interesting properties that are easily altered by small modifications in their structure, leading to changes in fluorescence to the desired part of the spectrum, without the aforementioned problems of cyanine dyes, turning them into promising probes[28,34].

BODIPYs have also been used to create chromophore systems for the study of artificial

photosynthetic models because of its high donor ability. These molecules normally exhibit absorption and fluorescence at around 500 and 520 nm. To shift wavelengths into the NIR region, the main modification strategies are peripheral annulation to expand π-conjugation, the introduction of push-pull substituents and heteroatom substitution[35].

1.4.1.1.   Peripheral annulation

Peripheral annulation is achieved by the fusion of aromatic rings to the BODIPY core, causing pronounced bathochromic shift[35].

Aromatic units can be fused at the [a] bond, [b] bond and the "zig-zag" edge of the BODIPY core. Fusion of aromatic units results in red shift to their absorption and emission spectra, impacting their photophysical properties (**figure 4**)[35,36].
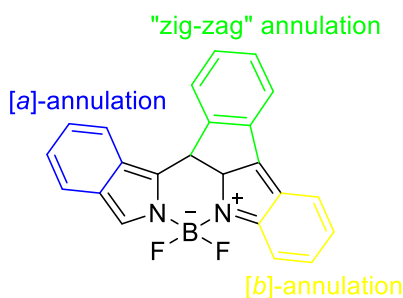
Figure 4- Examples of peripheral annulation designs using phenyl units[35].

1.4.1.2.   Aromatic [a]-fused BODIPY

[a]-Fused BODIPYs with aromatic units are obtained in various ways by retro-Diels–Alder reaction, using for example iso-indole fragments, or condensation of o-di-acetophenone with an ammonium salt, followed by boron complexation. The resulting derivatives have pronounced red shift in both absorption and emission spectra due to the extended π-conjugation[36,37]. The examples in **figure 5** are differently *meso*-substituted compounds not showing significant differences in absorption and emission wavelengths (respectively, λ_{abs} and $\lambda_{emi)}$[36].

7a, R- CH_3, EtOH, Φ_F-0.28

λ_{abs} -603 nm, λ_{emi} -609nm

7b, R- 4-iodophenyl, EtOH

Φ_F - 0.26, λ_{abs}-606nm, λ_{emi}-614nm
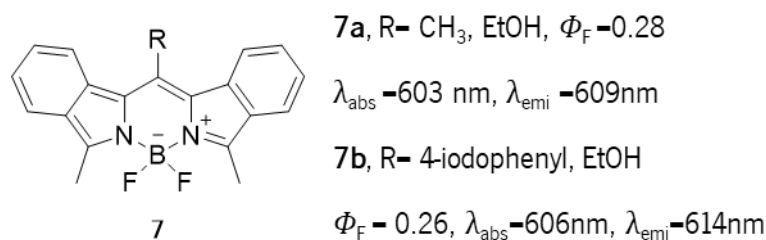
Figure 5- Example of two BODIPYs with [*a*]-annulation **7a** and **7b**[36].

1.4.1.3. Aromatic [*b*]-fused BODIPYs

Many strategies have been developed to fuse aromatic rings on BODIPYs [b]-bond. Condensation between 3-phenyl substituted indole fragments with an aromatic aldehyde, followed by oxidation, complexation with $BF_3 \cdot OEt_2$ produced dibenzo- [*b*]-fused BODIPY. The [*b*]-fused phenyl ring generally influences the LUMO energy level, while the HOMO energy level of the BODIPY core does not change[28,36].

An example of [*b*]-fused BODIPY dyes are the Keio Fluors (**figure 6**) that have furan rigs fused on the BODIPY core, which exhibited a significant spectral red shift with sharp absorption and fluorescence bands and outstanding bright fluorescence[36].

$CHCl_3$, Φ_F -0.56

λ_{abs}- 723nm, λ_{emi}- 738nm
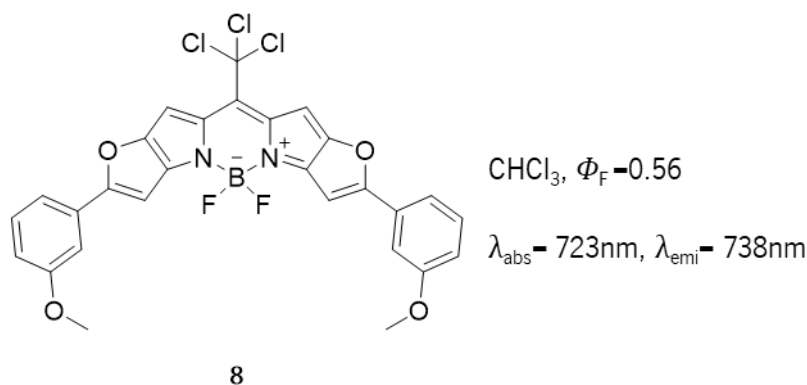
Figure 6- An example of Keio Fluors BODIPY **8**[36].

1.4.1.4. "Zig-zag" edge fusion

Intramolecular oxidative cyclodehydrogenation is a way to fuse an electron-rich aromatic unit to the "zig-zag" edge of the BODIPY **9** (**figure 7**). After fusion of aromatic moieties, the obtained BODIPY dyes exhibited red-shifted absorption spectra beyond 1000 nm. These compounds showed good photo- and chemical stability. When studied, they revealed an absorption band in the long-wavelength region that gave evidence for intramolecular charge transfer or aggregation profiles because of the highly extended

π-conjugation. For these reasons, these dyes always exhibited a low fluorescence quantum yield[36].

Toluene, $\Phi_F = 0.008$

$\lambda_{abs} = 670$ nm, 780 nm

$\lambda_{emi} = 742$ nm, 830 nm

9
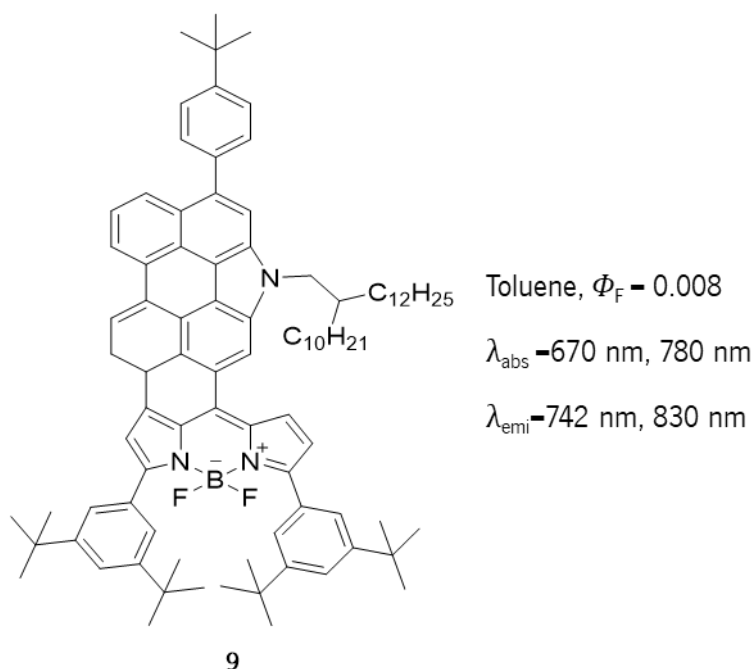
Figure 7- An example of "zig-zag" edge fusion design BODIPY **9**[36].

1.4.2. Push - pull substituents

The use of pull and push substituents is a BODIPY synthesis strategy that allows the delocalization of electrons through the introduction of aromatic rings at the α position. This strategy extends the conjugation system, but the bathochromic shift is limited. The use of heterocyclic aromatic substituents such as pyrrole and thiophene at the α positions can induce more pronounced red spectral shifts (**figure 8**)[36].

CH_2Cl_2, $\Phi_F = 0.82$

$\lambda_{abs} = 573$ nm, $\lambda_{emi} = 643$ nm

10
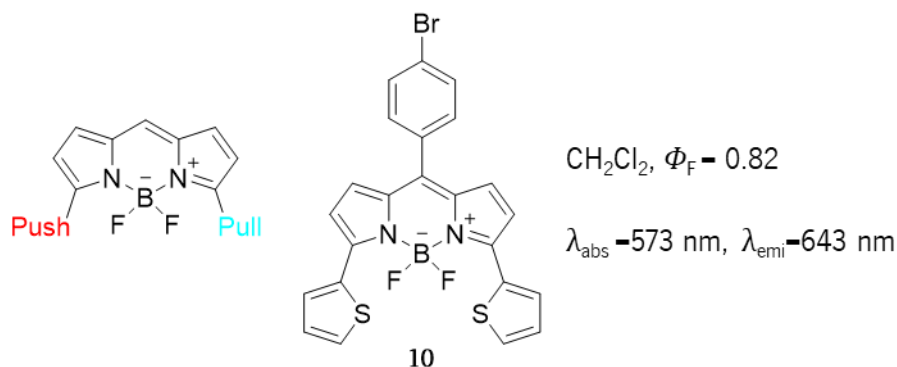
Figure 8- Push and pull layout and BODIPY **10** designed with this strategy[35,36].

.

1.4.3. Heteroatom substitution

The most common BODIPYs substituted with heteroatoms are the aza-BODIPYs where the carbon

atom at the *meso* position is replaced by an imine type nitrogen atom, such as BOBIPY **11** (**figure 9**). These molecules are obtained by the reaction of pyrrole and nitrosopyrrole and the addition between the chalcones and nitromethane, or cyanide. Followed by a condensation reaction with ammonium acetate, provided the aza-di-pyrromethenes, and complexation with BF$_3$·Et$_2$O gave the corresponding aza-BODIPYs.

Aza-BODIPYs are attractive because their red-shifted absorption/emission spectra and unmodified excellent properties from the classic BODIPYs include high molar extinction coefficients, narrow spectral bands, high fluorescence quantum yields and good stability[36].
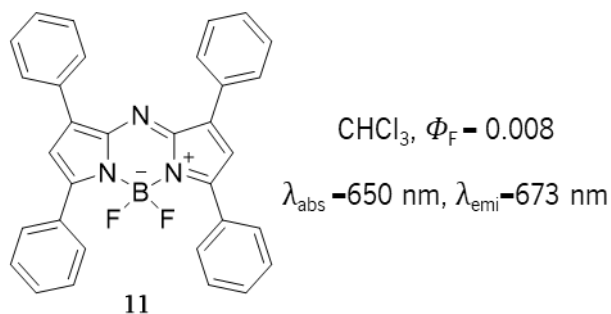
Figure 9- Example of an aza-BODIPY **11**[36].

1.5. Dicyanovinyl derivatives

Dicyanovinyl derivatives are widely used as colorimetric and fluorescent sensors based on nucleophilic addition reactions that shows both sensitivity and specificity to anions and molecules rich in eletrectons. Structurally they have strong electron-withdrawing effects and are used in presence of well-known recognition units. In literature is reported widely reported the addition of cyanide ion to the double bond of the dicyanovinyl moiety causing significant changes in color and fluorescence associated with ICT mechanism[33,38–41]

An excellent example is a novel dicyanovinyl derivative **12** studied by Ozdemir A. *et. al.*, a chemodosimeter sensor for cyanide (**figure 10**), where the anion is added to the β-position of the vinyl group.

12
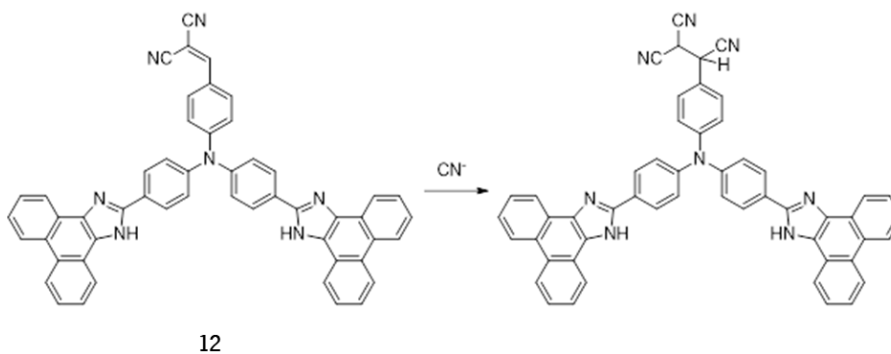
Figure 10- Novel dicyanovinyl derivative **12** and the respective product after addition of the cyanide ion[42].

In **figure 11** are presented the absorption (**a**) and emission (**b**) spectra of this compound in presence of different analytes showing the selectivity for cyanide. The differences in fluorescence and color are in the inset and it is possible to see the changes caused by the cut off of the ICT mechanism[42].
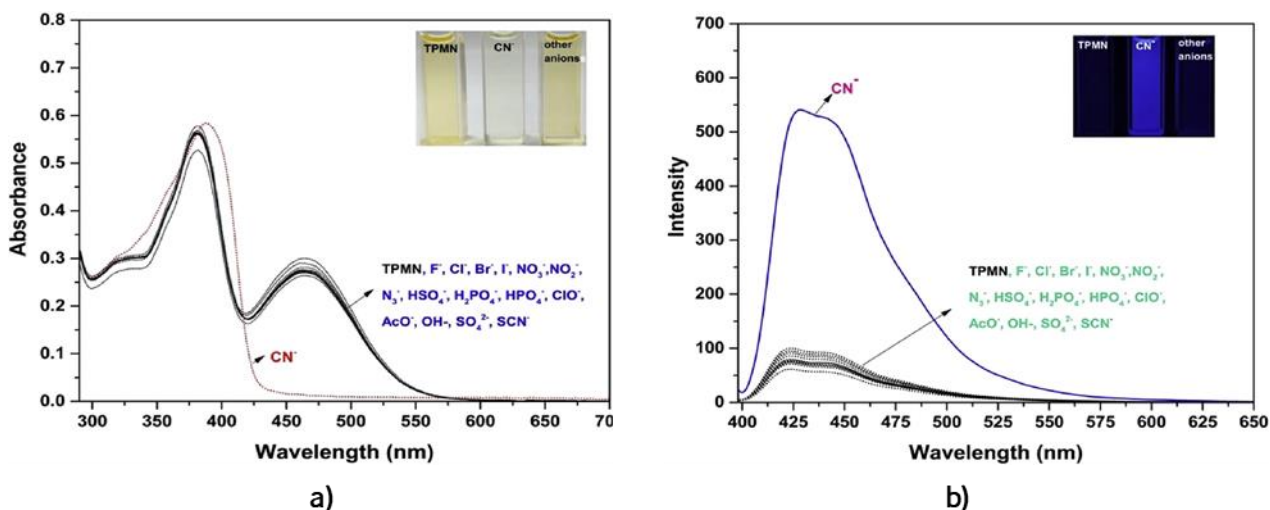
Figure 11- Absorption (**a**) and emission (**b**) spectra of the dicyanovinyl derivative **12** in presence of different anions. The inset represents the observable changes in fluorescence and color in presence of cianyde[42].

1.6. Ilicit drugs

The use of cigarettes and alcohol as legal drugs is common by the population. However, other drugs have been a problem for society for many years, causing several social situations such as increased crime, unemployment, health problems, among others. Because of this, in many countries some drugs are classified as illicit, but the use of the different drugs is not equally stigmatized[43,44].

Illicit drugs (ID) are associated with social prejudice, as the use of powdered cocaine, despite presenting health risks, is often seen as a demonstration of status, while the use of heroin or crack is associated with disadvantaged or marginalized groups. The granting of social status to users of ID can encourage their use and the social ills that accompany their consumption; however, their stigmatization can also affect people in a contrary way, due to the status with which they are sometimes associated. Despite that, both behaviors are health dangerous[43]. It is estimated that in the United States alone ID accounts for 30000 premature deaths per year and in Europe at least 8300 deaths in 2018[45,46]. To avoid these problems, governments around the world have developed programs to eradicate the sale and trafficking of ID, increasing the legal effects[44]. ID can cause acute intoxication and in extreme cases death, due to this it has become important to develop ways to determine the use of this type of substances[45].

A worrying situation related to drug abuse is the misuse of prescription medicines. This behavior

is the use of a medication without a prescription, differently from that prescribed, or for recreational purposes. According to various researches, prescription drugs used to treat pain, attention deficit, and anxiety disorders, are being used among ID users. Some of those drugs are opiates and cannabinoids[47], which cause addiction and dependence. The consequences of this abuse have steadily worsened, reflecting an increase in admissions to treatment, visits to emergency rooms, and overdose deaths[45,47]. To help with diagnosis, prevent serious situations, among others, there is a need to develop faster, more selective and less expensive techniques to detect these drugs. In this work, the targeted abuse drugs were the prescription drugs codeine and fentanyl and their main metabolites.

1.6.1. Cannabinoids

Cannabinoids are a class of chemical compounds of diverse origins that act on cannabinoid receptors on the cell membrane belonging to the G-protein-coupled receptor group (GPCR). Three main groups of cannabinoid receptor ligands have been identified dividing, consequently, the cannabinoids into three different types: endocannabinoids, phytocannabinoids, and synthetic cannabinoids[48]. For this work only phytocannabinoids and synthetic cannabinoids have interest.

1.6.1.1. Phytocannabinoids

Phytocannabinoids are produced by cannabis, a generic term used for drugs produced from plants belonging to the genus Cannabis. It is one of the most popular recreational drugs and it is also used in medical therapy to treat disease or alleviate symptoms. Cannabis's main application in medicine is in the treatment of chronically ill patients. Medications based on phytocannabinoids have been investigated in many clinical trials targeting diseases like multiple sclerosis, cancer, and noncancer pain, neurodegenerative disorders, and appetite suppression[48,49].

The most common phytocannabinoids are Δ^9-tetrahydrocannabinol (THC; 6, 6, 9-trimethyl-3-pentyl-6a, 7, 8, 10a-tetrahydro-6H-benzo[c]chromen-1-ol), which as the more pronounced psychoactivity of this group, the others are 6, 6, 9-trimethyl-3-pentyl-6H-benzo[c]chromen-1-ol, well-known as cannabinol, and (1'*R*, 2'*S*)-1', 2', 5'-trimethyl-4-pentyl-2'-(prop-1-en-2-yl)-1', 2', 3', 4'-tetrahydro-[1, 1'-biphenyl]-2, 6-diol, known as cannabidiol[48,49], which is non-psychoactive[50,51] (**Figure 12**).
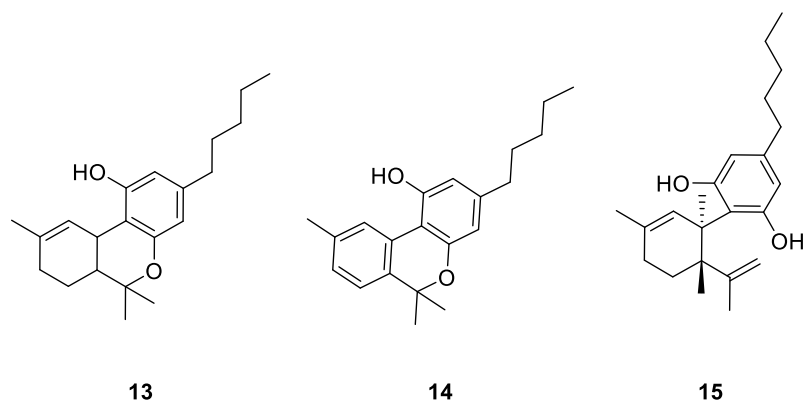
Figure 12- Chemical structures of the principal phytocannabinoids: THC (**13**), cannabinol (**14**) and cannabidiol (**15**)[48,51].

After being injected in the form of herb or resin preparations, the phytocannabinoids suffer various metabolic pathways. One of the major pathways occurs with THC, it involves the initial reaction of allylic hydroxylation at the C11 forming 11-hydroxy-Δ⁹-tetrahydrocannabinol with systematic name 6-(hydroxymethyl)-9, 9-dimethyl-2-pentyl-4b, 7, 8, 8a, 9, 10-hexahydrophenanthren-4-ol, furthermore is possible the oxidation to 11-nor-9-carboxy- Δ⁹-tetrahydrocannabinol with systematic name 5-hydroxy-10, 10-dimethyl-7-pentyl-1, 2, 4a, 9, 10, 10a-hexahydrophenanthrene-3-carboxylic acid, the major metabolite found in blood and urine (**scheme 3**)[52].
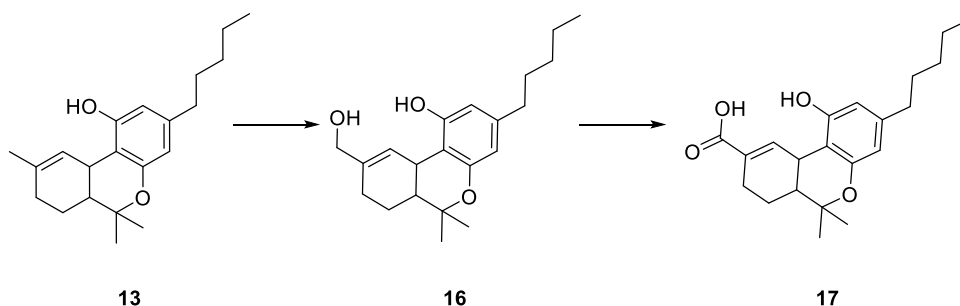
Scheme 3- The major metabolic pathway that occurs to phytocannabinoids taking as an example THC **13**. The first hydroxylation occurs forming compound **16** followed by oxidation forming **17**[52].

1.6.2. Opiates and opioids

Traditionally, the term opioid refers to all-natural and synthetic compounds that have morphine-like actions, while the term opiates refer to a compound derived from Papaver *somniferum*, such as morphine and codeine and its synthetic analogues, such as oxycodone and buprenorphine.

Opioids can be subdivided based on the ring structure of 4,5-epoxymorphine like morphine, codeine, heroin and naloxone, piperidine, and phenylpiperidines like meperidine, loperamide, fentanyl and others. Although these drugs have very different chemical structures, mechanisms, and rates of drug

distribution and elimination, their only common feature is interaction with the same receptor in the human body (μ opioid receptor). These compounds are used in medicine to treat acute and chronic pain. They have a narrow therapeutic index and great variability in response and are one of the most used IDs[53].

Many reports suggest that chronic exposure to opiates, such as morphine and heroin, can result in cognitive deficits, for example, heroin users perform worse in attention, verbal fluency, and memory tasks than controls[57,58]. The chemical structure of each synthetic opiate is unique and fails to follow the overall morphine like structure found in the natural compounds. Therefore, each one must be considered on its own when studying metabolism and the potential for pharmacokinetic drug-drug interactions[55].

1.6.2.1.   Codeine

Codeine, with systematic name (4*R*,7*S*,7a*R*)-9-methoxy-3-methyl-2,3,4,4a,7,7a-hexahydro-1*H*-4,12-methanobenzofuro[3,2-e]-isoquinolin-7-ol, is a natural constituent of *Papaver somniferum*, commonly known as opium poppy. Is usually used as an analgesic to treat mild and moderate pain[56].

The main pathways of codeine metabolization consist in *O*-demethylation, *N*-demethylation or both reactions forming the products shown in **scheme 4**[57,4].
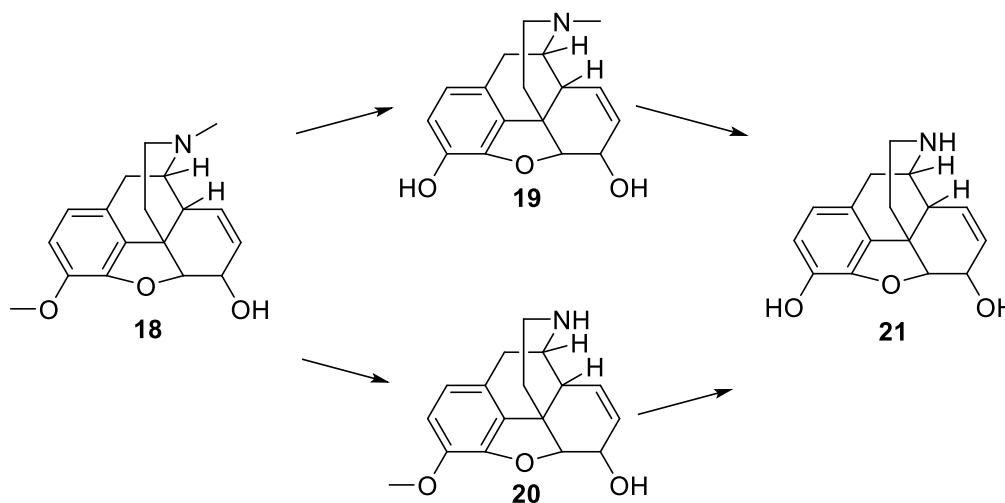
Scheme 4- Codeine (**18**) metabolites: morphine ((4*R*,7*S*,7a*R*)-3-methyl-2,3,4,4a,7,7a-hexahydro-1H-4,12-methanobenzofuro[3,2-e]isoquinoline-7,9-diol, **19**), norcodeine ((4*R*,7*S*,7a*R*)-9-methoxy-2,3,4,4a,7,7a-hexahydro-1H-4,12-methanobenzofuro[3,2-e]isoquinolin-7-ol, **20**) and normorphine ((4*R*,7*S*,7a*R*)-2,3,4,4a,7,7a-hexahydro-1H-4,12-methanobenzofuro[3,2-e]isoquinoline-7,9-diol, **21**)[4].

1.6.2.2.   Fentanyl

Fentanyl, with the systematic name *N*-(1-phenethylpiperidin-4-yl)-*N*-phenylpropionamide, is a synthetic opioid that acts as an opioid agonist. The exposure of humans to fentanyl can cause euphoria,

sedation, respiratory depression, physical tolerance and dependence, which are the same effect as exposure to other opioids such as morphine and heroin[58,59].

Oxidative *N*-dealkylation is fentanyl's primary pathway of metabolism in humans, being the main metabolite norfentanyl, a small percentage of fentanyl is metabolized by alkyl hydroxylation, combined with N-dealkylation and hydroxylation or amide hydrolysis to the inactive compounds hydroxyfentanyl, hydroxy norfentanyl, and despropionylfentanyl[58,60]. **Scheme 5** shows Fentanyl chemical structures and the metabolites.
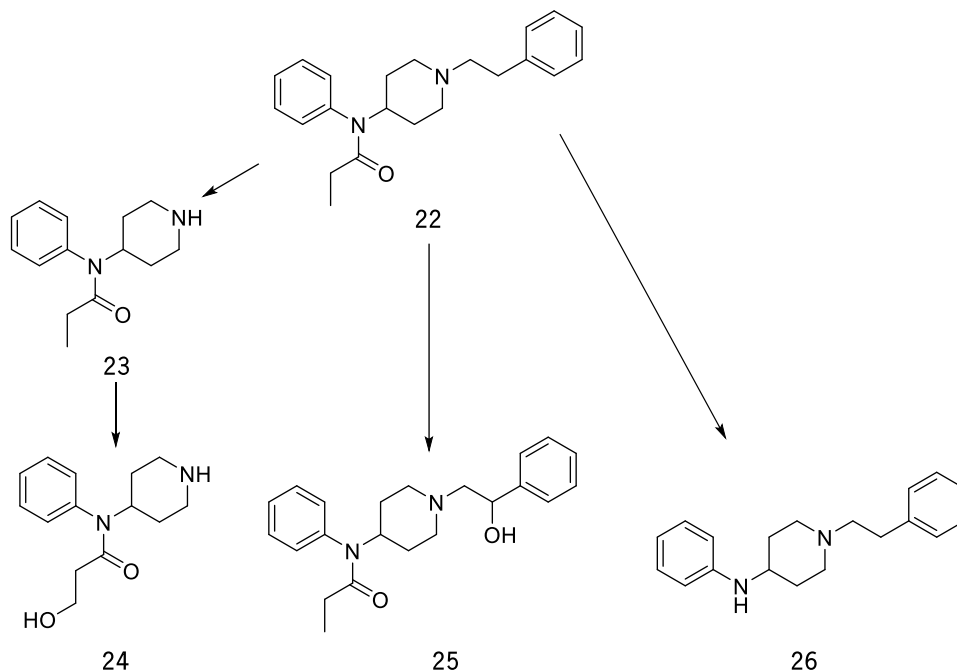
Scheme 5- Fentanil (**22**) metabolites: norfentanyl (*N*-phenyl-*N*-(piperidin-4-yl)propionamide, **23**), hydroxynorfentanil (3-hydroxy-*N*-phenyl-*N*-(piperidin-4-yl)propanamide, **24**), hydroxyfentanyl (*N*-(1-(2-hydroxy-2-phenylethyl)piperidin-4-yl)-*N*-phenylpropionamide, **25**) and despropionylfentanyl (1-phenethyl-*N*-phenylpiperidin-4-amine, **26**)[60].

1.6.3. Samples and analysis techniques used for ID

The most objective way to drug test humans is to analyze biological fluid and tissues. When it is intended to diagnose the use of a drug, the choice of the matrix to be analyzed must be considered. Every individual offers different information standards, in addition to the other need-to-know parameters such as the time of exposure, the form or modality of ingestion, the knowledge of the pharmacokinetics and pharmacodynamics of the substance[45].

The most common samples used in drugs analysis are blood and urine, however, there is a growing interest in the use of alternative body fluids and tissues, such as saliva, skin or skin excretions and hair for the diagnosis of drug use[45,61]. Most of the samples can be obtained non-invasively,

nevertheless, samples taken in a more invasive manner or with greater discomfort for the patient, such as blood and urine, may reveal more information about the metabolization of ID, among others, which may be important[62].

There are several analysis techniques for this type of drugs, such as those presented in **table 2**.

Table 2- Analytic techniques used for abuse drugs according to sample nature.

Drug and metabolites	Sample nature	Technique	Reference
Cannabinoids	Urine, saliva, tears and plasma	GC/MS	45,63
	Saliva	2D-GC/MS	64
	Urine	LC/MS	50, 65
		Immunoassay	66, 67
Codeine	Plasma and urine	HPLC	4, 68
		Immunoassay	68
	Urine	GC/MS	69
Fentanyl	Blood	LC/MS	70, 71
	Urine, saliva	GC/MS	72, 73
	Plasma and saliva	HPLC/MS	58

In this work, the type of sample targeted is urine. For that is important to know its constitution. Compounds present in the urine can act like interferents and may need to be separated from the sample in the pre-treatment stage of chromatography, for example, or in this case, the developed probes need to have specific recognition systems to avoid identification and quantification mistakes.

Urine is made up mostly of water, however various types of molecules and salts, such as sodium chloride, can be dissolved in the matrix. Larger molecules as peptides, proteins and small organic molecules are found. The most common small molecules in urine are urea (U), uric acid, creatinine (CRT) and some cholestenoic acids, the first three being the most abundant (**figure 13**)[74,75].
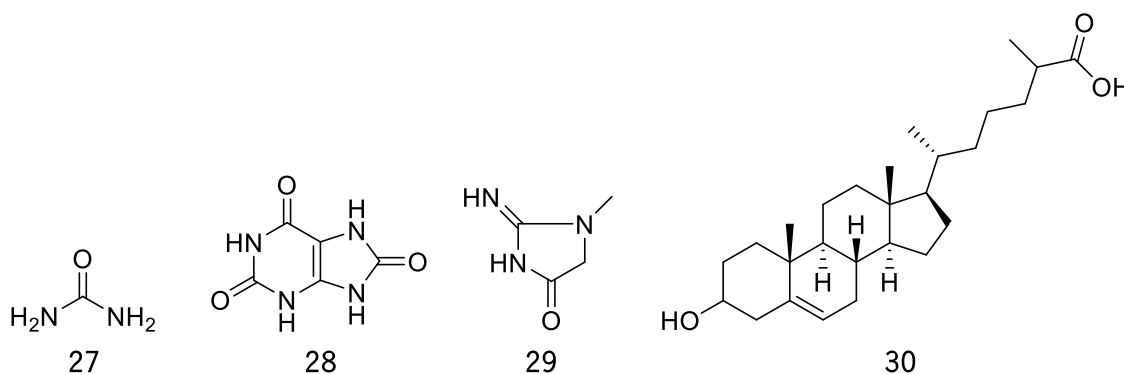
Figure 13- Chemical structure of principal components of urine: U (**27**), uric acid (7,9-dihydro-1*H*-purine-2,6,8(3*H*)-trione, **28**), CRT (2-imino-1-methylimidazolidin-4-one, **229**) and cholestenoic acid ((6*R*)-6-((8*S*,9*S*,10*R*,13*R*,14*S*,17*R*)-3-hydroxy-10,13-dimethyl-2,3,4,7,8,9,10,11,12,13,14,15,16,17-tetradecahydro-1*H*-cyclopenta[a]phenanthren-17-yl)-2-methylheptanoic acid, **30**) [74,75].

Another factor of the urine constitution that may affect the accurate detection of the target analytes is the pH. Urine's pH is not a constant value, usually it is in a range between 6.0 and 7.0 in normal situations. In case of drug addicts is found that the urine pH usually stays between 5 and 8 [76,77].

1.7. Ion importance and recognition

Ions play a fundamental role in several areas such as medicine, environment and biology, as they play important roles in living beings. Therefore, identification and quantification of these analytes has become important for the understanding of certain diseases and for the development of diagnostic methods [78].

1.7.1. Cation recognition

Metal ions play a fundamental role in several biochemical processes, such as in the nervous impulse transmission mechanism, where Na^+, K^+ and Ca^{2+} ions cause changes in the electrical potential of cell membranes [79,80].

Some metal ions such as Cu^+, Mg^{2+}, Mn^{2+}, Cu^{2+}, Zn^{2+}, Fe^{3+} are involved in the formation of complexes with proteins (metalloproteins) regulating the enzymatic activity or transporting molecules. In the presence of Fe^{2+}, hemoglobin is able to transport oxygen into the bloodstream [79,80]. On the other hand, significant variations in the concentrations of these ionic species can induce a deregulation of biological systems [84]. Recent studies have linked several pathologies with abnormal levels of ions in the human body. It is believed that the balance of ions in the patient's body is affected, with uncontrolled ions such as Cu^{2+}, Fe^{3+}

and Zn^{2+}, and consequently an accumulation in tissues and cells[78].

In the environment, large amounts of metals are dumped daily by industries into local rivers and watersheds. In an effort to effectively monitor these situations, many resources have been devoted to the development of new selective receptors for cations[82].

In this sense, it is increasingly necessary to develop new ways to detect these analytes effectively in order to prevent health and environmental problems.

Iron(II) and iron(III)

Iron is indispensable for life and Fe^{2+} and Fe^{3+} are the most abundant transition metals in the human body. It plays crucial roles in activities such as the growth and development of living systems and vital biochemical processes, such as oxygen detection and transport, electron transfer, catalysis of various enzymes, cell and DNA metabolism, RNA synthesis[81].

The detection of trivalent cations is of significant importance due to their crucial role in a wide range of environmental and biological processes. For example, the lack of Fe^{3+} in the body can lead to various diseases such as anemia, diabetes, hemochromatosis, Parkinson's disease and may even be associated with dysfunctions in the heart, pancreas, kidneys and liver[83].

Copper (II)

Copper (II) is the third most abundant and essential transition metal in the human body due to the vital roles it plays in several biological processes, such as the stimulation of endothelial cells, being necessary for the secretion of various angiogenic factors by tumor cells. However, given the extensive application in science and in the electrical and machinery and construction industry, has become a dangerous pollutant for the environment. Abnormal levels of copper(II) in organisms can cause symptoms similar to neutropenia, bone abnormality, hypopigmentation, impaired growth and osteoporosis, as well as serious health problems such as neurodegenerative diseases such as Alzheimer's, Parkinson's, Menke, prions and Wilson[84–86].

Zinc(II)

Zinc is the second most abundant transition metal ion in the human body. It is cytotoxic if consumed in large quantities, and unbalanced metabolism can lead to skin diseases, diabetes, epilepsy, ischemic stroke, Alzheimer's disease, prostatic adenocarcinoma and pancreatic islets, which play critical roles in insulin biosynthesis, storage and secretion, on the other hand, the considerable decrease in zinc

concentration may be associated with the development of cancer. Zinc is considered an environmental pollutant, and significant concentrations of this metal can reduce soil microbial activity causing phytotoxic effects and is a common contaminant in agriculture among others [78,87].

Palladium(II)

Palladium is widely used in catalysts, dental and medical devices, jewelry and fuel cells, it has high toxicity and, therefore, is highly harmful to the environment and human health. The threshold level of palladium in drugs has been limited to 5-10 ppm and its maximum dietary intake is restricted to ca. 1.5-15 μg per person. In organic synthesis, it is used as a catalyst for the synthesis of complex molecules, but owing to the frequent use of such catalysts, a high level of residual palladium is often found in the resulting product, which can be a danger to health [88-92].

Mercury(II)

Mercury (II) is a global pollutant that affects not only the ecosystem, but also human health. Mercury exists in three forms: elemental or metallic mercury, inorganic mercury compounds and organic mercury. The main sources of mercury are the burning of fossil fuels, mainly coal, municipal waste and incineration. Mercury is also released by natural evaporation from land and sea surfaces and by volcanoes. The most toxic form of mercury is methylmercury. Exposure to mercury, even at low concentrations induces digestive, brain, kidney and endocrine system diseases. this is especially associated with neurological diseases [93,94].

Nickel(II)

Nickel compounds have many industrial uses such as Ni-Cd batteries, machinery, pigments, welding, electroplating, tools and catalyst precursors. Nickel is also an important metal in biological systems. Overexposure to nickel ion can cause acute pneumonia, dermatitis, asthma, central nervous system disorders, and cancer of the nasal cavity and lungs. The adverse health effects of nickel depend on the route of exposure (inhalation, oral or dermal) and can be classified according to systemic, immunological, neurological, reproductive, developmental or carcinogenic effects after acute (1 day), subchronic (10-100 days) and chronic (100 days or more) exposure periods [95,96].

1.7.2. Anion recognition

Anions are also involved in several important biological processes, playing various roles, as well as in environmental and industrial applications[100]. The development of small molecules for anions, therefore, continues to attract a lot of research attention since its beginnings in the late 1960s and 1970s. Nowadays, is a fundamental pillar of supramolecular chemistry with applications in many areas including detection, extraction, transport through lipid bilayers and organocatalysis[98–100]. The design of anion receptors is a challenge because anions, in comparison to cations, are larger and therefore have a lower charge/radius ratio. They are also susceptible to pH, so that in an acidic environment they become protonated, losing their negative charge. The binding of the anion to the receptor can also be influenced by the solvent[98,100].

Fluoride

Fluoride is a very important analyte due to its biological and medicinal importance. Small amounts, on the order of 1 mg / L in the ingested water, have a beneficial effect, decreasing the rate of occurrence of tooth decay, especially in children, and it is also used in the treatment of osteoporosis. On the other hand, excess fluoride results in pathological changes in teeth and bones, such as dental and skeletal fluorosis, and can cause kidney failure. According to the World Health Organization (WHO), the maximum allowable limit of fluoride ions in drinking water is 1.5 mg/L[101–103].

Cyanide

Cyanide is a highly toxic substance for the environment and for mammals. Small amounts of cyanide can affect various functions in the human body, attacking the vascular, visual, central nervous, cardiac, endocrine and metabolic systems. The cyanide anion can be absorbed by the lungs, gastrointestinal tract and skin, causing vomiting, convulsions, unconsciousness and possibly leading to death. It is lethal to humans at concentrations in the range of 0.5-3.5 mg/kg body weight. In addition to being found in many foods and plants, cyanides are used industrially in the synthesis of organic chemicals, polymers, metallurgy, as well as in gold mining[104].

Acetate

The acetate ion is a vital component of several metabolic processes and specific roles in biochemical processes related to antibodies and enzymes. It has been widely used in the manufacture of paint, plastics, paper and the nylon industry[104,105].

1.8. From machine learning to chemometrics. Applications

In order to understand spectroscopic data and get a conclusion about them in a certain context is necessary to apply statistical tools. These tools allow relating the results to the work objective. Multivariate regression methods and design of experiments (DOE) are some of these tools. They appear as a consequence of the increase in the dimensionality of chemical data associated[106,107].

Multivariate analysis (MA) consists in simultaneously analyzing various variables with the purpose of understand how these variables correlate with each other, allowing interesting breakthroughs due to its ability to analyze high dimensionality data. However, its application was mostly based on multivariate regression methods, response surface's and pattern recognition, with the increasing amount of data acquired with novel technology and the growth and rise of artificial intelligence (AI) and machine learning (ML) methods it was a matter of time until ML methods started to be employed in analytical chemistry[107-109]. A rapid growth of the technology in terms of graphics processing units, powerful cloud-computing systems contributed to major breakthroughs in AI and ML[110–113].

Samuel *et al.* defined ML as "the field of study that gives computers the ability to learn without being explicitly programmed". In fact, this new approach was an important catalyst in bridging ML and chemistry originating the term chemometrics[109,114].Chemometrics means, no more than, performing calculations on chemical data[115].

Analytical chemistry is no exception and the application of these novel tools allowing exhaustive treatment of the chemical data permitting that the hidden information in chemical data acquired by several different methods could be understood. In what concerns the analytical chemistry process, this came to be its last big update in a long time[116].

Chemometric technics can be applied on spectroscopy data using mathematical, statistical and logic-based approaches to correlate analytical instrument data to quality, compositional, physical properties or discrete classification of the used samples[117].

1.9. Learning Algorithms

Learning algorithms are used to treat analytic data creating supervised ML models. The algorithms have a mathematical formalism but the important part is the form of how it works and the information given about the data. In practice, an algorithm is a step-by-step way to solve a problem. ML algorithms are most of the times called learners, contrasting with common algorithms that are base in a list organized rules, the concept of learners consent them to conclude the rules by analyzing a substantial amount of data.

Lots of ML algorithms are known and have specific applications intended to serve different purposes. Some of them are shown in **scheme 6**[118,119].

Scheme 6- Classification of the principal ML algorithms[118].

1.9.1. Principal component analysis (PCA)

PCA is a mathematical algorithm used to reduce the dimension of a data set while maintaining most of the variation of the original set. The reduction is made by identifying directions, called the principal components (PCs), which consider the variation in the data is maximal. Using, only, a few components, is possible to represent each sample with relatively few numbers instead of values for thousands of variables using algebra operations. Samples can then be represented, making possible to visually assess similarities and differences between the samples and determine if the samples can be grouped. PCA new variables are linear combinations of the original variables. Usually, are used two principal components, the first one embodies the largest variation of the data, otherwise, the second principal component has an uncorrelated direction to the first component along which the samples show the largest variation[120,121].

PCA extensively used to explore high-dimensional data sets. Three-dimensional visualizations are used for this exploration, and samples are either projected onto the components, or plotted according to their correlation with the components presenting their relation. Some information will be lost in two- or three-dimensional visualizations, it is important to systematically try different combinations of components

when picturing a data set to avoid this problem. As the principal components are uncorrelated, they may represent different characteristics of the samples. This suggests that PCA can serve as a useful first step before clustering or classification of samples[120].

In **figure 14** are shown two graphics related to an example which explains better PCA. The example is about breast cancer, the samples are classified as being either positive or negative for the estrogen receptor, and two genes whose expression is known to correlate with estrogen receptor status (**figure 14a**). The two principal components (PCs) are shown in **figure 14b**. The PC 1 has the direction along which the samples display the major variation. The PC 2 has the direction uncorrelated to the first component along which the samples show the largest variation. Individually, the components can be interpreted as their directions, which maximizes the variance of the samples when projected on the PC. Applying PCA, is calculated that PC 1 has different contribution from the two-original variable in different weights showing the sample-like pattern of all the data[120].
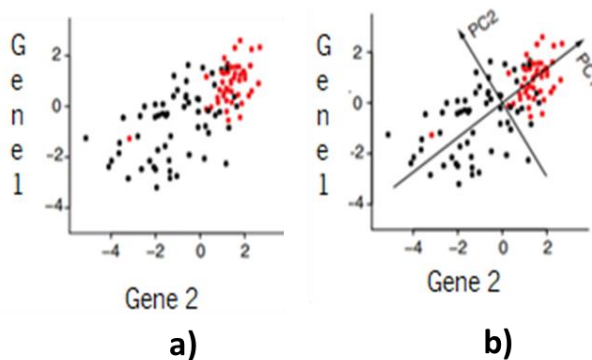
Figure 14- Data sets before (**a**) applying PCA and after (**b**), showing the PCs direction[120].

1.9.2. Partial least square regression (PLS)

Chemometricians are familiar with the concepts of regression methods and often select the use of main components or latent variables. Those aim to represent global orthogonal non- correlated variables deduced from the highly intercorrelated spectral sets. Spectroscopists, in the other hand, usually prefer variables or intervals of variables in the original traditional variable space because these represent interpretable chromophores, fluorophores, and other chemical species and because a strict orthogonal decomposition is not realistic.

The development of chemometric methods for spectral variable is important to improve the model's predictive ability. With respect to data reduction, variable selection may be a realistic method since spectral data contain a high degree of covariance and large amounts of redundant information. Because of that chemometric methods for variable where information is optimally preserved is needed

and consequently widely applied[122].

Multivariate analysis and latent variable methods, as PLS, are a possibility to project multivariate data into few dimensions in a graphical interface. PLS goal is to predict or analyze dependent variables from a set of independent variables (predictors). This prediction is accomplished by extracting from the predictors a set of orthogonal factors, the latent variables which have the finest predictive power. PLS regression is particularly useful to predict a set of dependent variables from a large set of predictors. It originated in the social sciences but became popular first in chemometrics due in part to Herman's son Svanteand in sensory evaluation[121–123].

For example, analyzing sugars in juice samples is hard because NIR spectra are, usually, broad and overlapped hiding important data. Appling PLS on the same NIR spectra data is possible to reobtain that hidden information and PLS makes use of the same information to establish analyte values associated with the spectra. After determining the right PCs and treat the data for outliers, then regression analysis is made leading to various PLS regression models. The best model is obtained by the second derivative processed spectra which indicates the linear relationship of the predicted values and reference values has the priority over other pre-treated and raw spectra. The best calibration equation can be applied to unknown samples to do quantification of the interest analites[124].

1.9.3. Multiple linear regression and principal component regression

Multiple linear regression (MLR) is an extension of simple linear regression (SLR), including more than one explanatory variable. In both cases, we still use the term "linear" because the response variable is directly related to a linear combination of variables. This type of regression usually presents collinearity (correlation of variables) problems, when spectral data are used, the great variability of these data leads to model instability since the coefficient of determination (r^2) changes easily[125].

PCA and MLR can be combined to improve the extrapolative capacity of MLR, this is known as principal component regression (PCR)[126].

This technique is popular in spectroscopic studies owing to its ability to accommodate spectral collinearity by excluding principal components with less information about the data. Thus, the inherent collinearity is reduced, leading to reliable and good predictive model with great stability[127].

In other words, PCR is a two-step multivariate calibration method: in the first step, a PCA, of the data matrix is performed and the measured variables, for example absorbances at different wavelengths, are converted into new ones, scores. This is followed by MLR between the scores obtained in the PCA step and the characteristic to be modelled, for example concentration[128].

Chapter 2

Materials and methods

2. Materials and methods

2.1. General considerations

The commercially available reagents and solvents were provided by Sigma-Aldrich, Acros and Fluka and used as received. Dicyanovinyl derivatives **4** and **5** were previously synthesized by the research group.

Thin layer chromatography was performed on Macherey-Nagel silica gel plates with 0.20 mm thick (DC-Fertigfolien ALUGRAM 60F254) and visualization was carried out under ultraviolet light (λ_{max} 254 and 365 nm) in a CN-15LC light chamber (Vilber Lourmat).

^{1}H and ^{13}C nuclear magnetic resonance (NMR) spectra were recorded on a Bruker Advance III at 400 MHz and 100.6 MHz, respectively, using the solvent peak as internal reference. The assignment of ^{1}H and ^{13}C signals was performed using two-dimensional heteronuclear correlation techniques (HMBC and HMQC) and distortionless enhancement by polarization transfer (DEPT). Deuterated solvents used in NMR spectroscopy were $CDCl_3$ with 99.8% degree of deuteration, containing 0.03% v/v of tetramethylsilane or deuterated acetonitrile (ACN-d_3) with 99.8% degree of deuteration tetramethylsilane from Aldrich.

Ultraviolet-visible (UV-vis) absorption spectra were obtained on a UV/2501PC spectrophotometer (Shimadzu) and fluorescence spectra were obtained on a FluoroMax-4 spectrofluorimeter (Horiba).

Low resolution mass spectra were obtained using a LC-MS LXQ Thermo equipment, *via* direct injection of an ACN/water (1:1) solution with 0,05% acetic acid with electrospray ionization method (ESI).

Infrared (IR) spectra were obtained on an ABB FTLA2000 instrument in KBr discs.

The ion salts used were in the form of tetrabutylammonium salts for anions and perchlorate for cations, except for Cu(I), Pd(II) and Li(II), in the form of tetrafluoroborate and Sn(II) in the form of chloride.

SpecAI by Tellspec software was used to develop the multivariate models for ions quantification and Microsoft Office Excel for the development of univariate models.

2.2. Synthesis of BODIPY derivatives

2.2.1. Synthesis of *meso*-triphenylamine BODIPY derivative **1**
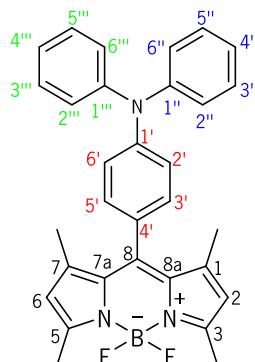
2,4-Dimethylpyrrole (69.6 mg, 0.731 mmol) and 4-(diphenylamino)benzaldehyde (100 mg, 0.366 mmol) were dissolved in anhydrous DCM (35mL). Two drops of TFA were added and the reaction mixture was stirred at room temperature for 50 minutes under N_2. A solution of DDQ (2,3-dichloro-5,6-dicyano-1,4-benzoquinone, 166.1 mg, 0.731 mmol) dissolved in dry DCM (35 mL) was added to the mixture, continuing the stirring for 50 minutes. Then Et_3N (0.88 mL, 6.29 mmol) was added and, after 15 minutes, $BF_3.OEt_2$ (1.31 mL, 10.6 mmol) was added and stirred for 30 minutes. The solvent was evaporated and the crude residue subjected to column chromatography (petroleum ether/DCM, 2:1) to obtain the pure product as a dark red solid (20.76 mg, 22%). The obtained sample was in agreement with a previously obtained compound, fully characterized by ^{1}H and ^{13}C NMR, IR spectroscopy and mass spectrometry, within the research group.

^{1}**H NMR** (400 MHz, CDCl₃): δ =1.60 (s, 6H, CH₃-1 e CH₃-7), 2.57 (s, 6H, CH₃-3 e CH₃-5), 6.02 (s, 2H, H-2 e H-6), 7.06-7.19 (m, 10H, 10 x Ar-H), 7.27-7.32 (m, 4H, 4 x Ar-H) ppm.

2.2.2. Synthesis of diformylated BODIPY derivative **2**
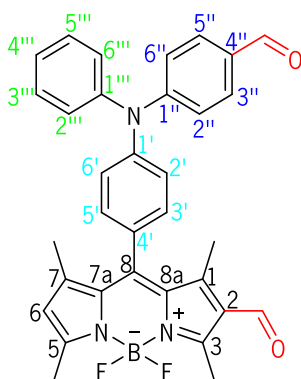
A mixture of $POCl_3$ (4.33 mL; 46.3 mmol) and dry DMF (4.44 mL; 60.3 mmol) was stirred in an ice bath for 5 minutes under N_2. The mixture was allowed to reach room temperature and then stirred for 30 minutes. BODIPY **1** (153.6 mg, 0.312 mmol) dissolved in dry DCM (10 mL) was added to the reaction mixture. The mixture was heated to 50°C under N_2 and stirred for 2 hours. After cooling to room temperature, the reaction mixture was slowly added to a saturated solution of $NaHCO_3$ (100 mL) in an ice bath. After the addition was completed, the mixture obtained was removed from the ice bath and kept under stirring for another 30 minutes. Ethyl acetate (2 x 20 mL) was added to the mixture and the combined organic phases were washed with distilled water (2 x 40 mL). Subsequently, the organic phase was dried over anhydrous $MgSO_4$, filtered and evaporated. The crude residue was purified by column chromatography using DCM/methanol (99:1) as eluent, to afford the pure product as a dark red solid (60 mg, 27%).

^{1}H NMR (400 MHz, $CDCl_3$): δ =1.64 (s, 3H, CH_3-7), 1.86 (s, 3H, CH_3-1), 2.63 (s, 3H, CH_3-5), 2.82 (s, 3H, CH_3-3), 6.20 (s, 1H, CH-6), 7.10 (d, J=8.8 Hz, 2H, H-2'' and H-6''), 7.18 (dd, J=1.2 and 8.4 Hz, 2H, H-3''' and H-5'''), 7.23 (m, 3H, H-4''', H-2' and H-6'), 7.32 (d, J=8,8 Hz, 2H, H-3' and H-5'), 7.38 (m, 2H, H-2''' and H-6'''), 7.75 (d, J=8,8 Hz, 2H, H-3'' and H-5''), 9.86 (s, 1H, C4''-CHO), 10.04 (s, 1H, C2-CHO).

^{13}C NMR (100.6 MHz, $CDCl_3$): δ =11.81 (CH_3-1), 12.87 (CH_3-3), 15.05 (CH_3-5 and CH_3-7), 120.81 (C2'' and C6''), 124.17 (C6), 125.62 (C4'''), 125.71 (C3' and C5'), 126.34 (C2, C3''' and C5'''), 129.19 (C2' and C6'), 129.61 (C4'), 129.88 (C1), 130.03 (C2''' and C6'''), 130.17 (C4''), 131.37 (C3'' and C5''), 134.19 (C7), 142.41 (C8a), 142.98 (C8), 145.87 (C1'''), 146.85 (C7a), 147.66 (C1'), 152.56 (C1''), 156.61 (C3), 161.82 (C5), 185.88 (C2-CHO), 190.38 (C4''-CHO).

IR (KBr): ν= 2920, 2850, 1664, 1654, 1589, 1508, 1384, 112, 1094, 823 cm^{-1}.

MS (ESI) m/z (%): 548.45 ($[M]^+$+1, 100), 405.38 (22), 324.41 (26), 296.37 (32), 268.33 (50), 240.32 (28).

2.2.3. Synthesis of nitrovinyl BODIPY derivative 3
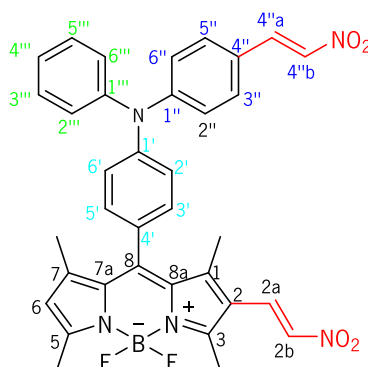
A mixture of ammonium acetate (56.3 mg 0.073 mmol) and nitromethane (1.0 mL; 18.68 mmol) was added to compound **2** (20,0 mg 0.037 mmol). The mixture was stirred and heated at 90°C for 14 h. Product formation was monitored with thin layer chromatography (TLC) using DCM as eluent. When the reaction was completed, distilled water (40 mL) was added and the mixture was extracted with DCM (3x15 mL). The organic layer was dried with anhydrous $MgSO_4$ and filtered. The solvent was evaporated and the crude was subjected to a dry flash chromatography using petroleum ether/DCM (9:1) as eluent, to afford the pure product as a dark red solid (14 mg, 63%).

¹H NMR (400 MHz, CDCl₃): δ =1.64 (s, 3H, CH₃-7), 1.69 (s, 3H, CH₃-1), 2.63 (s, 3H, CH₃-5), 2.72 (s, 3H, CH₃-3), 6.21 (s, 1H, H-6), 7.09 (d, J=8.4 Hz, 2H, H-2'' and H-6''), 7.17 (d, J=8.8 Hz, 2H, H-2''' and H-6'''), 7.21-7.27 (m, 3H, H-4''', H-3''' and H-5'''), 7.31 (dd, J= 2.8 and 8.4, 2H, H-2' and H-6'), 7.34 (d, J=14 Hz, 1H, H-2b), 7.39(d, J=5.2 Hz, 2H, H-3' and H-5'), 7.46 (d, J=8.4 Hz, 2H, H-3'' and H-5''), 7.53 (d, J=13.6, 1H, H-4''b), 7.97(d, J=13.2 Hz, 1H, H-4''a), 8.06(d, J=13.6, 1H, H-2a).

¹³C NMR (100.6 MHz, CDCl₃): 13.04 (CH3-1),14.09 (CH3-3), 15.12 (CH3-5 and CH3-7), 122.01 (C-2'' and C-6''), 123.47 (C-4''), 124.14 (C-6), 125.23 (C-2' and C-6'), 125.60 (C-4'''), 126.21 (C-2''' and C-6'''), 126.27 (C-1'), 129.22 (C-4'), 129.31 (C-3''' and C-5'''), 130.07 (C-3' and C-5'), 130.72 (C-2a), 130.76 (C-8a, C-3'' and C-5''), 133.80 (C-7), 134.72 (C-2b), 135.14 (C-4''b), 138.58 (C4''a), 139.98 (C-1), 145.88 (C-8), 146.42 (C-7a), 147.78 (C-1'''), 150.72 (C-1''), 154.29 (C-3), 161.58 (C-5).

IR (KBr): ν= 2923, 2852, 1589, 1552, 1508, 1465, 1321, 1178, 968, 819 cm⁻¹.

MS (ESI) m/z (%): 666.47([M]⁺+H₂O, 100), 634.49 ([M]⁺+1, 72), 607.44 (66), 393.39 (69), 284.40 (64), 219.16 (70).

2.3. Photophysical characterization of BODIPY derivatives **1-3** and dicyanovinyl derivatives **4-5**

The photophysical studies of compounds **1-3** were done using ACN solutions with concentrations between 1×10^{-6} M and 1×10^{-5} M. UV-Visible absorption spectra of the dilute solutions were obtained in the 200-800 nm range. Rhodamine 6G ($\Phi_F = 0.95$) was used as fluorescence standard in ethanol solution with a concentration of 1×10^{-5} M.

Dicyanovinyl compounds **4** and **5** were studied using both ACN and DCM solutions with concentrations between 1×10^{-6} and 1×10^{-5} M. UV-Visible absorption spectra of the dilute solutions were obtained in the 200-800 nm range. As fluorescence standards, 9,10-diphenylanthracene (DPA, $\Phi_F = 0.95$) was used in ethanol solution with a concentration of 1×10^{-5} M for compound **4** and quinine sulfate ($\Phi_F = 0.546$) in H_2SO_4 0.05 M for compound **5**.

BODIPY's **1-3** solutions were excited at 470 nm (the same for rhodamine 6G) and dicyanovinyl derivatives solutions were excited at 373 nm for derivative **4** (the same for DPA) and 421 nm for derivative **5** (the same for quinine sulfate) in quartz cells and the area under the fluorescence curve was determined.

The calculation of the relative quantum fluorescence yield of the prepared BODIPY and dicyanovinyl derivatives was performed using **equation 1**:

$$\frac{\phi_{comp}}{\phi_{stand}} = \frac{A_{stand}\times F_{comp}\times n^2_{stand}}{A_{comp}\times F_{stand}\times n^2_{comp}}$$

Equation 1

where A_{stand} and A_{comp} are the absorbances of the solutions at the excitation wavelengths of the standard and the compound under study, respectively; F_{stand} and F_{comp} are the areas under the fluorescence curve of the standard and the compound; n_{stand} and n_{comp} represent the refractive index value of the solvent for the standard and the compound under analysis, respectively.

2.3.1. Evaluation of BODIPY **1-3** derivatives and dicyanovinyl derivatives **4-5** as optical chemosensors of ions, amines and alcohols

The preliminary studies of the sensing capacity of compounds **1-5** allowed the quick and simple verification of the possible interaction of compounds **1-5** with metallic cations and anions, chosen due to their medical, biological and environmental importance, and various amines and alcohols, acting as models of drug.

For the ions sensing studies, solutions of compounds **1-5** were prepared in ACN (1×10^{-5} M) and ACN/H_2O (8:2, 8×10^{-6} M). Solutions of cations (Ag^+, K^+, Li^+, Na^+, Cu^+, TBT^+, Hg^{2+}, Ca^{2+}, Co^{2+}, Pb^{2+}, Mn^{2+}, Fe^{2+}, Zn^{2+}, Ni^{2+}, Cd^{2+}, Cu^{2+}, Pd^{2+}, Cs^{2+}, Sn^{2+}, Fe^{3+} and Al^{3+}) and anions ($H_2PO_4^-$, AcO^-, NO_3^-, ClO_4^-, HSO_4^-, BzO^-, Br^-, CN^-

, I⁻, and F⁻) were prepared in ACN (1×10^{-2} M). The solutions in ACN/H_2O (8:2) were prepared by adding 1.6 mL of solution in ACN (1×10^{-5} M) and 0.40 mL of distilled water directly to the vial.

For the model amines and alcohols sensing studies, solutions of BODIPY **2** were prepared in ACN (1×10^{-5} M) and ACN/phosphate buffer or ACN/phosphate-buffered saline (PBS, 3:1, 7.5×10^{-5} M) and solutions of dicyanovinyl derivative **4** were prepared in ACN and DCM (both 7.5×10^{-5} M) and ACN/phosphate buffer or ACN/PBS, (3:1, 7.5×10^{-5} M).

Buffer solutions were prepared in distilled water to maintain H^+ concentration in the range of urine pH, for tests with the amines and alcohols.

Phosphate buffer was prepared aiming pH 6.5 and 7 while PBS buffer was prepared at pH 7.4. The pH of all the buffers was adjusted using NaOH or HCl 6M. In **table 3** the concentrations of each salt in the buffers is presented.

Table 3- Preparation of buffer solutions.

Buffer	pH	Salts	Concentration (M)
Phosphate	6,5	Na_2HPO_4	2.65×10^{-2}
		NaH_2PO_4	7.35×10^{-2}
Phosphate	7.0	Na_2HPO_4	6.10×10^{-2}
		NaH_2PO_4	3.90×10^{-2}
PBS	7.4	NaCl	1.37×10^{-4}
		KCl	2.70×10^{-6}
		Na_2HPO_4	4.30×10^{-6}
		KH_2PO_4	1.47×10^{-6}

The solutions of ACN and aqueous buffer (3:1) were prepared by adding 1.5 mL of compounds' solution (1×10^{-5} M) and 0.5 mL of aqueous buffer.

Solutions of model amines (aniline (AN), triethylamine (TEA), diethylamine (DEA), dicyclohexylamine (DCHA) and hexylamine (HA)) and model alcohols (4-methoxyphenol (4MP), 2-butanol (2B), 1-pentanol (1P) and methanol) were prepared in ACN at a concentration of 1×10^{-2} M. Solutions of U and CRT were prepared in ACN at a concentration of 1×10^{-2} M.

2.3.2. Spectrophotometric and spectrofluorimetric titrations of BODIPY derivatives **1, 3** and dicyanovinyl derivative **5**

Spectrophotometric and spectrofluorimetric titrations were performed for the various compounds that showed colorimetric and/or fluorimetric responses in the preliminary sensing study. Solutions of compounds **1, 3** and **5** in ACN with concentration 1×10^{-5} M or ACN/H_2O (8:2) with concentration 8×10^{-5} M and ion solutions (Cu^{2+}, Fe^{3+}, F^- and CN^-) in ACN at concentration 1×10^{-2} M. A certain number of equivalents (eq) of each of the ions were successively added to the compound solutions and the absorption and/or fluorescence spectra were plotted after each addition.

2.3.3. ^{1}H-NMR titrations of dicyanovinyl derivative **5** with cyanide ion

A solution of compound **5** in ACN-d_3 with concentration of 3.8×10^{-5} M and cyanide ion with concentration of 2.65 M in ACN-d_3 were prepared. One equivalent of cyanide ion was successively added to the compound solution and the respective ^{1}H NMR spectrum was plotted after each addition.

2.4. Data mining methodologies

Spectral data were exported from Microsoft excel into SpecAI by Tellespec for pre-treatment and development of multivariate calibration models (**scheme 7**). Each sample from each titration was analyzed once without replicates.
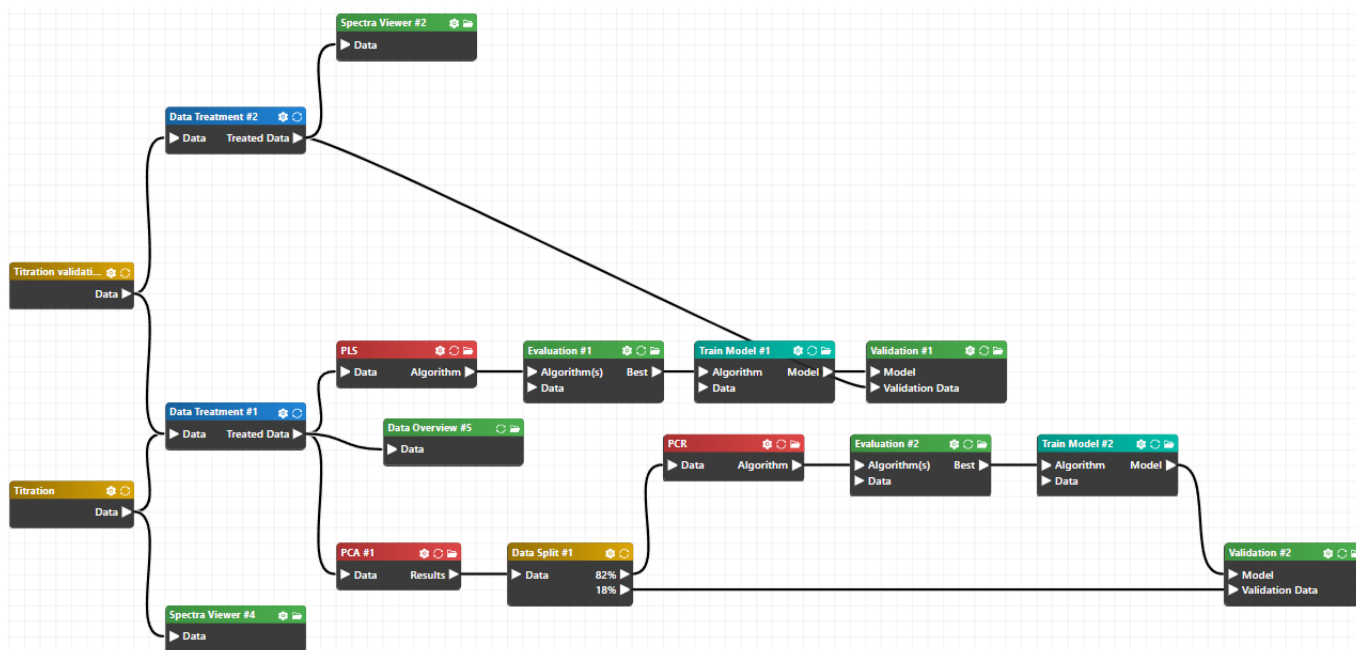
Scheme 7- Data mining workbench showing the different steps of data treatment and modeling.

Calibration models for measurement of ions in ACN and ACN/H_2O (8:2) solutions were performed

using PCR and PLS. Calibration models were developed using two samples of known concentration of ions for validation (one in beginning of the working range and other near the end) and the same concentration of compound used in the titration.

Spectral data were pre-treated before PCR and PLS modeling. The pretreatment was second derived Savitzky–Golay (2nd derived) with the purpose of smoothing the data, increasing the precision of the data without distorting the signal tendency.

Besides these two algorithms, linear regression is also applied to the same experimental data sets, choosing the maximum absorption and/ or emission wavelengths (univariate approach) for the study without previous data treatment. These models are developed in Microsoft office excel.

25 models were evaluated for the different ions using r^2 and root mean square error (RMSE).

R^2 is parameter commonly used to express the variation between variables, that way is possible to see the adjustment of these to the developed model (**equation 2**):

$$r^2 = 1 - \frac{\sum_{i=1}^{N}(\hat{y}_i - y_i)^2}{\sum_{i=1}^{N}(y_i - \bar{y}_i)^2}$$
Equation 2

where N is the sample size, y_i are the obtained data, $\hat{y}_i$ are the predicted results and $\bar{y}_i$ is the average value of the obtained data.

RMSE another parameter, usually used in machine learning to evaluate the quality of the predictions, in other words, this parameter measures the difference between the experimental data and the predictions (**equation 3**). This parameter is also used in the validation of the models.

$$RMSE = \sqrt{\frac{1}{N}\sum_{i=1}^{N}(y_i - \hat{y}_i)^2}$$
Equation 3

Where N is the sample size, y_i are the obtained data and $\hat{y}_i$ are the predicted results.

Chapter 3

Results and Discussion

3. Results and Discussion

3.1. Synthesis of BODIPY derivatives

In order to evaluate the effect of the functionalization of the BODIPY core on the photophysical properties and sensing capacity of these derivatives, it was decided to synthesize functionalized BODIPYs **1-3** with an aromatic electron donor group at the *meso* position and different electron withdrawing groups at positions 2 of the core and 4'' of the *meso*-substituent, to increase the conjugation of the π-system.

3.1.1. Synthesis of BOSIPY derivative **1**

The synthesis of the *meso*-functionalized BODIPY is usually carried out in two steps. In the first step a pyrrole derivative reacts with an aromatic aldehyde in presence of a catalytic amount of acid forming the dipyrromethane core. The second reactional step involves oxidizing dipyrromethane to dipyrromethene using DDQ. The intermediate is not isolated and immediately subjected to complexation with $BF_3.OEt_2$ in the presence of base[129].

The synthesis of BODIPY **1** was accomplished by reaction of 2,4-dimethylpyrrole and 4-(diphenylamino)benzaldehyde in presence of TFA, followed by oxidation with DDQ and cyclization with $BF_3.OEt_2$ in presence of Et_3N (**scheme 8**). The pure compound was isolated after dry-flash chromatography (petroleum ether/DCM, 2:1) as an orange solid. The overall yield was 22%, and the structure as well as the purity of the synthesized BODIPY was confirmed by ^{1}H NMR.
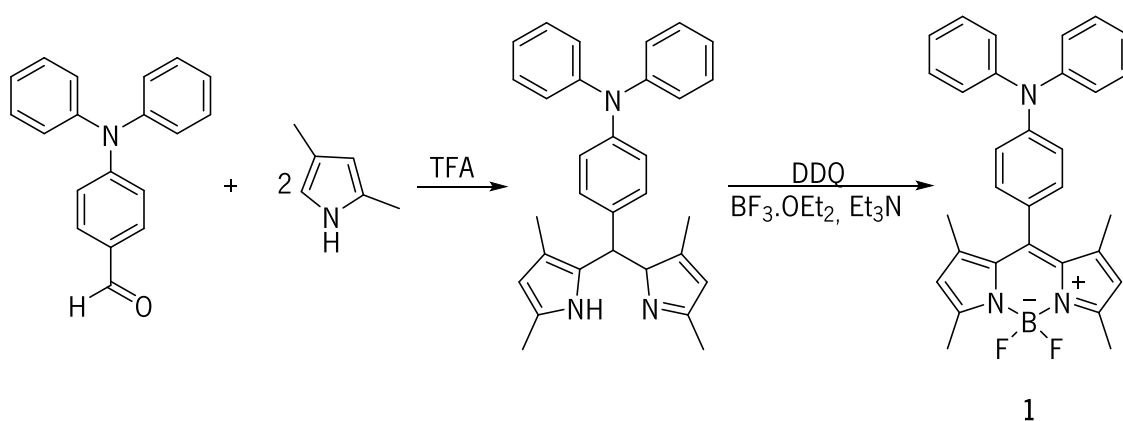
Scheme 8- Synthesis of BODIPY **1** accomplished in two steps.

In the ^{1}H NMR spectrum, the characteristic signs of the BODIPY core were visible, as well as a complex aromatic zone caused by the various aromatic rings of the *meso*-substituent. The signal corresponding to protons H2 and H6 appeared at a chemical shift of 6.02 ppm. The signal from the protons of the methyl groups at positions 1 and 7 appeared with a chemical shift of 1.60 ppm, while the

methyl groups at positions 3 and 5 appeared at 2.68 ppm.

3.1.2. Synthesis of BODIPY **2** through Vilsmeier-Haack reaction

Vilsmeier-Haack formylation consists of the reaction between electron-rich aromatic rings and the formylating agent (Vilsmeier's reagent) which acts as an electrophile. The electrophile is obtained through reaction between a substituted formamide and phosphorus oxychloride ($POCl_3$). As soon as the Vilsmeier reagent is formed, it will react with the aromatic compound through an electrophilic aromatic substitution, followed by hydrolysis in the presence of water, resulting in the final product functionalized with the aldehyde group[130].

In **scheme 9** it can be seen the functionalization of BODIPY **1**, carried out under the experimental conditions described above using DMF as formamide. The pure compound, formylated at positions 2 and 4'', was isolated after column chromatography (DCM/methanol, 99:1) as a dark red solid. The overall yield was 27%, and the structure as well as the purity of the synthesized BODIPY was confirmed by ^{1}H and ^{13}C NMR spectroscopy, IR spectroscopy and mass spectrometry.
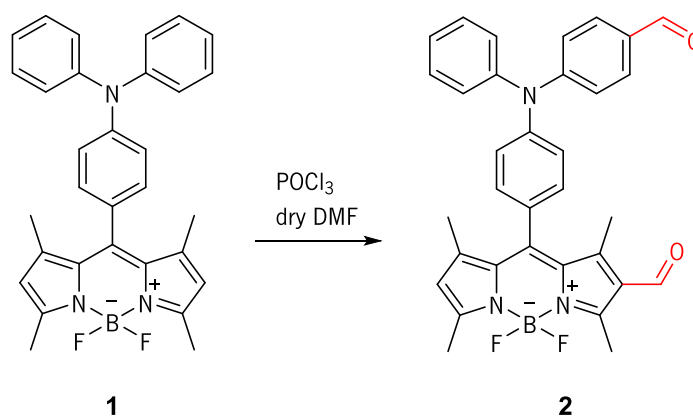
Scheme 9- Synthesis of BODIPY **2** by Vilsmeier-Haack formylation of BODIPY **1**.

Using unidimensional and bidimensional NMR techniques, it was possible to assign all the protons and related carbons. The signal corresponding to proton H6 appeared at 6.20 ppm and the respective carbon at 124.17 ppm. The signals corresponding to the aldehyde protons appeared at 9.86 and 10.04 ppm, respectively for C4''-C*H*O and C2-C*H*O, and the respective carbon atoms were found at 185.88 and 190.38 ppm, respectively C2 and C4''.

IR spectroscopy confirmed the functional groups present in BODIPY **2**, namely the N-C vibration at 1094 cm^{-1} found, the B-F vibration at 1508 cm^{-1} [134] and the C=O at 1664 and 1654 cm^{-1}.

The low-resolution mass spectrometry (LRMS) results via electrospray ionization showed a peak

at m/z 548 corresponding to the molecular ion (M⁺+1) as base peak.

3.1.3. Synthesis of BODIPY **3** through Henry reaction

The incorporation of a nitroalkene unit into a BODIPY transforms it into a strong Michael acceptor, which would be highly susceptible to suffer nucleophilic attack of certain analytes to the β-position of nitroalkane causing significant changes in color and fluorescence, resulting in a chemodosimeter approach.

In order to introduce a nitro vinyl group on BODIPY **2**, a Henry reaction was performed involving the electrophilic carbon of the aldehyde group and a nucleophile generated from nitromethane under basic conditions with ammonium acetate at 90 °C for 4 hours (**scheme 10**)[132]. The pure compound was isolated after dry-flash chromatography (petroleum ether/DCM, 9:1) as a dark red solid in 63% yield and fully characterized by uni- and bidimensional ¹H and ¹³C NMR spectroscopies, IR spectroscopy and low-resolution mass spectrometry.
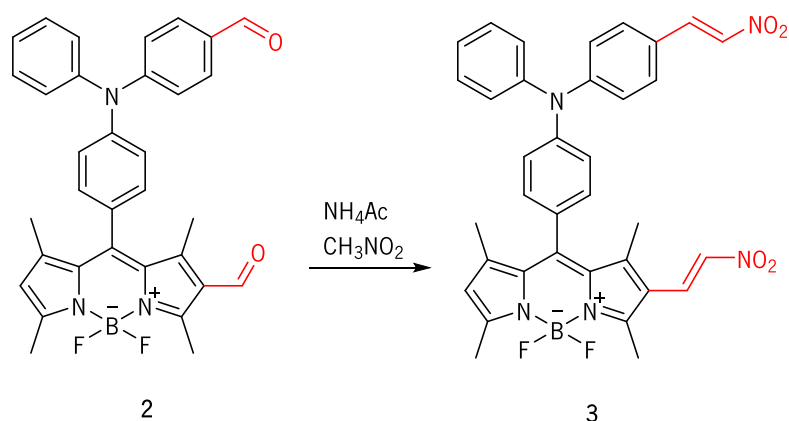
Scheme 10- Synthesis of nitrovinyl-BODIPY **3**.

In the ¹H NMR spectrum, the characteristic signal corresponding to H-6 appeared at 6.21 ppm. The signals relative to the vinyl protons were clearly visible: doublets for H-2a at 8.06 ppm (J= 13.6Hz) and H-2b at 7.34 ppm (J= 14Hz), thus indicating a *trans* configuration; also, as doublets in *trans* configuration, H-4a at 7.97 ppm (J= 13.2Hz) and H-4b at 7.53 ppm (J= 13.6 Hz).

IR spectroscopy confirmed the structure of BODIPY **3**. At 968 cm⁻¹ is found the C-H *trans* vibration, at 1175 is present the N-C vibration, at 1508 and 1552 cm⁻¹ are present the B-F vibrations[134], at 1321 and 1465 cm⁻¹ are the NO₂ group vibrations, at 1589 cm⁻¹ is the C=C vibration. In the LRMS results, it was seen a peak at 634 corresponding to the molecular ion (M⁺+1) with a 72% relative intensity.

3.2. Dicyanovinyl derivatives (**4** and **5**)

The synthesis of benzoindole and 2-(4-methoxyphenyl)thiophene dicyanovinyl derivatives, **4** and **5** respectively (**figure 16**) was achieved through a previously published procedure involving a Knoevenagel reaction of the corresponding aldehyde precursor and malononitrile, catalysed by piperidine in refluxing ethanol[133].

For the present work, both compounds were synthesized within the research group and were available for use and their purity was checked by ^{1}H NMR.
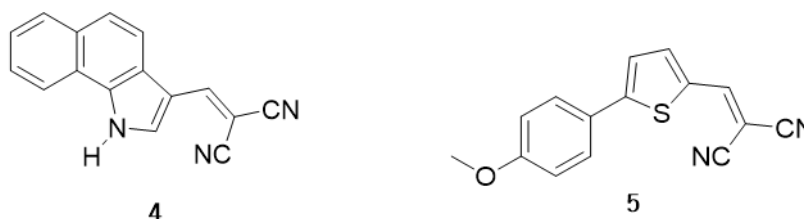
Figure 15- Dicyanovinyl derivatives **4** and **5**.

3.3. Photophysical characterization of the heterocyclic probes

3.3.1. BODIPY derivatives **1-3**

BODIPY derivatives synthesis with different groups at positions 2 and *meso* of the core was intended to diversify photophysical properties and optimize the recognition capability of these compounds and their application as optical probes. The characterization by UV-Vis absorption and fluorescence spectroscopies were carried out to evaluate the influence of the conjugated π-system and the electronic character of the substituents on their absorption/emission properties.

Photophysical studies of BODIPYs **1-3** were performed in acetonitrile solutions with concentrations of 1×10^{-6} to 1×10^{-5} M. The fluorescence spectra were obtained by exciting at 470 nm in order to visualize the entire fluorescence curve, due to the small Stokes' shift usually displayed by BODIPY derivatives. The data was compiled in **Table 4**. The fluorescence standard used to calculate the relative quantum yield of fluorescence was Rhodamine 6G in ethanol ($\Phi_F = 0.95$) with a concentration of 1×10^{-5} M.
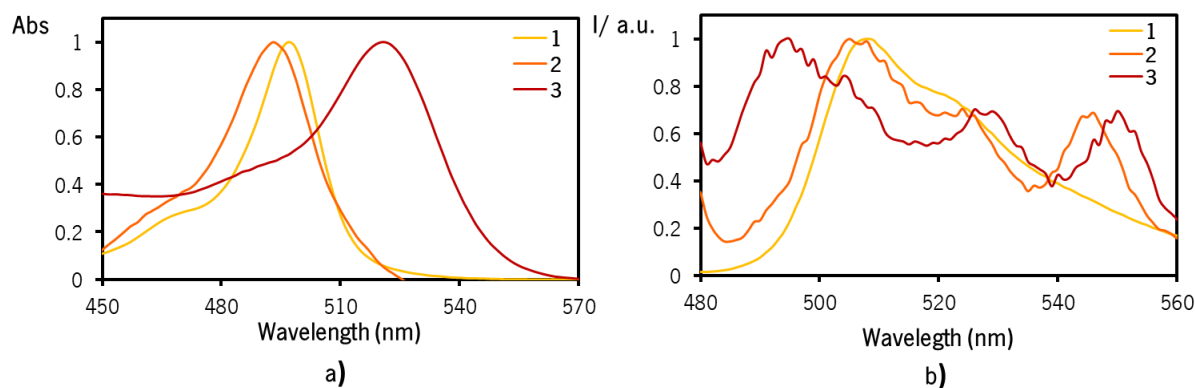
Figure 16- Normalized absorption (**a**) and fluorescence (**b**) spectra of BODIPYs **1** - **3** in ACN.

The compounds exhibited intense absorption bands (log ε =4.764, 4.004 and 4.362) in the spectral region comprised between 480-540 nm (**Figure 16a**). The maximum wavelength of absorption of the synthesized BODIPY derivatives suffers a shift according to the structure and electronic character of the functional group present in positions 2 and 4'' of the triphenylamine *meso*-substituent.

Considering derivative **1** as the reference compound, after introduction of the formyl groups (derivative **2**) there was a small hypsochromic shift of absorption from 497 nm to 493 nm that can be attributed to the electronic withdrawing effect of the functional group, which stabilizes HOMO inducing a greater energetic separation between LUMO and HOMO. On the other hand, compound **3** functionalized with a nitro vinyl group demonstrated an opposite behavior. In this case, there was a bathochromic shift of the absorption band to 546 nm, compared to the BODIPY **1**, due to the withdrawing effect of the functional group and increasing extension of the conjugated π-system. This derivative can establish an ICT complex between the nitro vinyl group and the BODIPY core, which can be interrupted and replaced by the PET mechanism through the possibility of nucleophilic addition reactions between the vinyl nitro group[33].

The emission spectra of the compounds demonstrated that the introduction of functional groups did not significantly influence the maximum emission wavelengths, having only occurred slight hipsochromic shifts of 3 and 5 nm for compound **2** and **3**, respectively, compared to the derivative without substituent (**Figure 16b**). Relative quantum fluorescence yields calculated for BODIPYs **1**, **2** and **3** were 0.003, 0.011 and 0.005 respectively.

Table 4- UV-vis absorption and fluorescence spectroscopy data of BODIPY 1-3 in ACN.

Compound	UV-vis			Fluorescence		
	λ_{abs} (nm)	log ε	λ_{exc} (nm)	λ_{emi} (nm)	Φ_F	Stokes' shift (nm)
1	497	4.764		508	0.003	11
2	493	4.004	470	546	0.011	53
3	521	4.362		550	0.005	29

3.3.2. Dicyanovinyl derivatives 4 and 5

Compounds 4 and 5 are based on benzoindole and 2-(4-methoxyphenyl)thiophene and modified with a dicyanovinyl group. The presence of this electron withdrawing group and different scaffolds intended to confer diverse photophysical properties and optimized recognition as optical probes in the respective applications. The characterization by UV-vis absorption and fluorescence spectroscopy was carried out to evaluate the influence of the different π-system and the electronic character of the scaffolds on their absorption/emission properties.

Benzoindole is a group known for the ability to donate electrons. The planar structure and the extended π conjugated system allow the establishment of ICT mechanism and highly absorbing spectra, revealing promising and adjustable photophysical properties as chemosensor[134,135]. The use of five-membered heterocyclic rings, such as thiophene, allows the establishment of an electron donor-acceptor relationship with chromophores by increasing π-conjugated systems. In addition to providing thermal and chemical stability, this type of compounds also improves delocalization of electrons and improved optical properties[133,136].

Photophysical studies of compounds 4 and 5 were performed in ACN solution with concentrations of 1×10^{-6} to 1×10^{-5} M. The fluorescence spectra were obtained by excitation at the maximum wavelength of absorption for each compound. The fluorescence standard used to calculate the quantum yield of fluorescence was DPA in ethanol (Φ_F = 0.95) and quinine sulphate (Φ_F = 0.546) in 0.05 M H_2SO_4 with concentrations of 1×10^{-5} M.
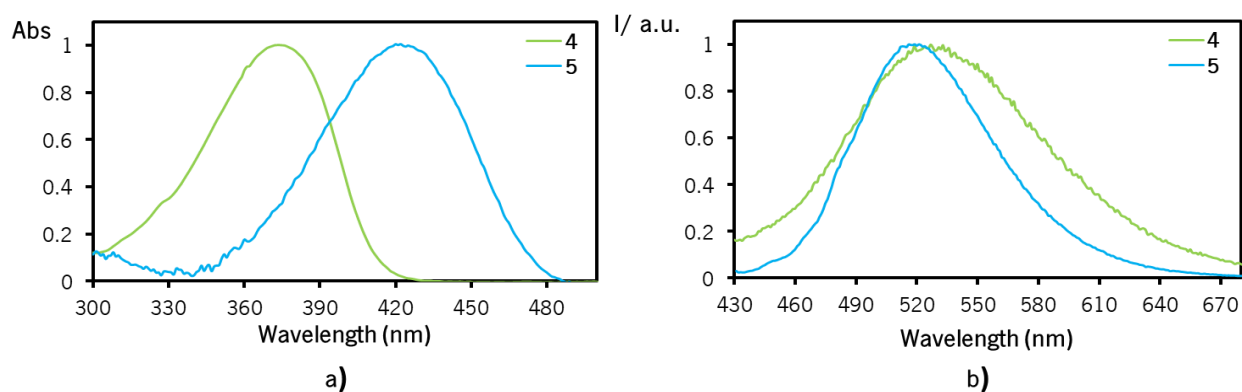
Figure 17- Normalized absorption (**a**) and fluorescence (**b**) spectra of dicyanovinyl derivatives **4** and **5** in ACN.

The compounds exhibited intense absorption bands (log ε =4.599 and 4.494) in the spectral region comprised between 300-480 nm (**Figure 17a**). As seen in the spectra, the maximum absorption wavelength of these derivatives has differences according to the structure and electronic character of the scaffolds conjugated with the dicyanovinyl group. Probe **5** has a maximum absorption peak at higher wavelength than compound **4**. The methoxyphenyl and thiophene groups are both electron rich aromatics and, in conjugation with the dicyanovinyl group, the push-pull effect is more evident causing the absorption to occur at higher wavelength for compound **5**. The fluorescence spectra (**figure 17b**) were obtained by exciting the samples at the maximum absorption wavelength, and both derivatives show low relative quantum fluorescence yields (**table 5**).

Table 5- UV-Vis absorption and fluorescence spectroscopy data of dicyanovinyl derivatives **4** and **5** in ACN.

Compound	UV-Vis		Fluorescence		
	λ_{abs} (nm)	log ε	λ_{emi} (nm)	Φ_F	Stokes' shift (nm)
4	373	4.599	527	0.001	154
5	421	4.203	519	0.012	98

3.4. Preliminary sensing assays for ions

A preliminary study of the interaction of BODIPY **1-3** derivatives and dicyanovinyl derivatives **4** and **5** with various cations and anions was carried out in order to make a quick assessment of the sensing capacity and understand the influence of the substituent groups in the sensing capacity. The solutions were visualized in natural light for the colorimetric assay and under a UV lamp at 365 nm to detect fluorimetric changes.

Solutions of the compounds were prepared with a concentration of 1×10^{-5} M and solutions of the cations and anions, selected due to their biological and environmental relevance, were prepared at 1×10^{-2} M. The studies were made in acetonitrile as it is an aprotic solvent, so it does not have the ability to establish hydrogen bonds and interfere with the recognition system of these analytes. The studies were also made in ACN/H_2O (8:2) with concentration of 8×10^{-6} M.

3.4.1. Assays in ACN

After adding 50 eq of each ion to the BODIPY **1-3** solutions in ACN, it was seen that compound **3** exhibited colorimetric and fluorimetric changes in the presence of certain ions, whilst compound **1** did not give colorimetric changes in presence of anions and compound **2** did not show colorimetric changes in the presence of cations.

In ACN solution, compound **1** signalized ClO_4^- and F- with an enhancement of the fluorescence intensity, while a quenching o fluorescence occurred with CN- **(figure 18)**.

Figure 18- Fluorimetric changes of BODIPY **1** in presence of 50 equiv of anions in ACN.

Considering the interaction of compound **1** with the different cations, there was a change in color from yellow to orange in presence of Hg^{2+} and from yellow to blue in presence of Cu^{2+} and Fe^{3+} **(figure 19a)**. The fluorescence intensity clearly increased in presence of Ag^+, TBT^+, Ni^{2+}, Sn^{2+} and was quenched in presence of Cu^{2+} and Fe^{3+} **(figure 19b)**.
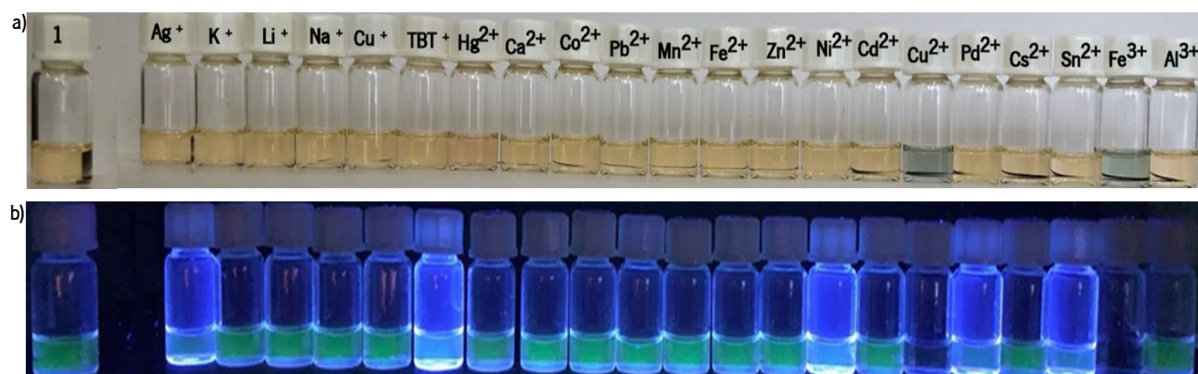
Figure 19- Colorimetric **(a)** and fluorimetric **(b)** changes of BODIPY **1** in presence of 50 equiv of cations in ACN.

BODIPY **2** showed a loss of color in the presence of CN⁻ and F⁻ (**figure 20 a**), and a fluorescence quenching in presence of F⁻ (**figure 20b**).

Figure 20- Colorimetric (**a**) and fluorimetric (**b**) changes of BODIPY **2** in presence of 50 equiv of anions in ACN.

For the interaction of compound **2** with the different cations, a very small quenching occurred in presence of Fe^{3+} and Al^{3+} (**figure 21**).

Figure 21- Fluorimetric changes of BODIPY **2** in presence of 50 equiv of cations in ACN.

BODIPY **3** showed a loss of color in the presence of CN⁻ and F⁻ (**figure 22a**), and fluorescence quenching in presence of ClO_4^-, HSO_4^-, CN⁻ and I⁻ (**figure 22b**).

Figure 22 -Colorimetric (**a**) and fluorimetric (**b**) changes of BODIPY **3** in presence of 50 equiv of anions in ACN.

As for the interaction of compound **3** with the different cations, there was a marked change in color from pink to yellow in presence of Cs^{2+} and a loss of color in presence of Al^{3+} (**figure 23a**). The

44

fluorescence intensity increased in presence of Ag^+, K^+, Li^+, Cu^+, Ca^{2+}, Zn^{2+}, Pd^{2+}, Sn^{2+}, Fe^{3+} and Al^{3+} (**figure 23b**).
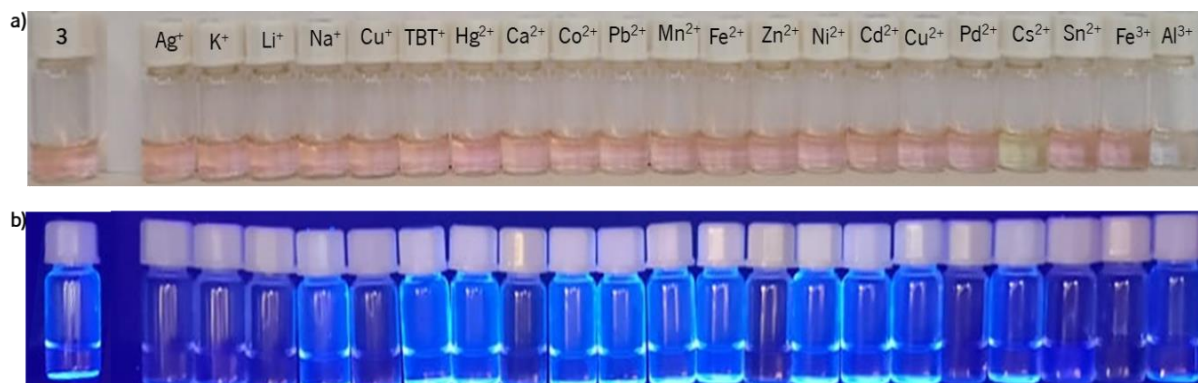
Figure 23- Colorimetric (**a**) and fluorimetric (**b**) changes of BODIPY **3** in presence of 50 equiv of cations in ACN.

For dicyanovinyl derivatives **4** and **5** in ACN solution, and after adding 50 equiv of each ion, it was seen that compound **4** and **5** exhibited colorimetric and fluorimetric changes only in the presence of anions, and fluorimetric changes in presence of cations.

In ACN solution, compound **4** developed a greenish yellow color in the presence of $H_2PO_4^-$, AcO^-, BzO^-, CN^- and F^- (**figure 24a**), and a fluorescence quenching in presence of HSO_4^-, BzO^-, Br^-, CN^- and I^- (**figure 24b**).
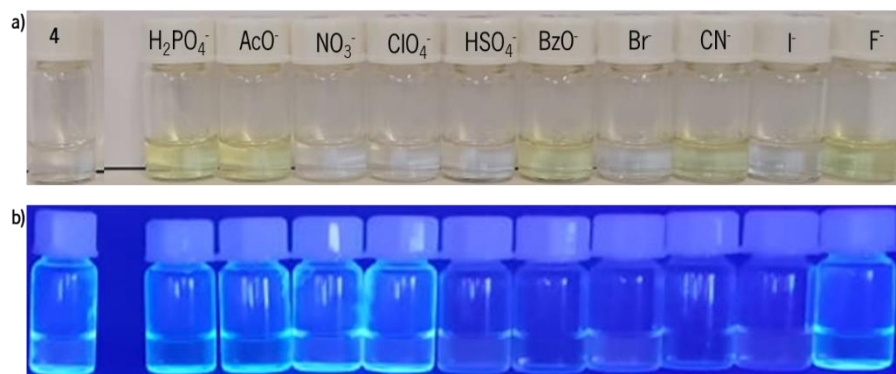
Figure 24 -Colorimetric (**a**) and fluorimetric (**b**) changes of compound **4** in presence of 50 equiv of anions in ACN.

The interaction of compound **4** with the different cations was seen by a fluorescence quenching in presence of Ag^+, K^+, Li^+, Na^+, Hg^{2+}, Ca^{2+}, Co^{2+}, Pb^{2+}, Cs^{2+} and Al^{3+} (**figure 25**).

Figure 25- Fluorimetric changes of BODIPY **4** in presence of 50 equiv of cations in ACN.

In ACN solution, compound **5** showed a loss of color in the presence of CN^- and F^- (**figure 26a**), and a enhancement in fluorescence intensity in presence of $H_2PO_4^-$, AcO^-, NO_3^-, BzO^-, I^- and F^- (**figure 26b**).
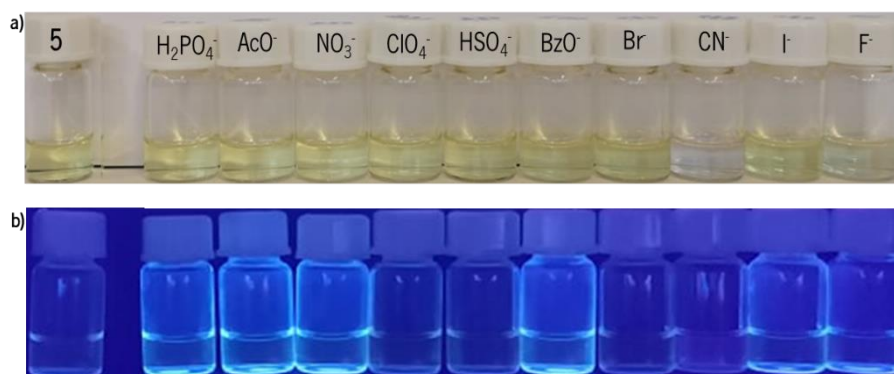
Figure 26 -Colorimetric (**a**) and fluorimetric (**b**) changes of compound **5** in presence of 50 equiv of anions in ACN.

As for cations, their interaction with compound **5** was visible through an enhancement in fluorescence intensity in presence of Ag^+, K^+, Na^+, Cu^+, TBT^+, Hg^{2+}, Co^{2+}, Pb^{2+}, Fe^{2+}, Zn^{2+}, Cu^{2+} and Pd^{2+} (**figure 27**).
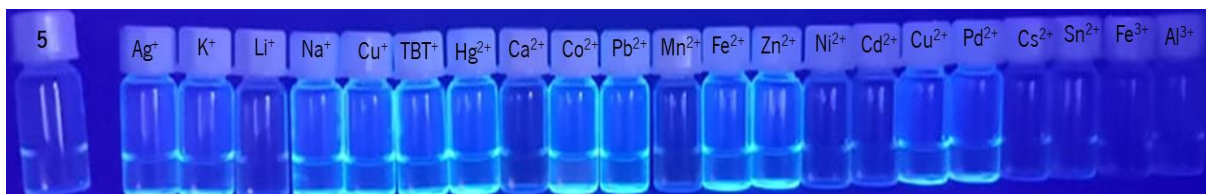
Figure 27- Fluorimetric changes of BODIPY **5** in presence of 50 equiv of cations in ACN.

In **table 6** is presented an overview of the colorimetric and fluorimetric changes for compounds **1-5** tested in ACN solution. Although there are some interesting results in terms of colorimetric and fluorimetric behavior, none of the compounds showed selectivity for only one ion.

Table 6- Colorimetric and fluorimetric changes for compounds 1-5 in ACN.

Compound	Colorimetric signal	Fluorimetric signal
1	Hg^{2+}, Cu^{2+} and Fe^{3+}	ClO_4^-, F^-, CN^-, Ag^+, TBT^+, Ni^{2+}, Sn^{2+} Cu^{2+} and Fe^{3+}
2	CN^- and F^-	F^-, Fe^{3+} and Al^{3+}
3	CN^-, F^-, Cs^{2+} and Al^3	ClO_4^-, HSO_4^-, CN^-, I^-, Ag^+, K^+, Li^+, Cu^+, Ca^{2+}, Zn^{2+}, Pd^{2+}, Sn^{2+}, Fe^{3+} and Al^{3+}
4	$H_2PO_4^-$, AcO^-, BzO^-, CN^- and F^-	HSO_4^-, BzO^-, Br^-, CN^-, I^-, Ag^+, K^+, Li^+, Na^+, Hg^{2+}, Ca^{2+}, Co^{2+}, Pb^{2+}, Cs^{2+} and Al^{3+}
5	$H_2PO_4^-$, CN^- and F^-	$H_2PO_4^-$, AcO^-, NO_3^-, I^-, F^-, Ag^+, K^+, Na^+, Cu^+, TBT^+, Hg^{2+}, Co^{2+}, Pb^{2+}, Fe^{2+}, Zn^{2+}, Cu^{2+} and Pd^{2+}

3.4.2. Assays in ACN/H$_2$O (8:2)

Assays were also conducted in aqueous mixture given the interest in sensing biological and environmentally relevant ions. After adding 50 eq of each ion to the BODIPY 1-3 in ACN/H$_2$O (8:2) solutions, it was found that compounds 1 and 3 exhibited colorimetric and fluorimetric changes in the presence of the anions and cations while compound 2 only showed a very faint colorimetric response with cations.

In ACN/H$_2$O (8:2) solution, compound 1 showed a loss of color in the presence of F$^-$ (**figure 28a**), an enhancement of fluorescence intensity in presence of ClO$_4^-$ and F- and a quenching in presence of CN$^-$ (**figure 28b**).
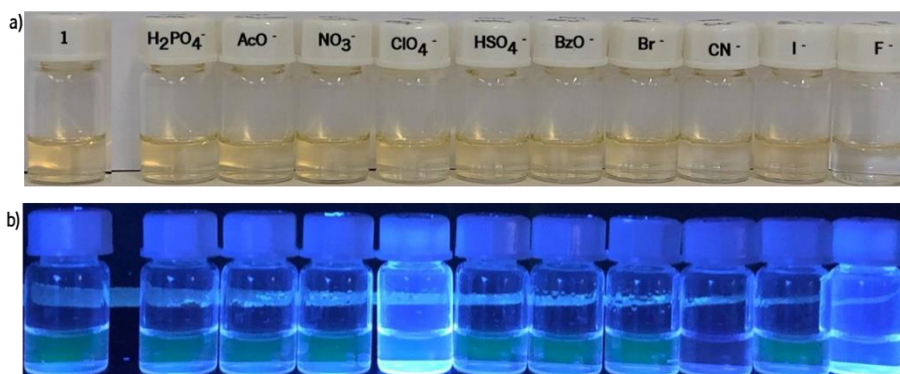
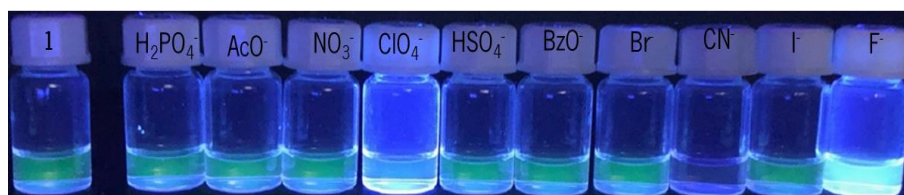Figure 28- Colorimetric (a) and fluorimetric (b) changes of BODIPY 1 in presence of 50 equiv of anions in ACN/H$_2$O (8:2).

The interaction of compound 1 with the different cations revealed a loss of color in presence of Cu^{2+} and a change of color from yellow to red in presence of Al^{3+} (**figure 29a**). The fluorescence intensity increased in presence of Ag^+, TBT^+, Ni^{2+}, Pd^{2+}, Sn^{2+} and diminished in presence of Cu^{2+} and Fe^{3+} (**figure**

29b).
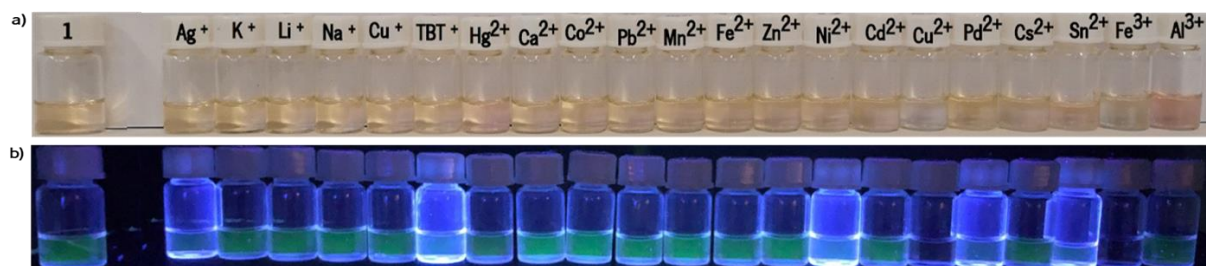
Figure 29-Colorimetric (**a**) and fluorimetric (**b**) changes of BODIPY **1** in presence of 50 equiv of cations in ACN/H$_2$O (8:2).

For compound **2** there was a loss of color in presence of CN$^-$ and F$^-$ (**figure 30a**), and a fluorescence quenching in presence of F$^-$ (**figure 30b**).
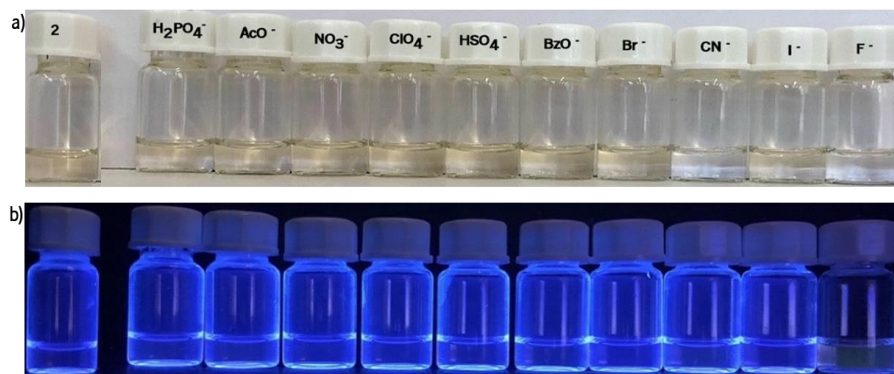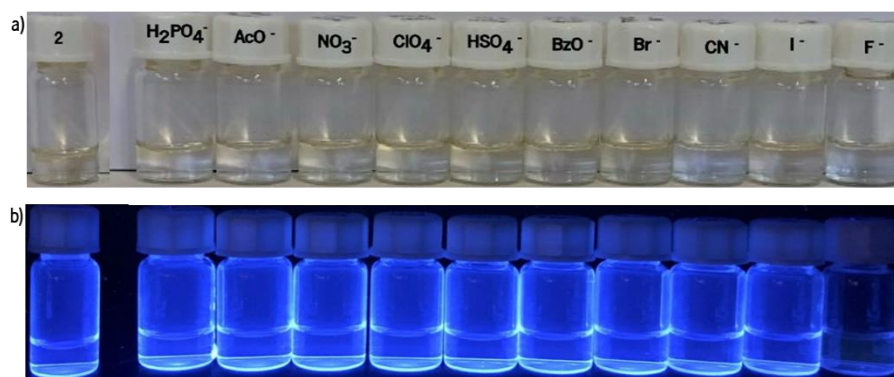

Figure 30- Colorimetric (**a**) and fluorimetric (**b**) changes of BODIPY **2** in presence of 50 equiv of anions in ACN/H$_2$O (8:2).

The interaction of compound **2** with the different cations revealed that in presence of Pd^{2+} and Fe^{3+} the solution developed a yellow color (**figure 31**).
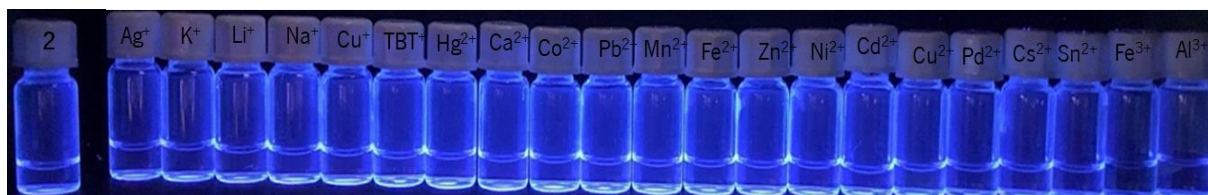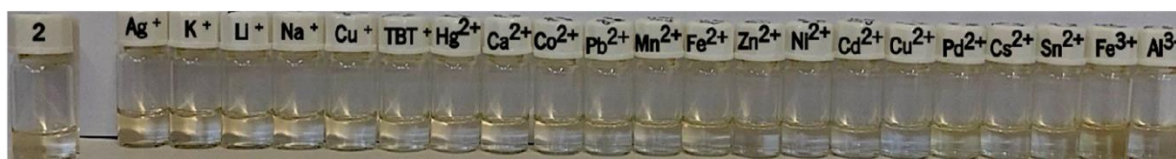

Figure 31- Colorimetric changes of BODIPY **2** in presence of 50 equiv of cations in ACN/H$_2$O (8:2).

Compound **3** showed a loss of color in the presence of CN$^-$, a change of color from red to light yellow in presence of I$^-$ (**figure 32a**), and a quenching in presence of F$^-$ (**figure 32b**).
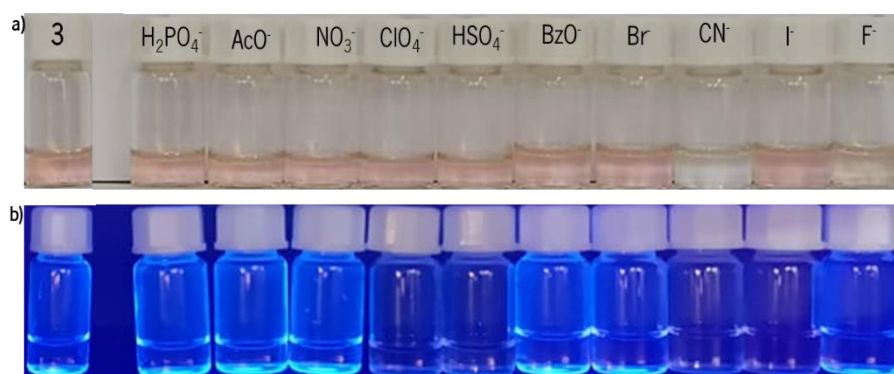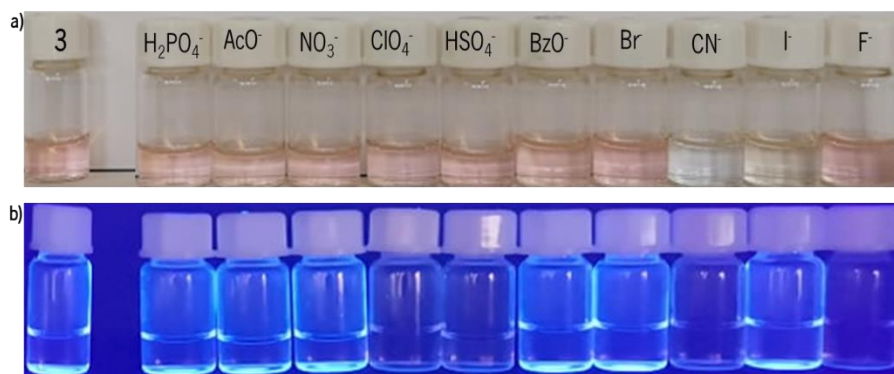
Figure 32- Colorimetric (**a**) and fluorimetric (**b**) changes of BODIPY **3** in presence of 50 equiv of anions in ACN/H$_2$O (8:2).

The interaction of compound **3** with the different cations revealed loss of color in presence of Cu^{2+} and a change of color from pink to orange in presence of Pd^{2+} (**figure 33a**). The fluorescence intensity of the solution was quenched in presence of Ag$^+$, K$^+$, Li$^+$, Cu$^+$, Ca^{2+}, Zn^{2+}, Pd^{2+}, Sn^{2+}, Fe^{3+} and Al^{3+} (**figure 33b**).
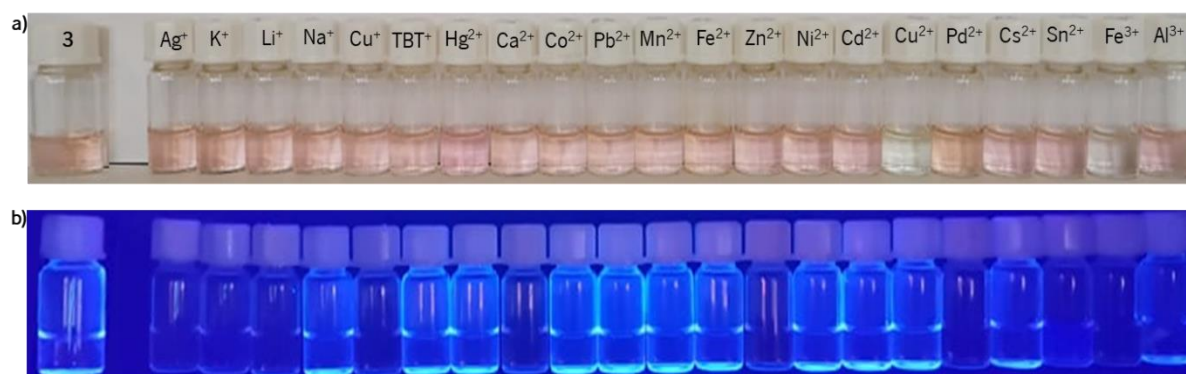
Figure 33- Colorimetric (**a**) and fluorimetric (**b**) changes of BODIPY **3** in presence of 50 equiv of cations in ACN/H$_2$O (8:2).

For dicyanovinyl derivatives **4** and **5** in ACN/H$_2$O (8:2) solutions, after addition of 50 equiv of each ion, it was seen that compound **4** exhibited fluorimetric changes in the presence of cations and anions, while compound **5** presented colorimetric and fluorimetric changes with anions, and only fluorimetric changes were observed with cations.

Compound **4** signalized HSO$_4^-$, BzO$^-$, Br$^-$, CN$^-$, I$^-$, and F$^-$ through fluorescence quenching (figure **34**).
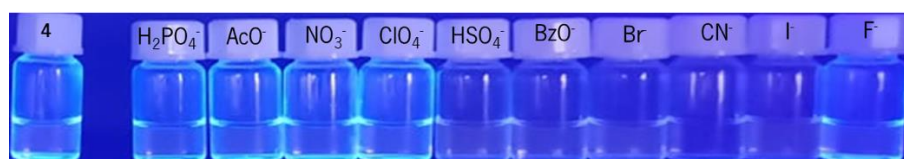
Figure 34- Fluorimetric changes of compound **4** in presence of 50 equiv of anions in ACN/H$_2$O (8:2).

Compound **4** showed a quenching of fluorescence in presence of Ag^+, K^+, Li^+, Na^+, Hg^{2+}, Ca^{2+}, Co^{2+}, Zn^{2+}, Pb^{2+}, Cs^{2+} and Al^{3+} (figure **35**).
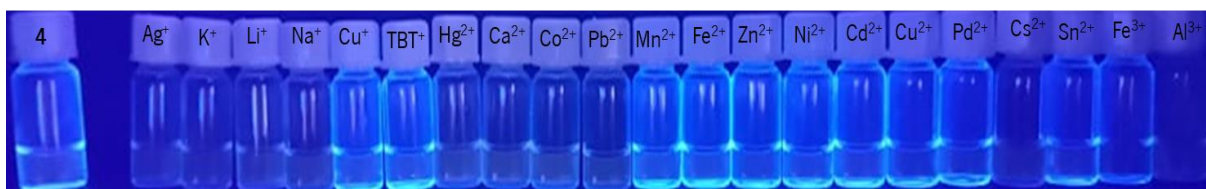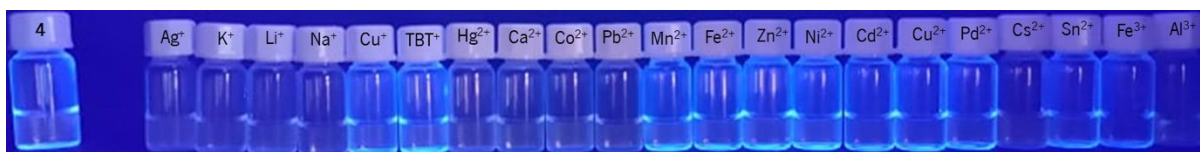

Figure 35- Fluorimetric changes of compound **4** in presence of 50 equiv of cations in ACN/H_2O (8:2).

Compound **5** showed a loss of color in the presence of CN^- and F^- (**figure 36a**), and a quenching in presence of HSO_4^-, BzO^-, Br^-, CN^- and I^- (**figure 36b**).
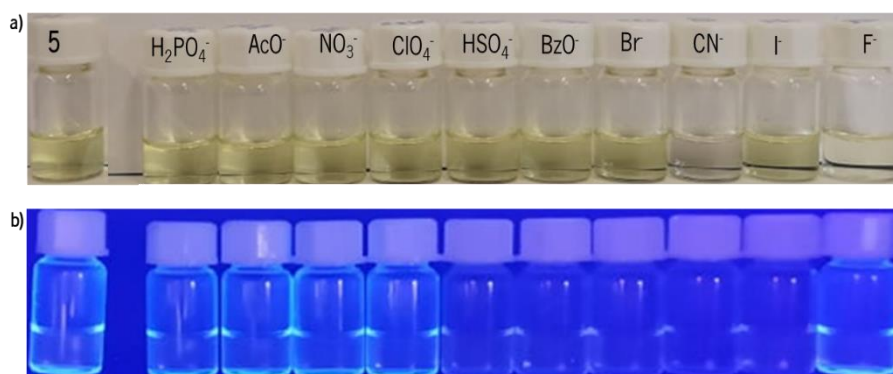
Figure 36- Colorimetric (**a**) and fluorimetric (**b**) changes of BODIPY **5** in presence of 50 equiv of anions in ACN/H_2O (8:2).

Compound **5** showed fluorescence quenching in presence of Ag^+, K^+, Li^+, Na^+, Hg^{2+}, Ca^{2+}, Co^{2+}, Pb^{2+}, Cs^{2+} and Al^{3+} (figure **37**).
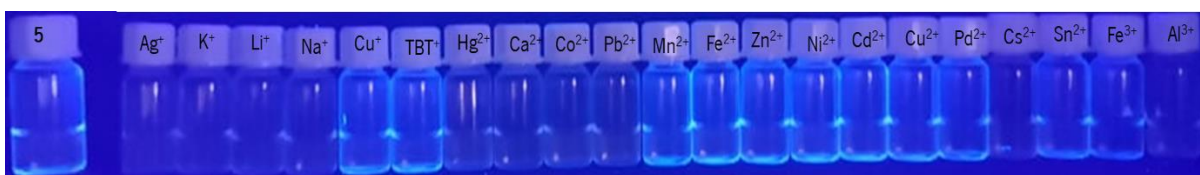
Figure 37- Fluorimetric changes of compound **5** in presence of 50 equiv of cations in ACN/H_2O (8:2).

In **table 7** is presented an overview of the colorimetric and fluorimetric responses of compounds **1-5** in ACN/H_2O (8:2) solution. The main differences between the assays in ACN and ACN/H_2O (8:2) were seen for compounds **2** and **4**. In ACN/H_2O (8:2) compound **2** showed fluorimetric selectivity for F^- and compound **4** lost the capacity to change color in presence of anions.

These results are quite promising considering the application of BODIPY and dicyanovinyl

derivatives as probes for ions in biological and environmental samples, since the studies imply the stability of the compounds and an efficiency of recognition under the conditions of the physiological/aqueous environment.

Table 7- Colorimetric and fluorimetric changes overview for compounds **1-5** in ACN/H_2O (8:2) solution.

Compound	Colorimetric signal	Fluorimetric signal
1	F-, Cu^{2+}, Al^{3+}	ClO_4^-, F-, CN-, Ag^+, TBT^+, Ni^{2+}, Sn^{2+} Cu^{2+} and Fe^{3+}
2	CN- and F-, Pd^{2+} and Fe^{3+}	F-
3	CN-, I-, Cu^{2+} and Pd^{2+}	F-, I-, Ag^+, K^+, Li^+, Cu^+, Ca^{2+}, Zn^{2+}, Pd^{2+}, Sn^{2+}, Fe^{3+} and Al^{3+}
4	——	HSO_4^-, BzO^-, Br, CN-, F-, Ag^+, K^+, Li^+, Na^+, Hg^{2+}, Ca^{2+}, Co^{2+}, Zn^{2+}, Pb^{2+}, Cs^{2+} and Al^{3+}
5	CN- and F-	HSO_4^-, BzO^-, Br, CN-, I-, Ag^+, K^+, Li^+, Na^+, Hg^{2+}, Ca^{2+}, Co^{2+}, Pb^{2+}, Cs^{2+} and Al^{3+}.

3.4.3. Spectrophotometric and spectrofluorimetric titrations of BODIPYs **1**, **3** and dicyanovinyl derivative **5** in presence of ions

Given the results obtained in the preliminary evaluation of the sensing capacity of BODIPY and dicyanovinyl derivatives with a view to their application as chemosensors, derivatives **1**, **3** and **5** proved to be colorimetric and fluorimetric sensors in ACN and in aqueous medium, so spectrophotometric and spectrofluorimetric titrations were carried out for selected ions.

Titrations were performed in ACN and ACN/H_2O (8:2) by sequentially adding solution of the ions (F-, CN-, Cu^{2+} and Fe^{3+}) to the solutions of the compounds, with the absorption/emission spectrum being plotted and recording changes in absorption/emission bands depending on the number of equiv of each added ion. The ions solutions were prepared at a higher concentration than compound solutions so that successive additions would not change the final volume of the solution. The graphics were normalized to allow a clearer understanding of the behavior as a function of the amount of ion added.

Titrations of compound **1** were carried out in ACN solution, and after addition of F-, Cu^{2+} and Fe^{3+}, the emission band of the compound changed according to what was observed in the preliminary tests. The same happened with Cu^{2+} and Fe^{3+} where the color changed from yellow to blue, as reflected by the appearance of a new absorption band in the absorption spectrum.

The spectrofluorimetric titration with F-, with successive additions the emission band at 509 nm

suffered an increase of 40% in intensity reaching a plateau at about 50 equiv (**figure 38**).

Figure 38- Normalized spectrofluorimetric titration of compound **1** with addition of F⁻ in ACN. Inset: normalized intensity at 509 nm as a function of [F]/[**1**]. ([**1**] =1x10⁻⁵ M, [F] = 1x10⁻² M).

Considering the absorption spectrum of **BODIPY 1** with successive additions of Cu^{2+} (**figure 39a**) the absorption band at 496 nm a suffered a decrease on absorbance of 40%, while a new band appeared at 695 nm. A plateau was reached with 25 equiv of the cation. With successive additions of Fe^{3+} (**figure 39b**) the absorption band at 497 nm a suffered a decrease on absorbance of 90%, while a new band appeared at 701 nm. A plateau was reached with 40 equiv of the cation. An isobestic point is clearly present in the spectrum with addition of 20 equiv of Fe^{3+}, both bands show the same absorbance at this point of the titration indicating that two species are present in solution, the uncomplexed BODIPY and the complex BODIPY-cation.
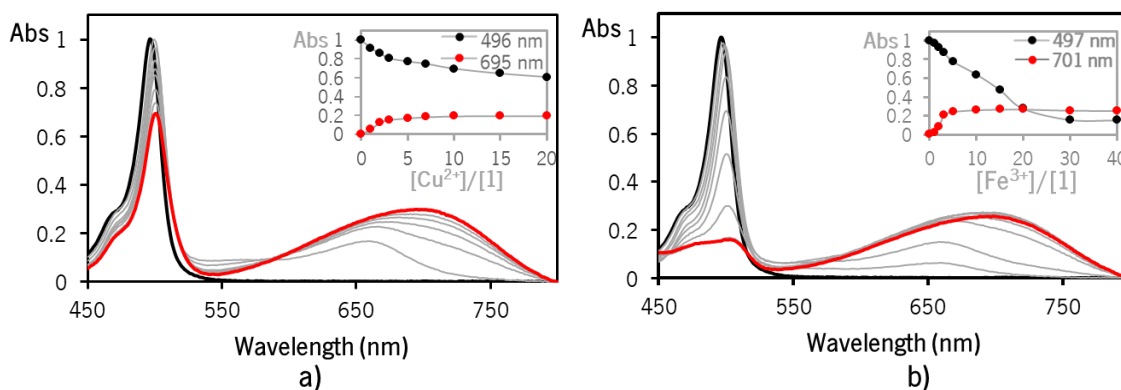
Figure 39 - Normalized spectrophotometric titrations of compound **1** with addition of Cu^{2+} (**a**) and Fe^{3+} (**b**) in ACN. Inset: normalized absorbance at 496/497 nm and 695/701 nm as a function of [cation]/[**1**]. ([**1**] =1x10⁻⁵ M, [cation] = 1x10⁻² M).

Considering the emission spectra of **BODIPY 1** with successive additions of Cu^{2+} and Fe^{3+} (**figure 40**), the emission bands at 520 and 509 nm suffered a decrease in intensity of 90%, reaching a plateau, respectively, at 20 and 10 equivalents.
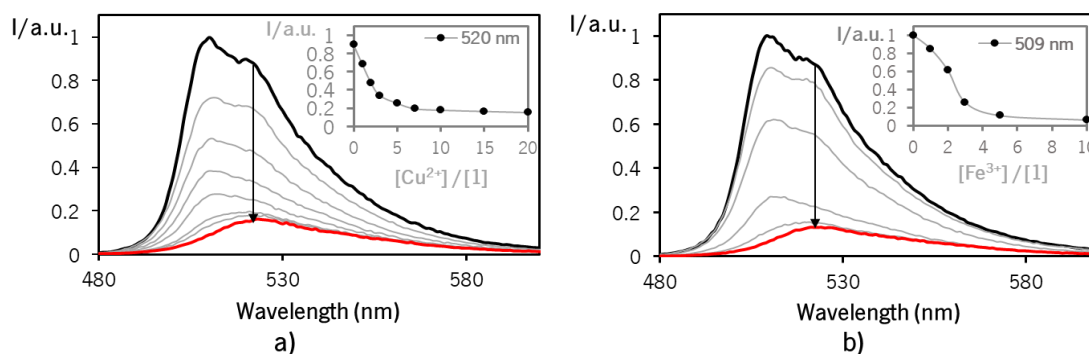
Figure 40 - Normalized spectrofluorimetric titrations of compound **1** with addition of Cu^{2+} (**a**) and Fe^{3+} (**b**) in ACN. Inset: normalized intensity at 520/ 509 nm as a function of [cation]/[**1**]. ([**1**] =$1x10^{-5}$ M, [cation] = $1x10^{-2}$ M).

Compound **3** was titrated with CN^- and Cu^{2+} in ACN and ACN/H_2O (8:2), respectively, showing a decrease in absorbance, matching the loss of color seen in the preliminary assays.

Observing the absorption spectrum of **BODIPY 3** with successive additions of CN^- (**figure 41**) the absorption band at 521 nm a suffered a decrease on absorbance of 50 % and the band was shifted to shorter wavelengths with 40 equiv of the anion.
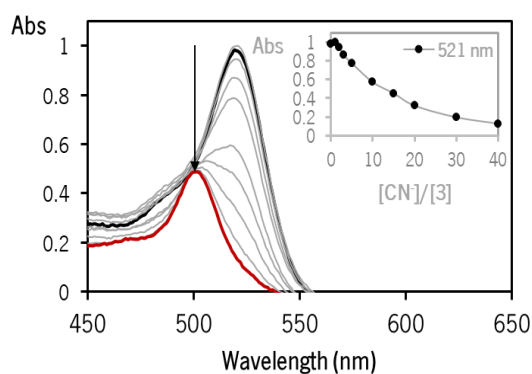
Figure 41 – Normalized spectrophotometric titration of compound **2** with addition of CN^- in ACN. Inset: normalized absorbance at 521 nm as a function of [anion]/[**3**]. ([**3**] =$1x10^{-5}$ M, [anion] = $1x10^{-2}$ M).

With regard to the absorption spectrum of **BODIPY 3** with successive additions of Cu^{2+} (**figure 42**), the absorption band at 521 nm suffered a decrease on absorbance of 98 % with 100 equiv of the cation.
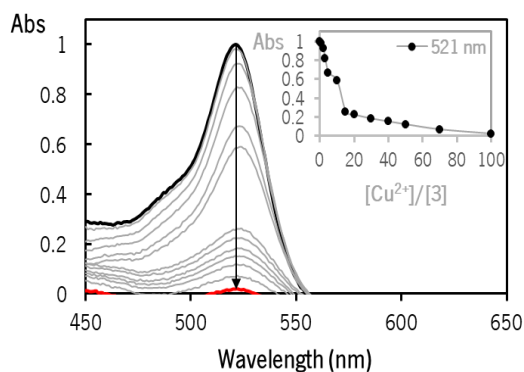
Figure 42- Normalized spectrophotometric titrations of compound **3** with addition of Cu²⁺ in ACN/ H₂O (8:2). Inset: normalized absorbance at 521 nm as a function of [Cu²⁺]/[**3**]. ([**3**] =8x10⁻⁶ M, [Cu²⁺] = 1x10⁻² M).

Compound **5** showed the most promising results, with the addition of a very small number of equiv of CN⁻ in ACN/H₂O (8:2), the absorption and emission bands suffered significant changes in absorbance and intensity, respectively. The results of the titration match the behavior of the compound in presence of the anions and cations seen in the preliminary tests.

Observing the absorption spectrum of dicyanovinyl derivative **5** with successive additions of CN⁻ (**figure 43**) the absorption band at 422 nm suffered a decrease on absorbance of 96 % with 4 equiv of the cation.
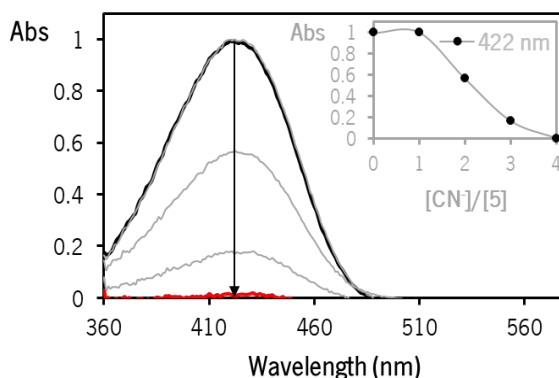
Figure 43- Normalized spectrophotometric titrations of compound **5** with addition of CN⁻ in ACN/ H₂O (8:2). Inset: normalized absorbance at 521 nm as a function of [CN⁻]/[**5**]. ([**5**] =8x10⁻⁶ M, [CN⁻] = 1x10⁻² M).

Regarding the fluorescence spectrum of dicyanovinyl derivative **5** with successive additions of CN⁻ (**figure 44**) the emission band at 521 nm suffered a decrease of intensity of 91 % with 6 equiv of the anion.
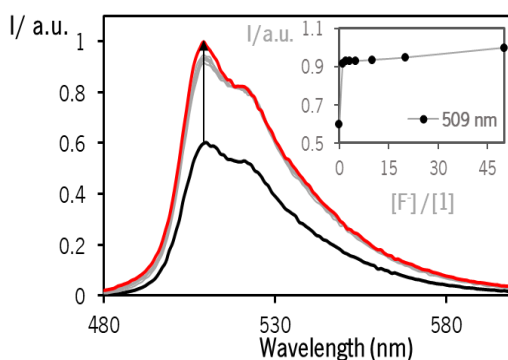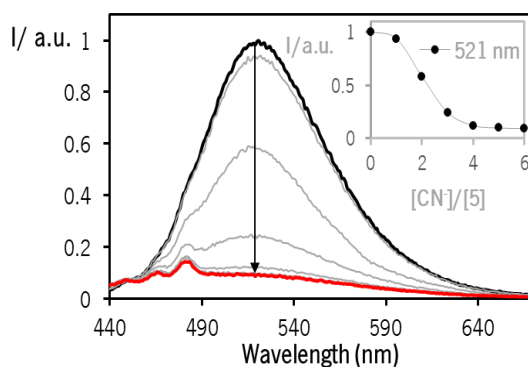
Figure 44- Normalized spectrofluorimetric titrations of compound **5** with addition of CN in ACN/ H₂O (8:2). Inset: normalized intensity at 521 nm as a function of [CN]/[**5**]. ([**5**] =8x10⁻⁶ M, [CN] = 1x10⁻² M).

The results of the titration match the behavior of the compounds in presence of the anions and cations seen in the preliminary tests (**table 8**).

Table 8- Overview of the obtained titrations results.

Compound	Analyte	Medium	Type of spectral data	[ion]/[compound]
1	F⁻	ACN	Emission	60
1	Cu²⁺	ACN	Absorption and emission	Both 20
1	Fe³⁺	ACN	Absorption and Emission	40 and 10
3	CN⁻	ACN	Absorption	40
3	Cu²⁺	ACN/H₂O (8:2)	Absorption	100
5	CN⁻	ACN/H₂O (8:2)	Absorption and emission	4 and 6

3.4.4. ¹H-NMR titration of dicyanovinyl derivative **5** with cyanide

Considering the chemodosimeter capacity of dicyanovinyl derivatives reported in the literature and the results obtained in the titrations of the dicyanovinyl derivative **5**, to gain further insight into the mechanism of interaction, a ¹H NMR titration of dicyanovinyl **5** (3.8×10^{-5} M) in presence of CN (2.65 M) was performed in ACN-d₃ to evaluate any differences in the chemical shifts after the addition of the ion.

Along the consecutive addition of 4 equiv of CN- to compound **5** is possible to see the signal of the double bound proton (2a) disappearing, while a new signal appears in the aliphatic region of the spectra corresponding to the proton (2a) in the new compound. The other proton signals corresponding to the phenyl and thiophene groups also display changes considering the alteration of the withdrawing electronic character of the vinylic double bond to a single bond. The originals signals disappear and new

signals appear at lower chemical shifts showing the formation of a new compound, as shown in **figure 45**.

This behavior is in total agreement with the spectrophotometric/spectrofluorimetric titrations and constitutes proof that compound **5** acts as a chemodosimeter for CN⁻, in accordance with published data for related dicyanovinyls.
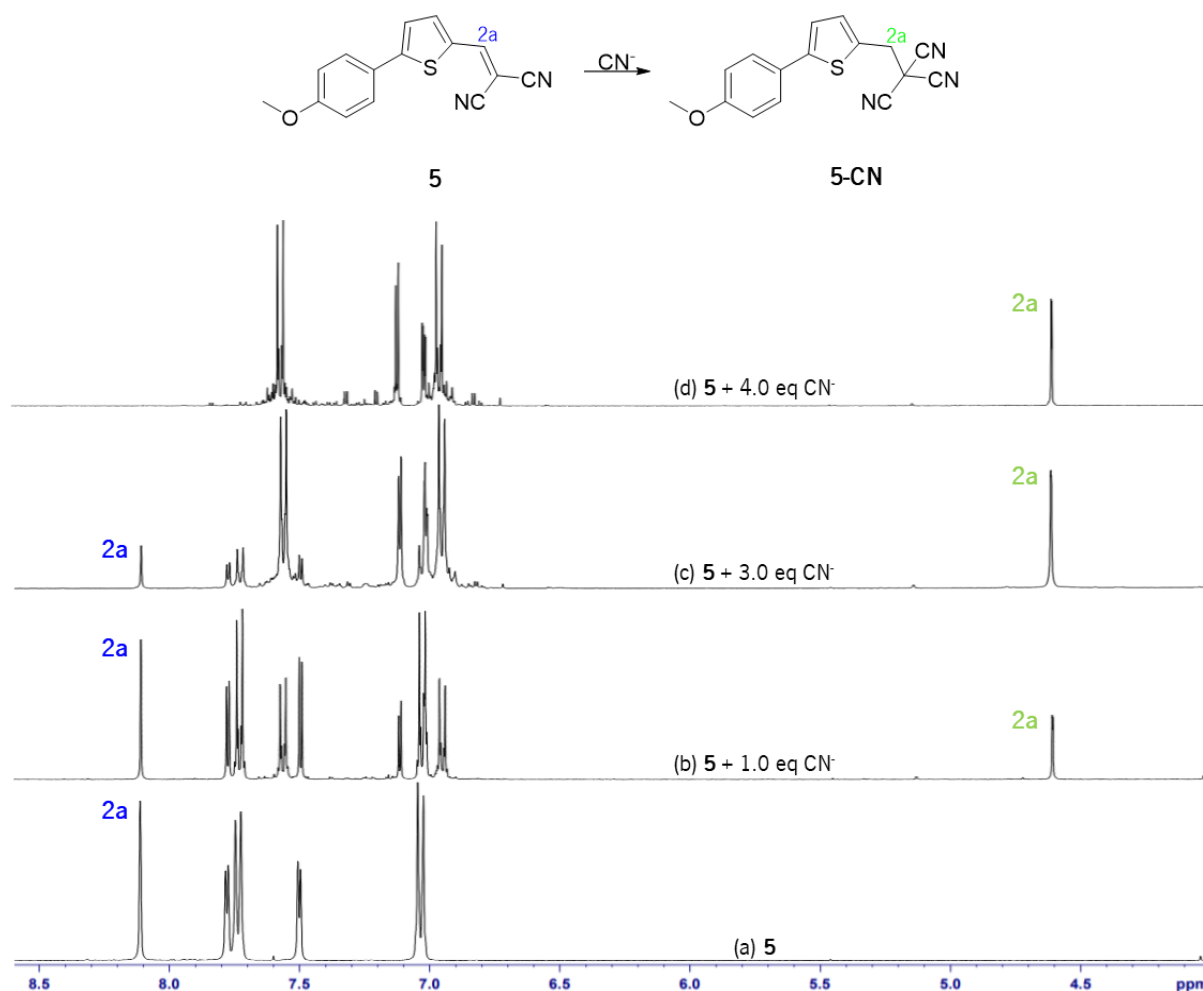
Figure 45- Partial ¹H NMR spectra of compound **5** (3.8×10⁵ M) in acetonitrile-d₃ in (a) the absence and (b) the presence of 1.0, (c) 3.0, (d) 4.0 eq of CN⁻.

3.5. Evaluation of BODIPY derivative **2** and dicyanovinyl derivative **4** as optical sensor for alcohols and amines

One of the initial goals for this work was the evaluation of the recognition ability of the synthesized compounds towards drugs of abuse such as fentanyl and codeine, aiming at the development of optical probes for testing these two analytes in simulated urine solutions through faster and simpler analyses. Fentanyl and codeine are prescription and over-the-counter authorized medicines but with a highly addictive profile. However, during the course of the work, it was not possible to obtain samples of the two

drugs to be tested and so, as an alternative, considering the functional groups present in the structure of codeine and fentanyl, a series of amines and alcohols were used as models for codeine and fentanyl.

Alcohols and amines (**figure 46**) were used to simulate, in a simplified way, the behavior of ID. For this purpose, alcohols and amines were chosen with different degrees of substitution, carbon chain length and also with different electronic structures (aromatic and aliphatic) in order to understand the selectivity of detection of these molecules. The model alcohols were: methanol, 2B,1P and 4MP. The model amines were: HA, DCHA, DEA, TEA and AN. This set of models included primary, secondary and aromatic alcohols, as well as primary, secondary, terciary and aromatic amines.
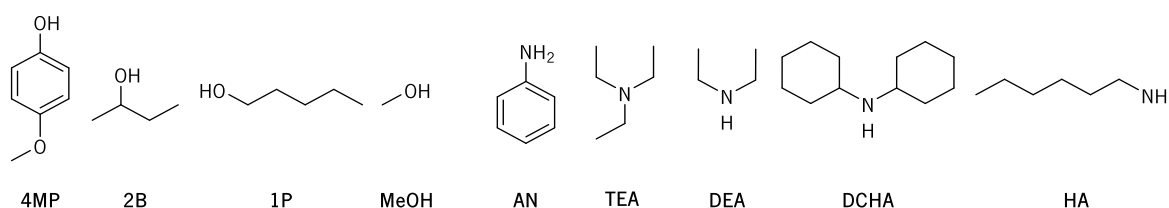
Figure 46- Chemical structures of the alcohols and amines used on preliminary assays.

Aiming at the preliminary study of the sensing ability of BODIPY derivative **2** and dicyanovinyl derivative **4** with various alcohols and amines, solutions of the compounds with a concentration of $1,0 \times 10^{-5}$ M in ACN were prepared and a solution of **5** in DCM with the same concentration. Solutions in acetonitrile ($1,0 \times 10^{-2}$ M) of the model alcohols and amines were also prepared.

In **section 1.6.1** and **1.6.2** the structures of the various groups of drugs of interest were presented, along with metabolic pathways, which revealed that amine and hydroxyl groups do not undergo metabolization and are comparable with the chosen analytes (**figure 46**), as well as in the cases where there is metabolization, the major metabolites still contain hydroxyl or amine groups.

The studies of compounds **2** and **4** with model amines and alcohols were conducted under various conditions shown in **table 9**.

Table 9- Conditions tested in the evaluation of compounds **2** and **4** as sensors of amines and alcohols in different media.

Condition	Compound			
	ACN		DCM	
	2	4	2	4
50 equiv of amines and alcohols	✓	✓	—	✓
50 equiv of amines and alcohols + pH 6.5 buffer	✓	✓	—	—
50 equiv of amines and alcohols + pH 6.5 buffer + interferents	✓	✓	—	—
50 equiv of amines and alcohols + pH 7.0 buffer	✓	✓	—	—
50 equiv of amines and alcohols + pH 7.0 buffer + interferents	✓	✓	—	—
50 equiv of amines and alcohols + pH 7.4 PBS	✓	✓	—	—
50 equiv of amines and alcohols + pH 7.4 PBS + interferents	✓	✓	—	—

The methodology adopted was similar to that of the ion sensing: 50 equiv of each alcohol and amine were added to solutions of compounds **2** and **4** and differences in color and fluorescence intensity were evaluated. The pictures for all these different tests were taken immediately after adding the analytes to the vial and after 2 hours to see if any changes had occurred in the meantime. To verify the possible reaction between the analytes and the dicyanovinyl group of compounds **4**, pictures were taken 1 week after the addition of the analytes.

The DCM solutions of compound **4** was used to test whether a different solvent altered the possible addition reaction time. These conditions also allow to see the effect of the pH, water, and the different salts in the compounds' fluorescence.

The possibility of interference by organic compounds usually present in urine were also tested by adding 50 equiv of U or CRT with concentration 1×10^{-2} M in ACN directly to the vial containing the compounds' ACN aqueous solution.

No color changes were observed in presence of the different analytes for compounds **2** and **4**.

3.5.1. Preliminary recognition assays for BODIPY **2**

After adding 50 equiv of each alcohol and amine to the BODIPY **2** solution in ACN (1×10^{-5}M), showed a selective increase in the fluorescence intensity in the presence of 4MP (**figure 47**). In presence of amines, BODIPY **2** solution did not show color or fluorescence changes. The behavior was maintained

after 2 hours (**appendix A, figure A1**).
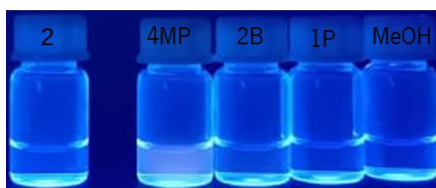
Figure 47- Fluorimetric changes of BODIPY **2** with 50 equiv of each alcohol in ACN.

After adding 50 equiv of each alcohol and amine to the BODIPY **2** solution in ACN/phosphate buffer pH 6.5 (3:1, 7.5×10⁻⁶M) no change in fluorescence happened for alcohols. In presence of amines, BODIPY **2** developed a fluorescence quenching in presence of DCHA and HA (**figure 48**). The behavior was maintained after 2 hours (**appendix A, figure A2**), no selectivity was achieved.
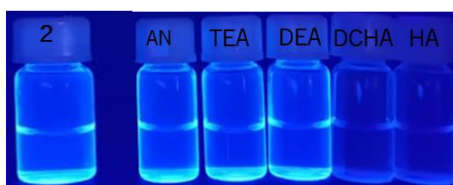
Figure 48- Fluorimetric changes of BODIPY **2** with 50 equiv of each amine in ACN/phosphate buffer pH 6.5 (3:1).

After adding 50 equiv of each alcohol or amine and U to BODIPY **2** in ACN/phosphate buffer pH 6.5 (3:1, 7.5×10⁻⁶ M) no change in fluorescence happened for alcohols. The solution of BODIPY **2** in presence of DEA developed a marked fluorescence quenching (**figure 49**). The same behavior was maintained after 2 hours (**appendix A, figure A3**), so in presence of U selectivity for DEA was achieved.

Figure 49- Fluorimetric changes of BODIPY **2** with 50 equiv of each amine and U in ACN/phosphate buffer pH 6.5 (3:1).

After adding 50 equiv of each alcohol or amine and CRT to the BODIPY **2** solution in ACN/ phosphate buffer pH 6.5 (3:1, 7.5 ×10⁻⁶M) in presence of CRT and MeOH showed a fluorescence quenching (**figure 50a**).

In presence of amines, BODIPY **2** displayed a quenching in presence of TEA (**figure 50b**). The same behavior was maintained after 2 hours (**appendix A, figure A4**), so no selectivity was achieved.

Figure 50- Fluorimetric changes of BODIPY **2** with 50 equiv of CRT and of each alcohol (**a**) and each amine (**b**) in ACN/phosphate buffer pH 6.5 (3:1).

After adding 50 equiv of each alcohol and amine to the BODIPY **2** solution in ACN/phosphate buffer pH 7.0 (3:1, 7.5×10^{6}M), in presence of 1P and MeOH, the quenching with 1P is more notorious (**figure 51**). The same behavior was maintained after 2 hours (**appendix A, figure A5**), so selectivity was achieved for 1P.
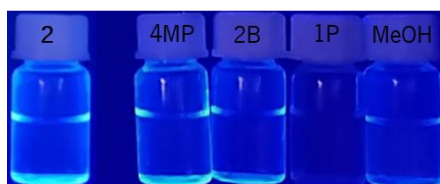
Figure 51- Fluorimetric changes of BODIPY **2** with 50 equiv of each alcohol in ACN/phosphate buffer pH 7.0 (3:1).

After adding 50 equivalents of each alcohol, amine and U to the BODIPY **2** solution in ACN/phosphate buffer pH 7.0 (3:1, 7.5×10^{-6} M), in presence of MeOH showed a new quenching (**figure 52a**). The same behavior was maintained after 2 hours (**appendix A, figure A6a**), so no selectivity was achieved.

In presence of amines, BODIPY **2** solution with DEA displayed a fluorescence quenching (**figure 52b**). The same behavior was maintained after 2 hours (**appendix A, figure A6b**), so selectivity was achieved for DEA.
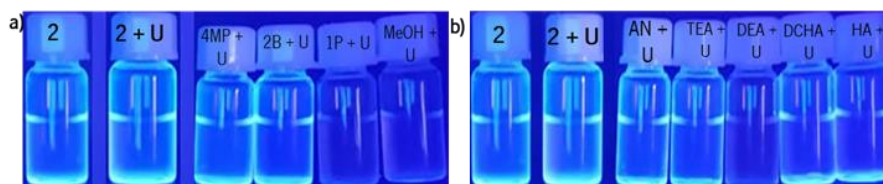
Figure 52- Fluorimetric changes of BODIPY **2** with 50 equiv of U and 50 equiv of each alcohol (**a**) and each amine (**b**) in ACN/phosphate buffer pH 7.0 (3:1).

After adding 50 equiv of each alcohol, amine and CRT to the BODIPY **2** solution in ACN/phosphate buffer pH 7.0 (3:1, 7.5×10^{6}M), no change in fluorescence happened for alcohols.

In presence of amines, BODIPY **2** solution with AN, DCHA and HA developed a new increase in the fluorescence intensity (figure **53**). The same behavior was maintained after 2 hours (**appendix A, figure A7**) so no selectivity was achieved.
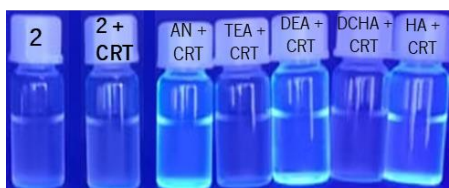
Figure 53- Fluorimetric changes of BODIPY **2** with 50 equiv of each amine and 50 equiv of CRT in ACN/phosphate buffer pH 7.0 (3:1).

After adding 50 equiv of each alcohol and amine to a BODIPY **2** solution in ACN/PBS pH 7.4 (3:1, 7.5×10^{-6} M), in presence of 4MP, 1P and MeOH showed a quenching, while in presence of 2B fluorescence intensity increased (**figure 54a**). The same behavior was maintained after 2 hours (**appendix A, figure A8a**), so no selectivity was achieved. In presence of amines, BODIPY **2** solution with DEA showed a quenching (**figure 54b**). The same behavior was maintained after 2 hours (**appendix A, figure A8b**), so selectivity was achieved for DEA.
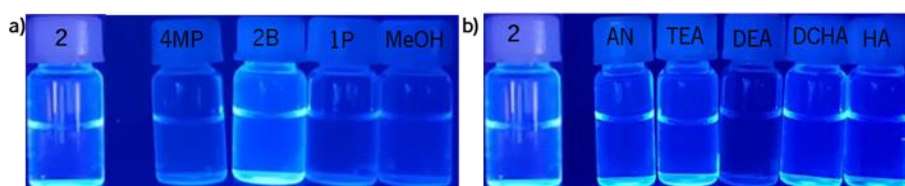
Figure 54- Fluorimetric changes of BODIPY **2** with 50 equiv of each alcohol (**a**) and each amine (**b**) in ACN/PBS pH 7.4 (3:1).

After adding 50 equiv of each alcohol, amine and U to the BODIPY **2** solution in ACN/PBS 7.4 (3:1, 7.5×10^{-6} M), in presence of 2B showed a new quenching (**figure 55a**). The same behavior was maintained after 2 hours (**appendix A, figure A9a**), so no selectivity was achieved. In presence of amines, BODIPY **2** solution with TEA, DCHA and HA showed a new quenching (**figure 55b**). The same behavior was maintained after 2 hours (**appendix A, figure A9b**), so no selectivity was achieved.
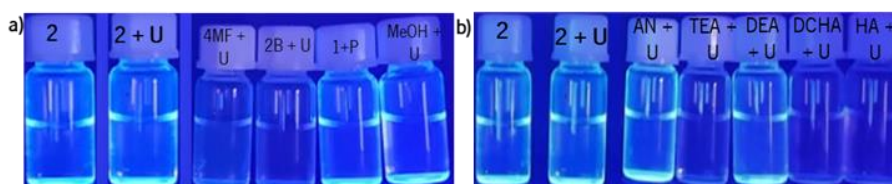
Figure 55- Fluorimetric changes of BODIPY **2** with 50 eq of U and 50 equiv of each alcohol (**a**) and each amine (**b**) in ACN/PBS pH 7.4 (3:1).

After adding 50 equiv of each alcohol, amine and CRT to the BODIPY **2** solution in ACN/PBS pH 7.4 (3:1, 7.5×10^{-6} M), no change in fluorescence happened for alcohols. In presence of amines, BODIPY **2** solution with AN, TEA, DCHA and HA showed a new quenching (**figure 56**). The same behavior was maintained after 2 hours and 1 week (**appendix A, figure A10**), so no selectivity was achieved.
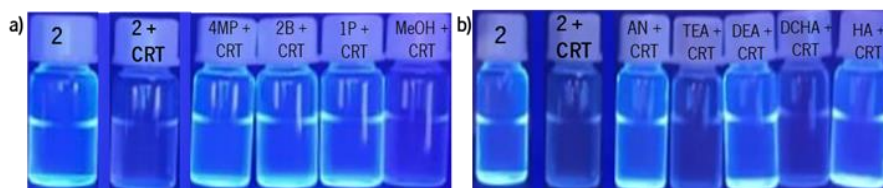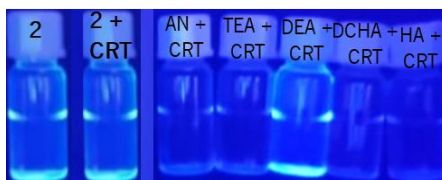

Figure 56- Fluorimetric changes of BODIPY **2** with 50 equiv of CRT and 50 equiv of each amine in ACN/PBS pH 7.4 (3:1)

The results for BODIPY **2** are systematized in **table 10**.

Table 10- Overview of preliminary sensing studies for probe **2** in presence of alcohols and amines.

Conditions	Interferents		Alcohols				Amines				
	U	CRT	4MP	2B	1P	MeOH	AN	TEA	DEA	DCHA	HA
ACN (50 equiv)			↑	—	—	—	—	—	—	—	—
pH 6.5			—	—	—	—	—	—	—	↓	↓
pH 6.5	—		—	—	—	—	—	—	↓	—	—
pH 6.5		↓	—	—	—	↓	—	↓	—	↓	—
pH 7			—	—	↓	↓	—	—	—	—	—
pH 7	—		—	—	↓	↓	—	—	↓	—	—
pH 7		—	—	—	—	—	↑	-	↑	—	↓
pH 7.4			↓	↑	↓	↓	—	—	↓	—	—
pH 7.4	—		↓	↓	—	—	—	↓	—	↓	↓
pH 7.4		—	—	—	—	—	↓	↓	—	↓	↓

Note: — represents no change in the probes' fluorescence, ↑ represent an enhancement in fluorescence intensity, ↓ represents the quenching and ▢ represents the absence of the interferent.

3.5.2. Preliminary recognition assays for dicyanovinyl derivative **4**

After adding 50 equiv of each alcohol and amine to the dicyanovinyl derivative **4** solution in ACN (1×10^5 M), in presence of 4MP showed an increase on fluorescence (**figure 57a**). The same behavior

was maintained after 2 hours and 1 week (**appendix A, figure A11**) so selectivity was achieved for 4MP. In presence of amines, with AN, TEA, DEA and DCHA also showed a fluorescence enhancement (**figure 27b**). The same behavior was maintained after 2 hours, 1 week (**appendix A, figure A12**), so no selectivity was achieved.

Figure 57- Fluorimetric changes of dicyanovinyl derivative **4** with 50 equiv of each alcohol (**a**) and each amine (**b**) in ACN.

After adding 50 equiv of each alcohol and amine to the dicyanovinyl derivative **4** solution in ACN/phosphate buffer pH 6.5 (3:1. 7.5×10^5M), in presence of 2B, 1P and MeOH showed a slight quenching (**figure 58a**). The same behavior was maintained after 2 hours and 1 week (**appendix A, figure A13**) so no selectivity was achieved. In presence of amines, with AN, TEA, DEA, DCHA and HA showed a slight quenching (**figure 58b**). The same behavior was maintained after 2 hours, 1 week (**appendix A, figure A14**), so no selectivity was achieved.

Figure 58 - Fluorimetric changes of dicyanovinyl derivative **4** with 50 equiv of each alcohol (**a**) and each amine (**b**) in ACN/phosphate buffer pH 6.5 (3:1).

After adding 50 equiv of each alcohol, amine and U to the dicyanovinyl derivative **4** solution in ACN/ phosphate buffer pH 6.5 (3:1, 7.5×10^5 M), in presence of 4MP and 1P, showed a quenching (**figure 59a**). The same behavior was maintained after 2 hours and 1 week (**appendix A, figure A15**) so no selectivity was achieved. In presence of amines with AN, DEA, DCHA, and HA showed quenching (**figure 59b**). The same behavior was maintained after 2 hours, 1 week (**appendix A, figure A16**), so no

selectivity was achieved.

Figure 59- Fluorimetric changes of dicyanovinyl derivative **4** with 50 equiv of U and 50 eq of each alcohol (**a**) and each amine (**b**), in ACN/phosphate buffer pH 6.5 (3:1).

After adding 50 equiv of each alcohol, amine and CRT to the dicyanovinyl derivative **4** solution in ACN/phosphate buffer pH 6.5 (3:1, 7.5×10^5 M), it was visible a fluorescence quenching with 2B and 1P (**figure 60a**). The same behavior was maintained after 2 hours and 1 week (**appendix A, figure A17**) so no selectivity was achieved. In presence of amines, with AN, DEA and DCHA showed quenching (**figure 60b**). The same behavior was maintained after 2 hours, 1 week (**appendix A, figure A18**), so no selectivity was achieved.


Figure 60- Fluorimetric changes of dicyanovinyl derivative **4** with 50 equiv of CRT and 50 eq of each alcohol (**a**) and each amine (**b**), in ACN/phosphate buffer pH 6.5 (3:1).

After adding 50 equiv of each alcohol and amine to the dicyanovinyl derivative **4** solution in ACN/phosphate buffer pH 7.0 (3:1, 7.5×10^5 M), there was an increase in fluorescence intensity for 4MP and 2B while in presence of 1P and MeOH showed a fluorescence quenching (**figure 61a**). The change in presence of 4MP was more notorious and the behavior was maintained after 2 hours and 1 week (**appendix A, figure A19**) so no selectivity was achieved. In presence of amines, with HA showed an increase in fluorescence intensity while with TEA, DEA and DCHA showed a quenching (**figure 61b**). The same behavior was maintained after 2 hours, 1 week (**appendix A, figure A20**), so selectivity was achieved

for HA.

Figure 61 -Fluorimetric changes of dicyanovinyl derivative **4** with 50 equiv of each alcohol (**a**) and each amine (**b**) in ACN/phosphate buffer pH 7.0 (3:1).

After adding 50 equiv of each alcohol, amine and U to the dicyanovinyl derivative **4** solution in ACN/phosphate buffer pH 7.0 (3:1, 7.5×10^5 M) in presence of MeOH the quenching persisted (**figure 62a**). The behavior was maintained after 2 hours and 1 week (**appendix A, figure A21**) so selectivity was achieved for MeOH. In presence of amines, with HA showed a new quenching (**figure 62b**). The same behavior was maintained after 2 hours, 1 week (**appendix A, figure A22**), so no selectivity was achieved.

Figure 62- Fluorimetric changes of dicyanovinyl derivative **4** with 50 equiv of U and 50 equiv of each alcohol (**a**) and each amine (**b**), in ACN/phosphate buffer pH 7.0 (3:1).

After adding 50 equiv of each alcohol, amine and CRT to the dicyanovinyl derivative **4** solution in ACN/phosphate buffer pH 7.0 (3:1, 7.5×10^5 M), in presence of 4MP showed a new quenching (**figure 63a**). The behavior was maintained after 2 hours and 1 week (**appendix A, figure A23**) so selectivity was achieved for 4MP. In presence of amines, with TEA and DCHA the quenching (**figure 63b**). The same behavior was maintained after 2 hours, 1 week (**appendix A, figure A24**), so no selectivity was achieved.

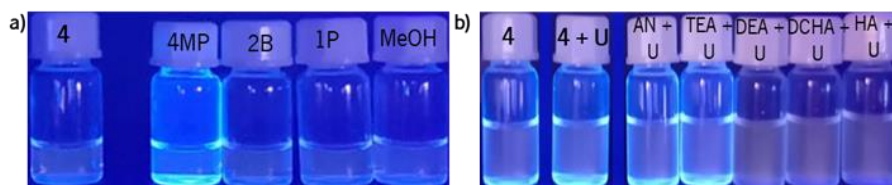**Figure 63**- Fluorimetric changes of dicyanovinyl derivative **4** with 50 equiv of CRT and 50 equiv of each alcohol (**a**) and each amine (**b**), in ACN/phosphate buffer pH 7.0 (3:1).

After adding 50 equiv of each alcohol and amine to the dicyanovinyl derivative **4** solution in

ACN/PBS pH 7.4 (3:1, 7.5×10^5 M), in presence of 2B, 1P and MeOH showed a fluorescence quenching (**figure 64a**). The behavior was maintained after 2 hours and 1 week (**appendix A, figure A125**), so no selectivity was achieved. In presence of amines, with HA showed a quenching (**figure 64b**). The same behavior was maintained after 2 hours and 1 week (**appendix A, figure A26**), so selectivity was achieved for HA.

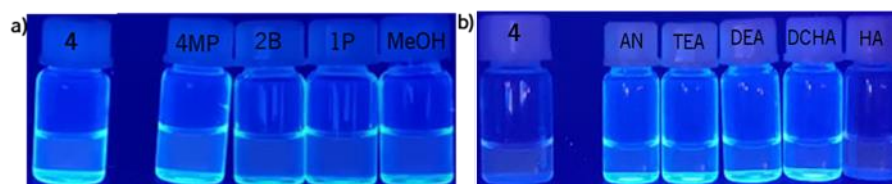**Figure 64** - Fluorimetric changes of dicyanovinyl derivative **4** with 50 equiv of each alcohol (**a**) and each amine (**b**) in ACN/PBS pH 7.4 (3:1).

After adding 50 equiv of each alcohol, amine and U to the dicyanovinyl derivative **4** solution in ACN/PBS pH 7.4 (3:1, 7.5×10^5 M), in presence of MeOH the quenching persisted (**figure 65a**). The behavior was maintained after 2 hours and 1 week (**appendix A, figure A27**) so selectivity was achieved for MeOH. In presence of amines, with DEA and HA showed a new quenching (**figure 65b**). The same behavior was maintained after 2 hours and 1 week (**appendix A, figure A28**), so no selectivity was achieved.
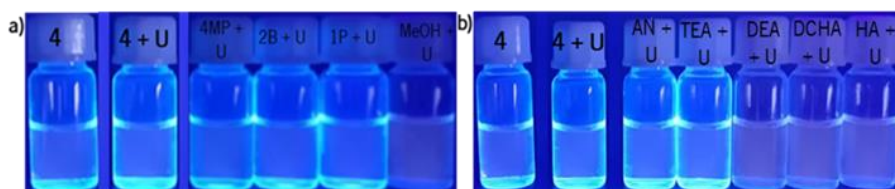
Figure 65- Fluorimetric changes of dicyanovinyl derivative **4** with 50 equiv of U and 50 equiv of each alcohol (**a**) and each amine (**b**) in ACN/PBS pH 7.4 (3:1).

After adding 50 equiv of each alcohol, amine and CRT to the dicyanovinyl derivative **4** solution in ACN/PBS pH 7.4 (3:1, 7.5×10^5 M), MeOH showed a fluorescence quenching (**figure 66a**). The behavior was maintained after 2 hours and 1 week (**appendix A, figure A29**) so no selectivity was achieved. In presence of amines, with AN, TEA and DEA displayed a fluorescence quenching (**figure 66b**). The same behavior was maintained after 2 hours and 1 week (**appendix A, figure A30**), so no selectivity was
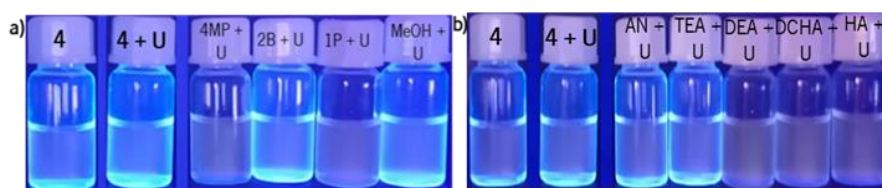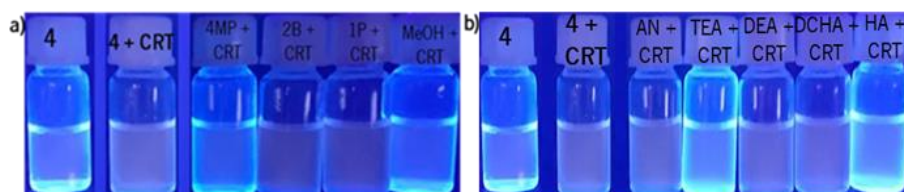
achieved.
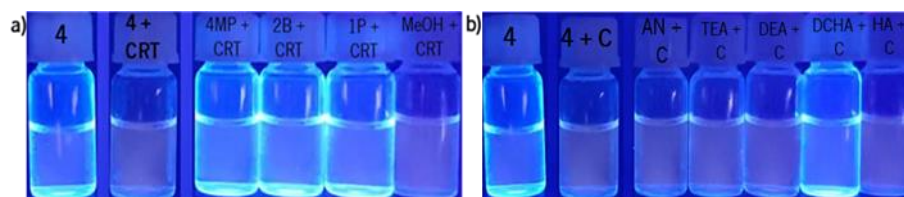
Figure 66- Fluorimetric changes of dicyanovinyl derivative **4** with 50 equiv of CRT and 50 equiv of each alcohol (**a**) and each amine (**b**), in ACN/PBS pH 7.4 (3:1).

After adding 50 equiv of each alcohol and amine to the compound **4** solution in DCM (1×10^{-5} M), no color change occurred. In terms of fluorescence, the compound **4** solution in the presence of 2B and MeOH showed an increase on fluorescence intensity (**figure 67a**). The same behavior was maintained after 2 hours and 1 week (**appendix A, figure A31**) so no selectivity was achieved. In presence of amines, with TEA, DEA and DCHA showed an increase in fluorescence intensity while with HA showed a quenching (**figure 67b**). The same behavior was maintained after 2 hours and 1 week (**appendix A, figure A32**), so selectivity was achieved for HA in the two groups because it is the only quenching.
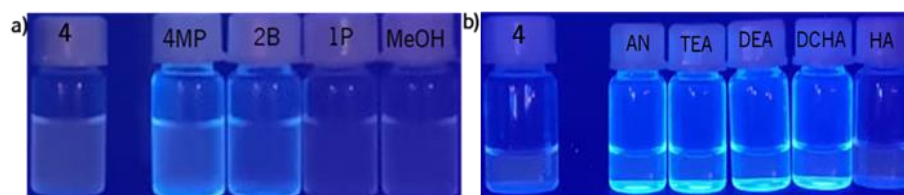

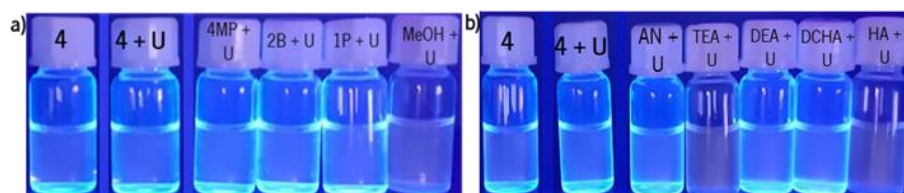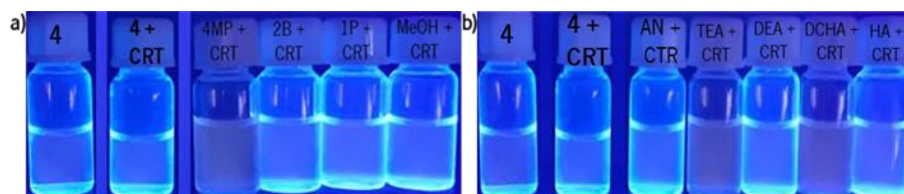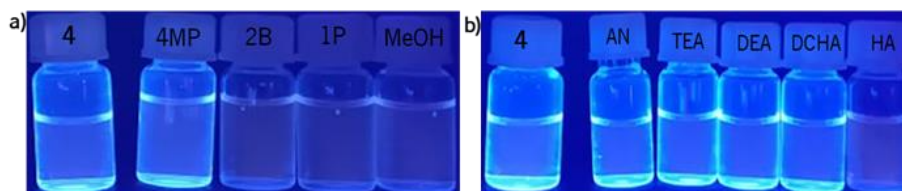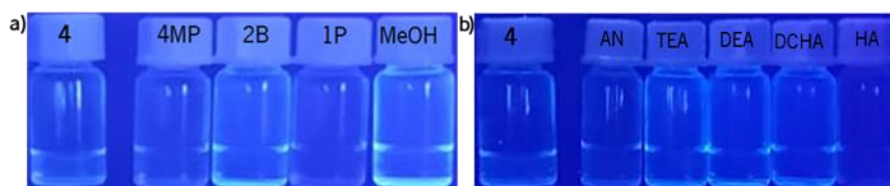**Figure 67**- Fluorimetric changes of dicyanovinyl derivative **4** with 50 equiv of each alcohol (**a**) and each amine (**b**) in DCM.

The results for dicyanovinyl derivative **4** are systematized in **table 11**.

Table 11- Overview of preliminary sensing studies for probe **4** in presence of alcohols and amines.

Conditions	Interferents		Alcohols				Amines				
	U	CRT	4MP	2B	1P	MeOH	AN	TEA	DEA	DCHA	HA
ACN (50 equiv)	■	■	↑	—	—	—	↑	↑	↑	↑	—
pH 6.5	■	■	—	↓	↓	↓	—	↓	↓	↓	↓
pH 6.5	—	■	↓	—	↓	—	—	—	↓	↓	↓
pH 6.5	■	↓	—	↓	↓	—	↓	—	↓	↓	—
pH 7	■	■	↑	↑	↓	↓	—	↓	↓	↓	↑
pH 7	—	■	—	—	—	↓	—	↓	—	—	↓
pH 7	■	—	↓	—	—	—	—	↓	—	↓	—
pH 7.4	■	■	—	↓	↓	↓	—	—	—	—	↓
pH 7.4	—	■	—	—	—	↓	—	↓	↓	↓	↓
pH7.4	■	↓	—	—	—	↓	↓	↓	↓	—	↓
DCM	■	■	—	↑	—	↑	—	↑	↑	↑	—

Note: — represents no change in the probe fluorescence, ↑ represent a enhancement in fluorescence intensity, ↓ represents the quenching and ■ represents the absence of the respective interferent.

Comparing the performance of compounds **2** and **4**, compound **2** seems to be more selective than **4** in ACN solution being able to recognize only 4MP. The selectivity of compound **2** is again better in ACN/phosphate buffer pH 6.5 (3:1) showing the capacity to detect different amines, and only MeOH in presence of creatinine.

In ACN/phosphate buffer pH 7 and in ACN/PBS pH 7.4 neither compound **2** or **4** show selectivity for one of the groups of analytes.

Both compounds have no interaction with U, so this molecule seems not to be an interferent.

3.5.2.1.   Media and salts effect on compound **2** and **4** color and fluorescence

Along the preliminary assays, it was clear that some factors could change the compounds' color and original fluorescence intensity.

For compound **2**, the effect of water and salts was visible: in ACN/phosphate buffer at pH 6.5 and 7.0 some turbidity appeared and a yellowish color developed at pH 7.0. In terms of fluorescence, at pH 7.0 the emission color was slightly changed and in ACN/PBS pH 7.4 the probe became non-fluorescent. These differences can be due to the establishment of hydrogen bonds with water or interactions with the salts used in the preparation of the buffers (**figure 68a**).

For compound **4** a similar behavior was seen: in ACN/phosphate buffer at pH 7.0 some turbidity appeared and in terms of fluorescence, it seemed that the compound had a more intense natural fluorescence. In ACN/PBS pH 7.4 the probe became less fluorescent with a change in the fluorescence color. In DCM the compound seemed to be less fluorescent than in ACN (**figure 68b**).
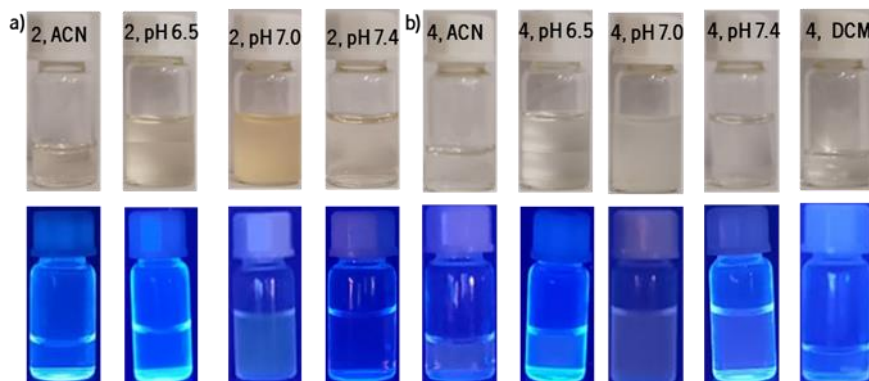
Figure 68- Differences in probe **2 (a)** and **4 (b)** color and fluorescence in different media and in presence of different salts.

3.6. Machine Learning Model Development

Figure 69 shows the raw spectral data for the spectrophotometric titration of Fe^{3+} in presence of compound **1** in ACN as a representative example for the rest of the titrations and model development. The spectrophotometric titration data was obtained between 200 and 800 nm.
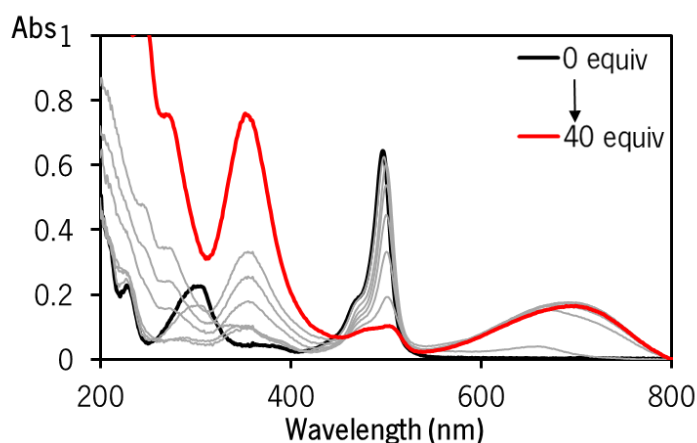
Figure 69- Raw absorption data of the titrations of compound **1** in presence of Fe^{3+} in ACN.

The preliminary analysis of PCA was developed for 4 components. As presented in **figure 70** and **table 12** the totality of data variance is explained just with PC1 and PC2, because of that all samples were used to move forward with calibration models and the other PCs were disregarded.

Through the scores plot bellow, we can easily see the relationship between PC1 and the concentration of samples. In the first four samples, where the concentration does not change significantly, the PC1

value does not change significantly either.

However, in the remaining samples where larger increases in concentration occur, the PC1 value also increases, showing the tendency between this main component and the concentration and how well PCA analysis maintain the overall tendency of the spectroscopic data.
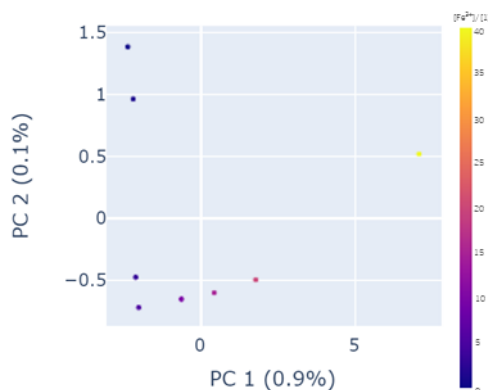
Figure 70- Scores plot of the two PCs for the raw data of the spectrophotometric titration of compound **1** in presence of Fe^{3+}.

In the following table are presented the results of the PCA analysis for all the titrations.

For the last titration only, SLR was applied to the data set because insufficient data were collected as the titration was finished with only a few equiv of CN^- in solution.

Table 12-Results of the PCA analysis presented as the percentage of variance explained with PC1 and PC2.

Titration	PC1 (%)	PC2 (%)
1+F^- (ACN, spectrofluorimetric)	100	0
1+Cu^{2+} (ACN, spectrofluorimetric)	100	0
1+Cu^{2+} (ACN, spectrophotometric)	90	10
1+Fe^{3+} (ACN, spectrofluorimetric)	100	0
1+Fe^{3+} (ACN, spectrophotometric)	90	10
3+CN^- (ACN, spectrophotometric)	90	10
3+Cu^{2+} (ACN/H_2O, spectrophotometric)	90	10
5+CN^- (ACN/H_2O, spectrophotometric)	100	0
5+CN^- (ACN/H_2O, spectrofluorimetric)	—	—

The same pre-treatment was performed to spectral data as cited above. Statistical results for SLR, PCR and PLS models for ion concentration predictions using absorption and emission spectra are shown in **table 13**. The statistical parameters are presented for all the models.

Table 13- Evaluation and validation statistic parameters obtained with LR, PLS and PCR.

Titration	Learner	Calibration		Validation
		R^2	RMSE	RMSE
1+F$^-$ (ACN, spectrofluorimetric)	SLR	0.23	47139.76	34413.73
	PLS	-21.95	83.92	5.51
	PCR	-0.30	22.73	189.99
1+Cu^{2+} (ACN, spectrofluorimetric)	SLR	0.52	114068.57	11110.25
	PLS	-33.57	37.60	3.48
	PCR	-0.05	7.65	4.71
1+Cu^{2+} (ACN, spectrophotometric)	SLR	0.82	0.034	0.033
	PLS	0.70	3.45	0.15
	PCR	0.58	4.49	54.55
1+Fe^{3+} (ACN, spectrofluorimetric)	SSLR	0.76	126052.96	141351.02
	PLS	-24.32	19.65	1.63
	PCR	-0.81	5.19	54.55
1+Fe^{3+} (ACN, spectrophotometric)	SLR	0.88	0.20	0.10
	PLS	0.98	1.72	0.33
	PCR	0.99	1.40	0.51
3+CN$^-$ (ACN, spectrophotometric)	SLR	0.89	0.022	0.015
	PLS	0.66	16.69	1.18
	PCR	0.95	6.65	0.39
3+Cu^{2+} (ACN/H$_2$O, spectrophotometric)	SLR	0.44	0.04	0.30
	PLS	0.76	11.32	0.33
	PCR	0.76	15.09	1.18
5+CN$^-$ (ACN/H$_2$O, spectrophotometric)	SLR	0.73	94367.82	341087.41
	PLS	-43.56	17.56	2.87
	PCR	0.08	2.96	0.76
5+CN$^-$ (ACN/H$_2$O, spectrofluorimetric)	SLR	0.94	0.019	0.016
	PLS	—	—	—
	PCR	—	—	—

As example, in **figure 71**, are presented the graphic models for the spectrophotometric and titration of compound **1** with Fe^{3+}.

a)

b)

c)
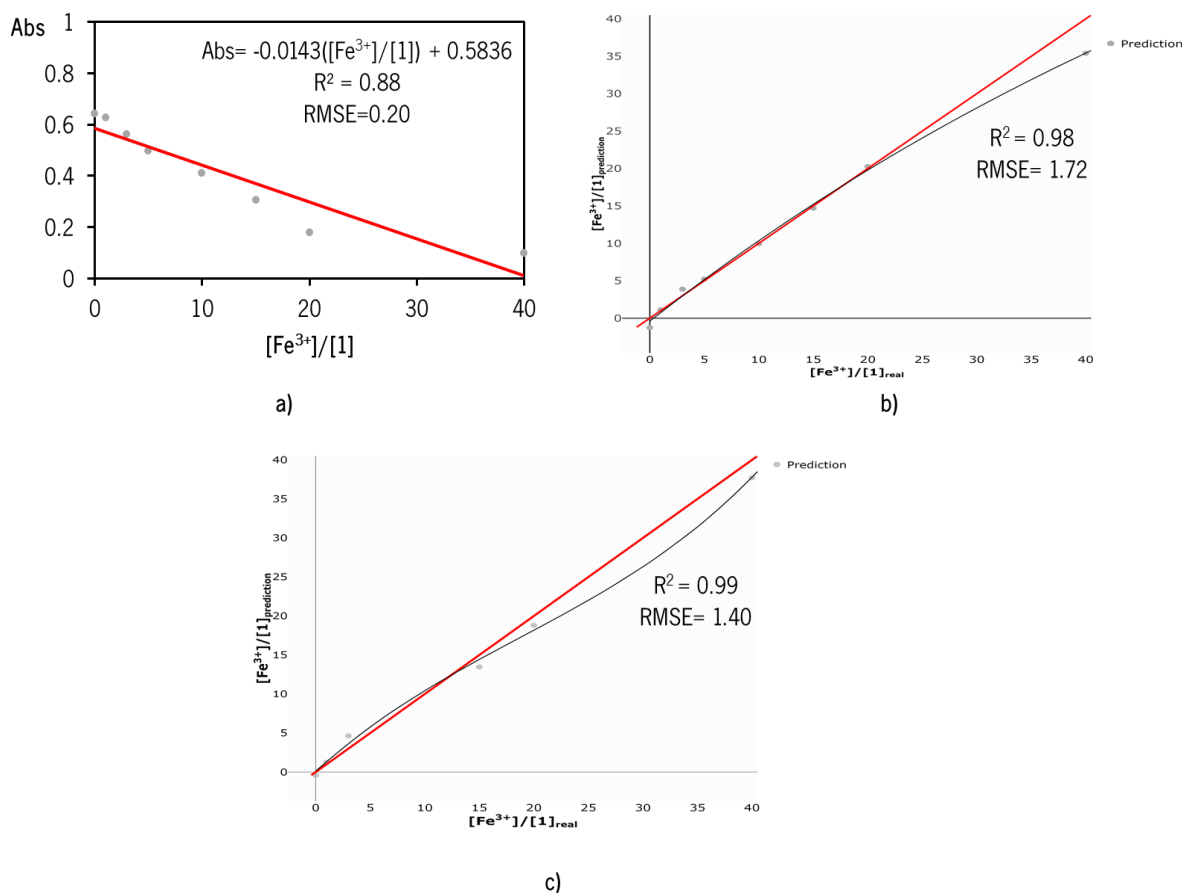
Figure 71- $[Fe^{3+}]/[1]$ predictive models: SLR (**a**), PLS (**b**) and PCR (**v**) using UV-vis spectral data.

For the SLR model, $[Fe^{3+}]/[1]$ was plotted against the absorbance at 497 nm, for the spectrophotometric titration. The changes in absorbance at 497 and 701 nm have information about the titration so both were studied showing that at 497 nm the fit between the data and the model is better, r^2 is closer to 1. The same strategy was applied for the other titration studies were important behavior is presented for two different wavelengths. In **table 14** are presented the considered wavelength for the SLR development.

Table 14- Spectrophotometric titration wavelengths considered for SLR models' development.

Probe	Ion	Important wavelengths (nm)	Chosen wavelength (nm)
1	Cu^{2+}	496 and 695	496
	Fe^{3+}	497 and 701	497

This disadvantage is overcome in the other models since the complete data sets are considered in the development, using all absorbances obtained for wavelengths between 200 and 800 nm.

Looking to the PLS and PCR models in **figure 71 b** and **c,** respectively, two lines appear. The red line is the calibration line while the black represents the fit of the results. The differences between the two lines can be compared to discuss the model performance. In this two cases is possible to see that the real value of $[Fe^{3+}]/[1]$ is similar to the predicted and the points tend to overlay the calibration line witch indicated a good performance of the model. The same conclusion can be taken with r^2 and RMSE values. In this specific case both PLS and PCR models can be used to predict the concentration of Fe^{3+} in presence of compound 1 with UV-vis spectral data.

When a lack of fit of the results happen the black line shows that the behavior of results are poor explained by the model and the different points tend to be far from the calibration, in other words the real value of $[Fe^{3+}]/[1]$ is completely different from the predicted, showing that the model cannot be used.

The lack of fit of the results and the poor predictions are accompanied with small r^2, and elevated values of RMSE.

As shown in **table 13**, although most models have statistical parameters that demonstrate the lack of fit of the spectral data to the predicted, some cases were found in which the ion concentration could be predicted by the model ($R^2 \approx 1$ and RMSE is near 0).

Attending to the results, 3 models can be used: PLS and PCR for quantification of Fe^{3+} with compound **1** based on UV-vis data and PCR for quantification of CN^- with compound **3** based on UV-vis data.

The validation of these two models is also satisfactory, when two new data sets correspondents to [ion]/[compound], in the working range, are tested the RMSE is almost 0 which indicates that difference between the experimental data and the predictions is minimum and the predictions are accurate.

The contrary also happens, for example in the quantification of CN^- with compound **5**. The models show a lack of fit between the predictions and the real values, and when studying the validation the predictions of $[CN^-]/[5]$ were inaccurate.

Based on the r^2 of the models where the same [ion]/[compound] was determined with data from different spectroscopies, the models developed with UV-vis data showed better fit of the results to de model which indicates that UV-Vis spectroscopy, is more useful for quantification of those specific ions (Cu^{2+} and Fe^{3+} in presence of compound **1**) than emission spectroscopy.

Chapter 4

Conclusions and Future Work

4.   Conclusion and Future work

New BODIPY derivatives functionalized with different functional groups were obtained through distinct synthetic pathways with moderate yields (22 - 63%). Derivative **1** h been synthesized through the condensation reaction between 2,4-dimethylpyrrole and 4-(diphenylamino)benzaldehyde. The functionalization of compound **1** with the formyl group at position 2 and 4'' through the Vilsmeier-Haack reaction gave derivative **2**. Derivative **3** functionalized with the vinyl-nitro group at position 2 and 4''was obtained through the Henry reaction between the formylated precursor **2** and nitromethane. All the derivatives were obtained through simple synthetic methodologies and an easy purification procedure.

The synthesized BODIPYs **2** and **3** were characterized by LRMS, IR spectroscopy, uni- and bidimensional ^{1}H and ^{13}C NMR spectroscopies, from which it was possible to confirm the chemical structures and the purity of the compounds.

The influence of the extension of the π-conjugate system and the electronic character of the functional groups on the photophysical properties of BODIPY derivatives and dicyanovinyl derivatives was evaluated by absorption and fluorescence spectroscopies in acetonitrile solutions. The results obtained demonstrated that the introduction of an electron-withdrawing group (derivative **2**) induces a hypsochromic shift in the absorption band; on the other hand, increasing the extension of the π-conjugate system through functionalization with a vinyl-nitro group, which has also electron-withdrawing character (derivative **3**) induces a bathochromic shift.

The dicyanovinyl derivatives showed that the functionalization with different types of aromatic moieties influenced the absorption band wavelength, thus proving that photophysical properties can be easily modulated for this type of compounds.

With regard to fluorescence spectra, no significant displacements of the emission bands happened for the BODIPYs as expected, since these compounds are known to display small Stokes' shifts, while the dicyanovinyl derivatives show significant Stokes' shifts.

The low quantum yield determined in acetonitrile for the all derivatives (Φ_F ≤0.012) may be related to the signaling mechanisms (PET and ICT).

The evaluation of BODIPY and dicyanovinyl derivatives as optical sensors was carried out through a preliminary study involving the addition of a fixed amount of ion (50 equiv) and, depending on the results obtained in the preliminary study, spectrophotometric and spectrofluorimetric titrations in acetonitrile and acetonitrile/water (8:2) were carried out for selected ions. It was possible to conclude that the functionalization of the BODIPY nucleus at position 2 and 4'' with different functional groups influences not only the selectivity and sensitivity of BODIPY but also the type of response obtained in the ion

recognition process. The BODIPY **1** derivative exhibited potential as a colorimetric sensor for Fe^{3+} and as fluorimetric sensor for F^-, and Fe^{3+}, in acetonitrile. On the other hand, the BODIPY **2** derivative proved to be a colorimetric sensor for CN^- in acetonitrile and, simultaneously, a colorimetric sensor for Cu^{2+} in acetonitrile/water (8:2). As for dicyanovinyl derivative **5**, it showed colorimetric and fluorimetric recognition behavior for CN^- in acetonitrile/water (8:2).

To complement this result, an ^1H NMR titration of compound **5** with CN^- in deuterated acetonitrile was performed showing the chemodosimeter capacity of this compound through the disappearance of the original signals and the development of a new set of signals corresponding to the new compound after addition of the cyanide to the vinyl double bond.

The evaluation of BODIPY and dicyanovinyl derivatives as optical sensors for selected amines and alcohol, acting as models for drugs of abuse such as codeine and fentanyl, in different media (ACN, DCM, ACN/phosphate buffer and ACN/PBS buffer), in presence and absence of possible interferents (urea and creatinine) was also carried out. These studies showed the influence of the media and salts on the fluorescence intensity and recognition ability of alcohols and amines.

Neither one of the compounds can be used as a selective probe for one specific alcohol or amine, but compound **2** reveals less interaction with the analytes than compound **5** mainly in at pH 6.5. Testing the capacity of recognition of amines and alcohols over time did not show significant differences. For these two compounds, urea is not an interferent in any media tested while creatinine in some cases changes the original fluorescence of the compounds.

The spectrophotometric and spectrofluorimetric raw data from the titrations were used to develop quantification models using different learning algorithms (SLR, PLS and PCR). Most of the developed models didn't show a satisfactory fit to the used regressions, but it was possible to develop models to quantify accurately Cu^2, Fe^{3+}, CN^- knowing the exact concentration of compounds **1**, **3** and **5**, respectively.

As future perspectives, compounds **1 - 5** could be evaluated as probes for metal cations in aqueous mixtures with higher water content in the presence of a surfactant such as sodium dodecylsulfate (SDS). Recent literature has reported that poorly water-soluble organic optical chemosensors can be embedded into the inner hydrophobic core of the SDS micelles, allowing optical detection of metal cations in aqueous solution. Also, it would be interesting to test the drugs, as originally intended, and their main metabolites. In terms of the chemometric model development, other learning algorithms, usually used for small data sets, can be tested to see the adjustment of the data, for example quadratic regression.

Chapter 5

Bibliography

5. Bibliography

1) Bhalla, V. Supramolecular chemistry from molecule to molecular machines. Reson. 2018, 23, 277–290. https://doi.org/10.1007/s12045-018-0617-z.

2) You, L.; Zha, D.; Anslyn, E. v. Recent advances in supramolecular analytical chemistry using optical sensing. *Chem. Rev.* **2015**, *115* (15), 7840–7892. https://doi.org/10.1021/cr5005524.

3) Fabbrizzi, L.; Poggi, A. sensors and switches from supramolecular chemistry. *Chem. Soc. Rev.* **1995**, *24* (3), 197–202. https://doi.org/10.1039/CS9952400197.

4) Svensson, J. O.; Yue, Q. Y.; Säwe, J. Determination of codeine and metabolites in plasma and urine using ion-pair high-performance liquid chromatography. *J. Chromatogr. B Biomed. Appl.* **1995**, *674* (1), 49–55. https://doi.org/10.1016/0378-4347(95)00292-1.

5) Berhanu, A. L.; Gaurav; Mohiuddin, I.; Malik, A. K.; Aulakh, J. S.; Kumar, V.; Kim, K. H. A review of the applications of schiff bases as optical chemical sensors. *Trends Anal. Chem.* **2019**, *116*, 74–91. https://doi.org/10.1016/j.trac.2019.04.025.

6) Schäferling, M. The Art of fluorescence imaging with chemical sensors. *Angew. Chem. Int. Ed.* **2012**, *51* (15), 3532–3554. https://doi.org/10.1002/anie.201105459.

7) Kolesnichenko, I.; Anslyn, E. Practical applications of supramolecular chemistry. *Chem. Soc. Rev.* **2017**, *46* (9), 2385–2390. https://doi.org/10.1039/c7cs00078b.

8) Wencel, D.; Abel, T.; McDonagh, C. Optical chemical pH sensors. *Anal. Chem.* **2014**, *86* (1), 15–29. https://doi.org/10.1021/ac4035168.

9) Frankær, C.; Sørensen, T. A unified approach for investigating chemosensor properties-dynamic characteristics. *R. Soc. Chem.* **2019**, *144* (7), 2208–2225. https://doi.org/10.1039/c9an00268e.

10) Wu, J.; Liu, W.; Ge, J.; Zhang, H.; Wang, P. New sensing mechanisms for design of fluorescent chemosensors emerging in recent years. *Chem. Soc. Rev.* **2011**, *40* (7), 3483–3495. https://doi.org/10.1039/c0cs00224k.

11) De Silva, A. P.; Gunaratne, H.; Gunnlaugsson, T.; Huxley, A.; McCoy, C.; Rademacher, J.; Rice, T. Signaling recognition events with fluorescent sensors and switches. *Chem. Rev.* **1997**, *97* (5), 1515–1566. https://doi.org/10.1021/cr960386p.

12) Basak, S.; Chattopadhyay, K. Studies of protein folding and dynamics using single molecule fluorescence spectroscopy. *Phys. Chem. Chem. Phys.* **2014**, *16* (23), 11139–11149. https://doi.org/10.1039/c3cp55219e.

13) Feng, G.; Zhang, G.-Q.; Ding, D. Design of superior phototheranostic agents guided by jablonski diagrams. *Chem. Soc. Rev.* **2020**, *49*, 8179-8234. https://doi.org/10.1039/d0cs00671h.

14) Andersson, P.; Gillbro, T. Photophysics and dynamics of the lowest excited singlet state in long substituted polyenes with implications to the very long-chain limit. *J. Chem. Phys.* **1998**, *103* (7), 2509. https://doi.org/10.1063/1.469672.

15) Berezin, M.; Achilefu, S. Fluorescence lifetime measurements and biological imaging. *Chem. Rev.* **2010**, *110* (5), 2641–2684. https://doi.org/10.1021/CR900343Z.

16) Ramprasad, M.; Shankar P. Bhattacharyya. An overview of the ICT process. In *Intramolecular Charge Transfer: Theory and Applications*; Weinheim, 1st Ed.; Wiley-VCH Verlag: Germany, **2018**; pp 1–3

17) De Silva, A. P.; Moody, T. S.; Wright, G. D. Fluorescent PET (photoinduced electron transfer) sensors as potent analytical tools. *Analyst* **2009**, *134* (12), 2385–2393. https://doi.org/10.1039/b912527m.

18) Escudero, D. Revising intramolecular photoinduced electron transfer (PET) from first-principles. *Acc. Chem. Res.* **2016**, *49* (9), 1816–1824. https:// doi.org/10.1021/acs.accounts.6b00299.

19) Yang, Y.; Zhao, Q.; Feng, W.; Li, F. Luminescent chemodosimeters for bioimaging. *Chem. Rev.* **2012**, *113* (1), 192–270. https://doi.org/10.1021/CR2004103.

20) Quang, D.; Kim, J. Fluoro- and chromogenic chemodosimeters for heavy metal ion detection in solution and biospecimens. *Chem. Rev.* **2010**, *110* (10), 6280–6301. https://doi.org/10.1021/CR100154P.

21) O'sullivan, J.; Colleran, J.; Heaney, F. Highly selective fluorimetric turn-off detection of copper(II) by two different mechanisms in calix[4]arene-based chemosensors and chemodosimeters. *ChemPlusChem* **2019**, *84* (10), 1610–1622. https://doi.org/10.1002/cplu.201900448.

22) Suganya, S.; Naha, S.; Velmathi, S. A critical review on colorimetric and fluorescent probes for the sensing of analytes via relay recognition from the Year 2012-17. *ChemistrySelect* **2018**, *3* (25), 7231-7268. https://doi.org/10.1002/slct.201801222.

23) Rasheed, T.; Li, C.; Bilal, M.; Yu, C.; Iqbal, H. M. N. Potentially Toxic Elements and Environmentally-Related Pollutants Recognition Using Colorimetric and Ratiometric Fluorescent Probes. *Sci. Total Environ.* **2018**, *640–641*, 174–193. https://doi.org/10.1016/j.scitotenv.2018.05.232.

24) Baumes, L. A.; Sogo, M. B.; Montes-Navajas, P.; Corma, A.; Garcia, H. A Colorimetric sensor array for the dtection of the date-rape drug g-hydroxybutyric acid (GHB): a supramolecular approach. *Chem. Eur. J.* **2010**, *16*, 4489–4495. https:// doi.org/10.1002/chem.200903127.

25) Rai, A.; Singh, A. Tripathi, K.; Sonkar, A.; Chauhan, B.; Srikrishna, S.; James, T.; Mishra, L. A quick and selective rhodamine based "smart probe" for "signal-on" optical detection of Cu^{2+} and Al^{3+} in water, cell imaging, computational studies and solid state analysis. *Sens. Actuators B Chem.* **2018**, *266*, 95–105. https://doi.org/10.1016/J.SNB.2018.02.019.

26) Aryal, G. H.; Hunter, K. W.; Huang, L. A Supramolecular red to near-infrared fluorescent probe for the detection of drugs in urine. *Org. Biomol. Chem.* **2018**, *16* (40), 7425–7429. https://doi.org/10.1039/C8OB02180E.

27) Niu, X.; Ye, K.; Wang, L.; Lin, Y.; Du, D. A review on emerging principles and strategies for colorimetric and fluorescent detection of alkaline phosphatase activity. *Anal. Chim. Acta* **2019**, *1086*, 29–45. https://doi.org/10.1016/J.ACA.2019.07.068.

28) Lu, H.; MacK, J.; Yang, Y.; Shen, Z. Structural Modification Strategies for the Rational Design of Red/NIR Region BODIPYs. *Chem. Soc. Rev.* **2014**, *43* (13), 4778–4823. https://doi.org/10.1039/c4cs00030g.

29) Luo, S.; Zhang, E.; Su, Y.; Cheng, T.; Shi, C. A review of NIR dyes in cancer targeting and imaging. *Biomaterials* **2011**, *32* (29), 7127–7138. https://doi.org/10.1016/j.biomaterials.2011.06.024.

30) Clarke, R. G.; Hall, M. J. Recent Developments in the Synthesis of the BODIPY Dyes. In *Advances in Heterocyclic Chemistry*; Scriven; Eric, Ramsden; Christopher, Eds.; Academic Press, **2019**; Vol. 128, pp 181–261. https://doi.org/10.1016/bs.aihch.2018.12.001.

31) Llano, R. S.; Zaballa, E. A.; Bañuelos, J.; Durán, C. F. A. G.; Vázquez, J. L. B.; Cabrera, E. P.; Arbeloa, I. L. Tailoring the Photophysical Signatures of BODIPY Dyes: Toward Fluorescence Standards across the Visible Spectral Region. In *Photochemistry and Photophysics - Fundamentals to Applications*; Saha, S., Mondal, S., Eds.; IntechOpen, **2018**; pp 21–40. https://doi.org/10.5772/intechopen.74848.

32) Niu, S. L.; Ulrich, G.; Ziessel, R.; Kiss, A.; Renard, P. Y.; Romieu, A. water-soluble BODIPY derivatives. *Org. Lett.* **2009**, *11* (10), 2049–2052. https://doi.org/10.1021/ol900302n.

33) Isik, M.; Ozdemir, T.; Turan, I. S.; Kolemen, S.; Akkaya, E. U. Chromogenic and fluorogenic sensing of biological thiols in aqueous solutions using BODIPY-based reagents. *Org. Lett.* **2013**, *15* (1), 216–219. https://doi.org/10.1021/ol303306s.

34) Liu, M.; Ma, S.; She, M.; Chen, J.; Wang, Z.; Liu, P.; Zhang, S.; Li, J. Structural modification of BODIPY: improve its applicability. *Chin. Chem. Lett.* **2019**, *30* (10), 1815–1824. https://doi.org/10.1016/j.cclet.2019.08.028.

35) Shimizu, S. Aza-BODIPY synthesis towards vis/NIR functional chromophores based on a schiff base forming reaction protocol using lactams and teteroaromatic amines. *Chem. Commun.* **2019**, *55* (60), 8722–8743. https://doi.org/10.1039/c9cc03365c.

36) Ni, Y.; Wu, J. Far-red and near infrared BODIPY dyes: synthesis and applications for fluorescent pH probes and bio-imaging. *Org. Biomol. Chem.* **2014**, *12* (23), 3774–3791. https://doi.org/10.1039/c3ob42554a.

37) Jean-Gérard, L.; Vasseur, W.; Scherninski, F.; Andrioletti, B. Recent advances in the synthesis of [*a*]-benzo-fused BODIPY fluorophores. *Chem. Commun.* **2018**, *54* (92), 12914–12929. https://doi.org/10.1039/c8cc06403b.

38) Ferreira, R.; Costa, S.; Raposo, M. Heterocyclic dicyanovinyl derivatives: synthesis and evaluation of the chemosensory ability in aqueous solution. *Proceedings* **2017**, *1* (2), 30. https://doi.org/10.3390/ECSA-3-B001.

39) Wang, L.; Li, L.; Cao, D. A BODIPY-based dye with red fluorescence in solid state and used as a fluorescent and colorimetric probe for highly selective detection of cyanide. *Sens. Actuators B Chem.* **2017**, *239*, 1307–1317. https://doi.org/10.1016/J.SNB.2016.09.112.

40) Li, Q.; Cai, Y.; Yao, H.; Lin, Q.; Zhu, Y.; Li, H.; Zhang, Y.; Wei, T. A colorimetric and fluorescent cyanide chemosensor based on dicyanovinyl derivatives: utilization of the mechanism of intramolecular charge transfer blocking. *Spectrochim. Acta A Mol. Biomol. Spectrosc.* **2015**, *136* (B), 1047–1051. https://doi.org/10.1016/J.SAA.2014.09.128.

41) El-Shishtawy, R.; Al-Zahrani, F.; Al-amshany, Z.; Asiri, A. Synthesis of a new fluorescent cyanide chemosensor based on phenothiazine derivative. *Sens. Actuators B Chem.* **2017**, *240*, 288–296. https://doi.org/10.1016/J.SNB.2016.08.168.

42) Ozdemir, A.; Erdemir, S. Phenanthroimidazole and dicyanovinyl-substituted triphenylamine for the selective detection of CN^-: DFT salculations and practically applications. *J. Photochem. Photobiol.* **2020**, *390*. https://doi.org/10.1016/j.jphotochem.2019.112328.

43) Ahern, J.; Stuber, J.; Galea, S. Stigma, discrimination and the health of illicit drug users. *Drug and Alcohol Dependence* **2007**, *88* (2–3), 188–196. https://doi.org/10.1016/j.drugalcdep.2006.10.014.

44) Saffer, H.; Chaloupka, F. The demand for illicit drugs. *Econ. Inq.* **1999**, *37* (3), 401–411. https://doi.org/10.1111/j.1465-7295.1999.tb01439.x

45) De Giovanni, N.; Fucci, N. The current status of sweat testing for drugs of abuse: a review. *Curr. Med. Chem.* **2013**, *20* (4), 545–561. https://doi.org/10.2174/0929867311320040006.

46) Agência Lusa. Pelo menos 8.300 mortos em 2018 na Europa por "overdose" de drogas ilícitas https://observador.pt/2020/09/22/pelo-menos-8-300-mortos-em-2018-na-europa-por-overdose-de-drogas-ilicitas/ (accessed 2021 -06 -26)

47) Volkow, N. D. Prescription Drugs: Abuse and Addiction. *National Institutes of Health*. **2001**, pp 1–16.

48) Le Boisselier, R.; Alexandre, J.; Lelong-Boulouard, V.; Debruyne, D. Focus on cannabinoids and synthetic cannabinoids. *Clinical Pharmacol. Ther.* **2017**, *101* (2), 220–229. https://doi.org/10.1002/cpt.563.

49) Whiting, P.; Wolff, R.; Deshpande, S.; Di Nisio, M.; Duffy, S.; Hernandez, A.; Keurentjes, J.; Lang, S.; Misso, K.; Ryder, S.; Schmidlkofer, S.; Westwood, M.; Kleijnen, J. Cannabinoids for medical use: a systematic review and meta-analysis. *JAMA* **2015**, *313* (24), 2456–2473. https://doi.org/10.1001/jama.2015.6358.

50) Andersson, M.; Scheidweiler, K.; Sempio, C.; Barnes, A.; Huestis, M. Simultaneous quantification of 11 cannabinoids and metabolites in human urine by liquid chromatography tandem mass spectrometry using WAX-S tips. *Anal. Bioanal. Chem.* **2016**, *408* (23), 6461–6471. https://doi.org/10.1007/s00216-016-9765-8.

51) Messina, F.; Rosati, O.; Curini, M.; Marcotullio, M. C. Cannabis and Bioactive Cannabinoids. *Stud. Nat. Prod. Chem.* **2015**, 45, 17–57. https://doi.org/10.1016/B978-0-444-63473-3.00002-2.

52) Kemp, P.; Abukhalaf, I.; Manno, J.; Manno, B.; Alford, D.; Mc Williams, M.; Nixon, F.; Fitzgerald, M.; Reeves, R.; Wood, M. Cannabinoids in humans. ii. the influence of three methods of hydrolysis on the concentration of THC and two metabolites in urine. *J. Anal. Toxicol.* **1995**, *19* (5), 292–298. https://doi.org/10.1093/jat/19.5.292.

53) Somogyi, A.; Barratt, D.; Coller, J. Pharmacogenetics of opioids. *Clin. Pharm. Therap.* **2007**, *81* (3), 429–444. https://doi.org/10.1038/sj.clpt.6100095.

54) Eisch, A.; Barrot, M.; Schad, C.; Self, D.; Nestler, E. Opiates inhibit neurogenesis in the adult rat hippocampus. *PNAS* **2000**, *97* (13), 7579–7584. https://doi.org/10.1073/pnas.120552597.

55) Armstrong, S.; Wynn, G.; Sandson, N. Pharmacokinetic drug interactions of synthetic opiate analgesics. *Psychosomatics* **2009**, *50* (2), 169–176. https://doi.org/10.1176/appi.psy.50.2.169.

56) Sindrup, S. H.; Brøsen, K. The Pharmacogenetics of Codeine Hypoalgesia. *Pharmacogenetics* **1995**, *5* (6), 335–346. https://doi.org/10.1097/00008571-199512000-00001.

57) Kirchheiner, J.; Schmidt, H.; Tzvetkov, M.; Keulen, J.; Lötsch, J.; Roots, I.; Brockmöller, J. Pharmacokinetics of codeine and its metabolite morphine in utra-rapid metabolizers due to CYP2D6 duplication. *Pharmacogenomics* **2007**, *7* (4), 257–265. https://doi.org/10.1038/sj.tpj.6500406.

58) Bista, S.; Lobb, M.; Haywood, A.; Hardy, J.; Tapuni, A.; Norris, R. Development, validation and Application of an HPLC-MS/MS method for the determination of fentanyl and nor-fentanyl in human plasma and saliva. *J. Chromatogr. B: Anal. Technol. Biomed. Life Sci.* **2014**, *960*, 27–33. https://doi.org/10.1016/j.jchromb.2014.04.019.

59) Qin, N.; Xiang, P.; Shen, B.; Zhuo, X.; Shi, Y.; Song, F. Application of a validated UHPLC-MS/MS method for 28 fentanyl-analogue and novel synthetic opioids in whole blood in authentic forensic cases. *J J. Chromatogr. B: Anal. Technol. Biomed. Life Sci.* **2019**, *1124*, 82–99. https://doi.org/10.1016/j.jchromb.2019.05.025.

60) Wilde, M.; Pichini, S.; Pacifici, R.; Tagliabracci, A.; Busardò, F.; Auwärter, V.; Solimini, R. Metabolic pathways and potencies of new fentanyl analogs. *Front. Pharmacol.* **2019**, *10*, 1–16. https://doi.org/10.3389/fphar.2019.00238.

61) Cone, E. J. Legal, workplace, and treatment drug testing with alternate biological matrices on a global scale. *Forensic Sci. Int.* **2001**, *121* (1–2), 7–15. https://doi.org/10.1016/S0379-0738(01)00446-7.

62) Maralikova, B.; Weinmann, W. Confirmatory analysis for drugs of abuse in plasma and urine by high-performance liquid chromatography-tandem mass spectrometry with respect to criteria for compound identification. *J. Chromatogr. B: Anal. Technol. Biomed. Life Sci.* **2004**, *811*(1), 21–30. https://doi.org/10.1016/j.jchromb.2004.04.039.

63) Kemp, P.; Abukhalaf, I.; Manno, J.; Manno, B.; Alford, D.; Abusada, G. Cannabinoids in humans. I. Analysis of Δ⁹-tetrahydrocannabinol and six metabolites in plasma and urine using GC-MS. *J. Anal. Toxicol.* **1995**, *19* (5), 285–291. https://doi.org/10.1093/jat/19.5.285.

64) Milman, G.; Barnes, A; Lowe, R.; Huestis, M. Simultaneous quantification of cannabinoids and metabolites in oral fluid by two-dimensional gas chromatography mass spectrometry. *J. Chromatogr. A* **2010**, *1217* (9), 1513–1521. https://doi.org/10.1016/j.chroma.2009.12.053.

65) Sobolevsky, T.; Prasolov, I.; Rodchenkov, G. Detection of urinary metabolites of AM-2201 and UR-144, two novel synthetic cannabinoids. *Drug Test. Anal.* **2012**, *4* (10), 745–753. https://doi.org/10.1002/dta.1418.

66) Diao, X.; Huestis, M. A. Approaches, challenges, and advances in metabolism of new synthetic cannabinoids and identification of optimal urinary marker metabolites. *CPT* **2017**, 101 (2), 239–253. https://doi.org/10.1002/cpt.534.

67) Arntson, A.; Ofsa, B.; Lancaster, D.; Simon, J. R.; McMullin, M.; Logan, B. Validation of a novel immunoassay for the detection of synthetic cannabinoids and metabolites in urine specimens. *J. Anal. Toxicol.* 2013, 37 (5), 284–290. https://doi.org/10.1093/jat/bkt024.

68) Nelson, P.; Fletcher, S.; Moffat, A. A combined high-performance liquid chromatography and immunoassay method for the analysis of morphine, codeine and their metabolites in biological fluids. *J. Forensic Sci.* **1980**, *20* (3), 195–202. https://doi.org/10.1016/S0015-7368(80)71339-7.

69) Wasels, R.; Belleville, F. Gas chromatographic-mass spectrometric procedures used for the identification and determination of morphine, codeine and 6-monoacetylmorphine. *J. Chromatogr. A* 1994, *674* (1–2), 225–234. https://doi.org/10.1016/0021-9673(94)85227-8.

70) Fogarty, M.; Papsun, D.; Logan, B. Analysis of fentanyl and 18 novel fentanyl analogs and metabolites by LC-MS-MS, and report of fatalities associated with methoxyacetylfentanyl and cyclopropylfentanyl. *J. Anal. Toxicol.* **2018**, *42* (9), 592–604. https://doi.org/10.1093/jat/bky035.

71) Strayer, K.; Antonides, H.; Juhascik, M.; Daniulaityte, R.; Sizemore, I. LC-MS/MS-based method for the multiplex detection of 24 fentanyl analogues and metabolites in whole blood at sub ng mL^{-1} concentrations. *ACS Omega* **2018**, *3* (1), 514–523. https://doi.org/10.1021/acsomega.7b01536.

72) Silverstein, J.; Rieders, M.; McMullin, M.; Schulman, S.; Zahl, K. An analysis of the duration of fentanyl and its metabolites in urine and saliva. *Anesth. Analg.* **1993**, *76* (3), 618–621. https://doi.org/10.1213/00000539-199303000-00030.

73) Camann, W. Identification and quantitative determination of fentanyl metabolites in patients by gas chromatography-mass spectrometry. *Anesthesiology* 1992, *77* (5), 73-77.

74) Axelson, M.; Mork, B.; Sjovallt, J. Occurrence of 3β-hydroxy-5-cholestenoic acid, 3β, 7α-dihydroxy-5-Cholestenoic Acid, and 7α - hydroxy-3-oxo-4-cholestenoic acid as normal constituents in human blood. **1988**, *29*, 629–641. https://doi.org/10.1016/S0022-2275(20)38509-6

75) Willems, P.; Peter W.; Verdaasdonk, R.; van Swol, C.; Jansen, G. Urine analysis by laser raman spectroscopy. *Lasers Surg. Med.* **2001**, *28* (4), 330–334. https://doi.org/10.1002/lsm.1058.

76) Chipako, T.; Randall, D. Urine treatment technologies and the importance of pH. *J. Environ. Chem. Eng.* **2020**, *8* (1), 103622. https://doi.org/10.1016/J.JECE.2019.103622.

77) Lin, S.; Lee, H.; Lee, J.; Chen, B. Urine specimen validity test for drug abuse testing in workplace and court settings. *J. Food Drug Anal. Analysis* **2018**, *26* (1), 380–384. https://doi.org/10.1016/J.JFDA.2017.01.001.

78) Qian X.; Xu, Z. Fluorescence imaging of metal ions implicated in diseases. *Chem. Soc. Rev* **2015**, *44* (14), 4487–4493. https://doi.org/10.1039/C4CS00292J.

79) Williams, R.; Phil, D. Role of transition metal ions in biological processes. R.I. C. Reviews **1968**, *1*(1), 13-38.

80) Valeur, B.; Leray, I. Design principles of fluorescent molecular sensors for cation recognition. *Coord. Chem. Rev.* **2000**, *205* (1), 3–40. https://doi.org/10.1016/S0010-8545(00)00246-0.

81) Robert Crichton. *Biological inorganic chemistry: a new introduction to molecular structure*, 2nd ed.; Elsevier: Amsterdam, 2012.

82) Wang, H.; Xue, L.; Jiang, H. Ratiometric fluorescent sensor for silver ion and its resultant Complex for iodide anion in aqueous solution. *Org. Lett.* **2011**, *13* (15), 3844–3847. https://doi.org/10.1021/OL2013632.

83) Kim, H.; Kim, K.; Song, E.; Hwang, I.; Noh, J.; Kim, P.; Jeong, K.; Kim, C. Turn-on selective fluorescent probe for trivalent cations. *Inorg. Chem. Commun.* **2013**, *36*, 72–76. https://doi.org/10.1016/J.INOCHE.2013.08.025.

84) Okda, H.; el Sayed, S.; Otri, I.; Ferreira, R.; Costa, S.; Raposo, M.; Martínez-Máñez, R.; Sancenón, F. A simple and easy-to-prepare imidazole-based probe for the selective chromo-fluorogenic recognition of biothiols and Cu(II) in aqueous environments. *Dyes Pigm.* **2019**, *162*, 303–308. https://doi.org/10.1016/j.dyepig.2018.10.017.

85) Okda, H.; el Sayed, S.; Otri, I.; Ferreira, R.; Costa, S.; Raposo, M.; Martínez-Máñez, R.; Sancenón, F. 2,4,5-Triaryl imidazole probes for the selective chromo-fluorogenic detection of Cu(II). prospective use of the Cu(II) complexes for the optical recognition of biothiols. *Polyhedron* **2019**, *170*, 388–394. https://doi.org/10.1016/j.poly.2019.05.055.

86) Yang, Z.; Zhao, Y.; Chen, S.; Bu, Y.; Zhu, X.; Du, Y.; Li, F. A highly sensitive and selective colorimetric "off-on" chemosensor for Cu^{2+} in aqueous media based on a rhodamine derivative bearing thiophene group. *Sens. Actuators B Chem.* **2016**, *235*, 414–419. https://doi.org/10.1016/j.snb.2016.05.084.

87) Dong, W.; Akogun, S.; Zhang, Y.; Sun, Y.; Dong, X. A reversible "turn-on" fluorescent sensor for selective detection of Zn^{2+}. *Sens. Actuators B Chem.* **2017**, *238*, 723–734. https://doi.org/10.1016/j.snb.2016.07.047.

88) Ferreira, R.; Costa, S.; Gonçalves, H.; Belsley, M.; Raposo, M. Fluorescent phenanthroimidazoles functionalized with heterocyclic spacers: synthesis, optical chemosensory ability and two-photon absorption (TPA) properties. *New J. Chem.*, *41* (21), 12866–12878. https://doi.org/10.1039/c7nj02113e.

89) Batista, R.; Oliveira, E.; Costa, S.; Lodeiro, C.; Raposo, M. (Oligo)thienyl-imidazo-benzocrown ether derivatives: synthesis, photophysical studies and evaluation of their chemosensory properties. *Talanta* **2011**, *85* (5), 2470–2478. https://doi.org/10.1016/J.TALANTA.2011.07.107.

90) Kielhorn, J.; Melber, C.; Keller, D.; Mangelsdorf, I. Palladium – a review of exposure and effects to human health. *Int. J. Hyg. Environ. Health* **2002**, *205* (6), 417–432. https://doi.org/10.1078/1438-4639-00180.

91) Garrett, C.; Prasad, K. The art of meeting palladium specifications in active pharmaceutical ingredients produced by Pd-catalyzed reactions. *Adv. Synth. Catal.* **2004**, *346* (8), 889–900. https://doi.org/10.1002/ADSC.200404071.

92) Batista, R. M.; Oliveira, E.; Costa, S.; Lodeiro, C.; Raposo, M. Imidazo-benzo-15-crown-5 ethers bearing arylthienyl and bithienyl moieties as novel fluorescent chemosensors for Pd^{2+} and Cu^{2+}. *Tetrahedron* **2011**, *67* (37), 7106–7113. https://doi.org/10.1016/J.TET.2011.06.106.

93) Ha, E.; Basu, N.; Bose-O'Reilly, S.; Dórea, J.; McSorley, E.; Sakamoto, M.; Chan, H. Current progress on understanding the impact of mercury on human health. *Environ. Res.* **2017**, *152*, 419–433. https://doi.org/10.1016/J.ENVRES.2016.06.042.

94) Vergilio C.; Carvalho C.; Melo E. Metercury-Induced Dysfunctions in Multiple Organelles Leading to Cell Death. *Toxicology in Vitro* **2015**, *29* (1), 63–71.

95) Melber; C.; Keller; D.; Mangelsdorf; I. *Palladium*; World Health Organization: Geneva, 2002.

96) Zhou, Y.; Huang, Q.; Zhang, Q.; Min, Y.; Wang, E. A simple-structured acridine derivative as a fluorescent enhancement chemosensor for the detection of Pd^{2+} in aqueous media. *Spectrochim. Acta A Mol. Biomol. Spectrosc.* **2015**, *137*, 33–38. https://doi.org/10.1016/J.SAA.2014.08.018.

97) Martínez-Máñez, R.; Sancenón, F. Fluorogenic and chromogenic chemosensors and reagents for anions. *Chem. Rev.* **2003**, *103* (11), 4419–4476. https://doi.org/10.1021/cr010421e.

98) Busschaert, N.; Caltagirone, C.; Rossom, W.; Gale, P. Applications of supramolecular anion recognition. *Chem.Rev.* **2015**, *115* (15), 8038–8155. https://doi.org/10.1021/ACS.CHEMREV.5B00099.

99) Gale, P.; Howe, E.; Wu, X. Anion receptor chemistry. *Chem.* **2016**, *1* (3), 351–422. https://doi.org/10.1016/J.CHEMPR.2016.08.004.

100) Langton, M.; Serpell, C.; Beer, P. Anion recognition in water: recent advances from a supramolecular and macromolecular perspective. *Angew. Chem. Int. Ed.* **2016**, *55* (6), 1974–1987. https://doi.org/10.1002/ANIE.201506589.

101) Ferreira, R.; Costa, S.; Gonçalves, H.; Belsley, M.; Raposo, M. Fluorescent phenanthroimidazoles functionalized with heterocyclic spacers: synthesis, optical chemosensory ability and two-photon absorption (TPA) properties. *New J. Chem.* **2017**, *41* (21), 12866–12878. https://doi.org/10.1039/C7NJ02113E.

102) Ayoob, S.; Gupta, A. Fluoride in drinking water: a review on the status and stress effects. **2007**, *36* (6), 433–487. https://doi.org/10.1080/10643380600678112.

103) World Health Organization. *Guidelines for Drinking-Water Quality*; WORLD HEALTH ORGANIZATION: Geneva, 2004; Vol. 1.

104) Batista, R.; Costa, S.; Raposo, M. Selective colorimetric and fluorimetric detection of cyanide in aqueous solution using novel heterocyclic imidazo-anthraquinones. *Sens. Actuators B Chem.* **2014**, *191*, 791–799. https://doi.org/10.1016/j.snb.2013.10.030.

105) Ho, T.; Scranton, M.; Taylor, G.; Varela, R.; Thunell, R.; Muller-Karger, F. Acetate cycling in the water column of the cariaco basin: seasonal and vertical variability and implication for carbon cycling. *Limnol. Oceanogr. Lett.* **2002**, *47* (4), 1119–1128. https://doi.org/10.4319/LO.2002.47.4.1119.

106) Sternberg, J.; Stillo, H.; Schwendeman, R. Spectrophotometric Analysis of Multicomponent Systems Using the Least Squares Method in Matrix Form. *Anal. Chem.* **1960**, *32* (1), 84–90. doi.org/10.1021/ac60157a025

107) Hansch, C.; Fujita, T. A method for the correlation of biological activity and chemical structure. *J. Am. Chem. Soc.* **1964**, *86* (8), 1616–1626. https://doi.org/10.1021/ja01062a035.

108) Maeder, M.; Neuhold, Y. Introduction. In *Practical data analysis in chemistry*; Rutan, S., Walczak, B., Eds.; Elsevier: Callaghan, 2007; Vol. 26, pp 1–6. (112) Samuel, A. L. Some Studies in Machine Learning Using the Game of Checkers. *IBM Journal* **1959**, 535–554.

109) Samuel, A. L. Some Studies in Machine Learning Using the Game of Checkers. *IBM Journal* **1959**, *3* (3), 210–229. https://doi.org/10.1147/rd.33.0210

110) Raina, R.; Madhavan, A.; Ng, A. Y. Large-Scale Deep Unsupervised Learning Using Graphics Processors. In *Proceedings of the 26th International Conference On Machine Learning, ICML 2009*; Canada, 2009; pp 873–880.

111) Lecun, Y.; Bengio, Y.; Hinton, G. Deep learning. *Nature* **2015**, *521* (7553), 436–444. https://doi.org/10.1038/nature14539.

112) Bahrami, M.; Singhal, M. The Role of Cloud Computing Architecture in Big Data. In *Information Granularity, Big Data, and Computational Intelligence*; Pedrycz, W., Chen SM., Eds.; Springer Internation: Switzerland, 2015; Vol. 8, pp 275–295. https://doi.org/10.1007/978-3-319-08254-7_13.

113) Li, H.; Phung, D. Journal of Machine Learning Research: Preface. *JMLR* **2014**, *39* (2014), i–ii.

114) Samuel, A. Some studies in machine learning using the game of checkers. II-Recent Progress. *IBM J.* **1967**, *11* (6), 601–617. https://doi.org/10.1147/rd.116.0601.

115) Luu-Tan, R.; Cella, R. Experimental Design: Introduction. In *Comprehensive Chemometrics: Chemical and Biochemical Data Analysis*; Brown, S., Tauler, R., Eds.; Elsevier: Newark, 2009; Vol. 1, pp 247–250.

116) Helbing, D.; Frey, B. S.; Gigerenzer, G.; Hafen, E.; Hagner, M.; Hofstetter, Y.; van den Hoven, J.; Zicari, R. v.; Zwitter, A. Will Democracy Survive Big Data and Artificial Intelligence? In *Towards Digital Enlightenment: Essays on the Dark and Light Sides of the Digital Revolution*; Springer International Publishing, 2018; pp 73–98. https://doi.org/10.1007/978-3-319-90869-4_7.

117) Wang, X.; Esquerre, C.; Downey, G.; Henihan, L.; O'Callaghan, D.; O'Donnell, C. Development of chemometric models using vis-NIR and raman Spectral data fusion for assessment of infant formula storage temperature and time. *Innov Food Sci Emerg Technol.* **2020**, *67*,102551. https://doi.org/10.1016/j.ifset.2020.102551.

118) Sridharan, M. Machine learning algorithms mindmap https://jixta.wordpress.com/2015/07/17/machine-learning-algorithms-mindmap/ (accessed 2020 -12 -13).

119) Osisanwo, F.; Akinsola, J.; Hinmikaiye, O.; Olakanmi, O.; Akinjobi, J. Supervised machine learning algorithms: classification and comparison. *IJCTT* **2017**, *48* (3), 128–138. https://doi.org/10.14445/22312803/ijctt-v48p126.

120) Ringnér, M. What is principal component analysis? *Nat. Biotechnol.* **2008**, *26* (3), 303–304. https://doi.org/10.1038/nbt0308-303.

121) Kumar, K. Principal component analysis: most favourite tool in chemometrics. *Resonance* **2017**, *22* (8), 747–759. https://doi.org/10.1007/s12045-017-0523-9.

122) Nørgaard, L.; Wagner, J., Nielsen, P.; Munck, L.; Saudland, A.; Engelsen, S. Interval partial least-squares regression (IPLS): a comparative chemometric study with an example from near-infrared spectroscopy. *Appl. Spectrosc.*2000, *54* (3), 413–419.

123) Sampaio, P.; Soares, A.; Castanho, A.; Almeida, A.; Oliveira, J.; Brites, C. Optimization of rice amylose determination by NIR-spectroscopy using PLS chemometrics algorithms. *Food Chem.* **2018**, *242*, 196–204. https://doi.org/10.1016/j.foodchem.2017.09.058.

124) Xie, L.; Ye, X.; Liu, D.; Ying, Y. Quantification of glucose, fructose and sucrose in bayberry juice by NIR and PLS. *Food Chem.* **2009**, *114* (3), 1135–1140. https://doi.org/10.1016/j.foodchem.2008.10.076.

125) Tranmer, M.; Murphy, J.; Elliot, M.; Pampaka, M. *Multiple Linear Regression*, 2nd ed.; 2020.

126) Mevik, B.; Cederkvist, H. Mean squared error of prediction (MSEP) estimates for principal component regression (PCR) and partial least squares regression (PLSR). *J. Chemom.* **2004**, *18* (9), 422–429. https://doi.org/10.1002/cem.887.

127) Sutter, J.; Kalivas, J.; Lang, P. Which principal components to utilize for principal component regression. *J. Chemom.* **1992**, *6* (4), 217–225. https://doi.org/10.1002/CEM.1180060406.

128) Walczak, B.; Chem, I.; D.espagne, F.; de Maesschalck, R.; Estienne, F.; Verdú-Andrés, J.; Candolfi, A.; Centner, V.; Despagne, F.; Jouan-Rimbaud, D.; Walczak, B.; Massart, D.; de Jong, S.; de Noord, O; Puel, C.; Vandeginste, B. The Development of calibration models for spectroscopic data using principal component regression. *Internet J.Chem*, **1999**, *2* (19).

129) Lakshmi, V.; Rao, M.; Ravikanth, M. Halogenated boron-dipyrromethenes: synthesis, properties and applications. *Org. Biomol. Chem.* **2015**, *13* (9), 2501–2517. https://doi.org/10.1039/C4OB02293A.

130) Utiel, E.; Montalvillo, L.; Esnal, I.; Montero, R.; Agarrabeitia, A.; García, I.; Bañuelos, J.; López, I.; Moya, S.; Ortiz, M. Controlling Vilsmeier-Haack processes in meso-methylBODIPYs: a new way to modulate finely photophysical properties in boron dipyrromethenes. *Dyes Pigm.* **2017**, *141*, 286–298. https://doi.org/10.1016/j.dyepig.2017.02.030.

131) Zhang, X.; Feng, N. Photoinduced electron transfer-based halogen-free photosensitizers: covalent meso-aryl (phenyl, naphthyl, anthryl, and pyrenyl) as electron donors to effectively induce the formation of the excited triplet state and singlet oxygen for BODIPY compounds. *Chem. Asian J* **2017**, *12* (18), 2447–2456. https://doi.org/10.1002/asia.201700794.

132) Neelakandeswari, N.; Sangami, G.; Emayavaramban, P.; Karvembu, R.; Dharmaraj, N.; Kim, H. Mesoporous nickel hydroxyapatite nanocomposite for microwave-assisted Henry reaction. *Tetrahedron Lett.* **2012**, *53* (24), 2980–2984. https://doi.org/10.1016/j.tetlet.2012.03.086.

133) Herbivo, C.; Comel, A.; Kirsch, G.; Fonseca, A.; Belsley, M.; Raposo, M. Synthesis and characterization of novel, thermally atable 2-aryl-5-dicyanovinylthiophenes and 5-aryl-5′-dicyanovinyl-2,2′-bithiophenes as potentially promising non-linear optical materials. *Dyes Pigm.* **2010**, *86* (3), 217–226. https://doi.org/10.1016/J.DYEPIG.2010.01.006.

134) Khopkar, S.; Jachak, M.; Shankarling, G. Viscosity Sensitive semisquaraines based on 1, 1, 2-trimethyl-1H-benzo[e]indole: photophysical properties, intramolecular charge transfer, solvatochromism, electrochemical and DFT study. *J. Mol. Liq.* **2019**, *285*, 123–135. https://doi.org/10.1016/J.MOLLIQ.2019.03.173.

135) Ye, S.; Wu, C.; Gu, P.; Xiang, T.; Zhang, S.; Jing, T.; Wang, S.; Yang, X.; Li, Y.; Huang, W. A benzoindole-cored building block for deep blue fluorescent materials: synthesis, photophysical properties, and applications in organic light-emitting diodes. *J. Mater. Chem. C*, *8* (47), 16870–16879. https://doi.org/10.1039/D0TC04221H.

136) Pina, J.; Melo, J.; Batista, R.; Costa, S.; Raposo, M. The influence of the relative position of the thiophene and pyrrole rings in donor–acceptor thienylpyrrolyl-benzothiazole derivatives. A photophysical and theoretical investigation. *Phys. Chem. Chem. Phys.* **2010**, *12* (33), 9719–9725. https://doi.org/10.1039/C002434A.

Appendix

Preliminary assays with alcohols and amines supplementary figures
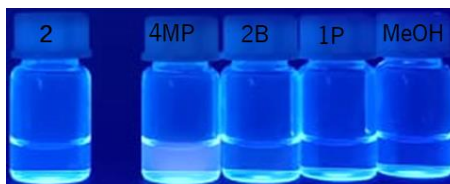
Figure A1-Fluorimetric changes of BODIPY 2 with 50 equiv of each alcohol in ACN, 2 hours after addition.
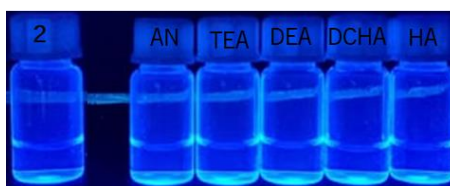
Figure A2- Fluorimetric changes of BODIPY 2 with 50 equiv of each amine in ACN/phosphate buffer pH 6.5 (3:1), 2 hours after addition.
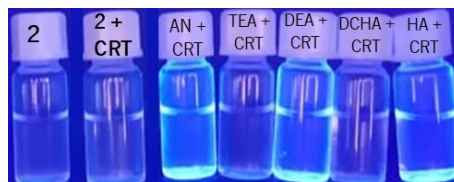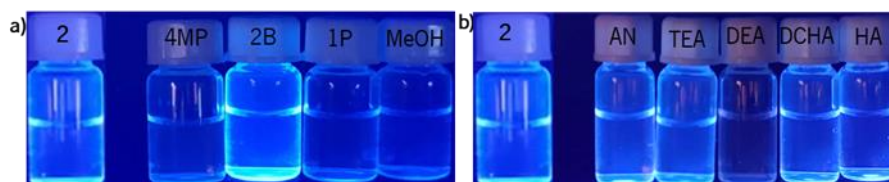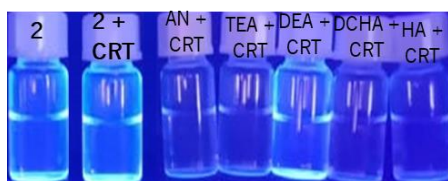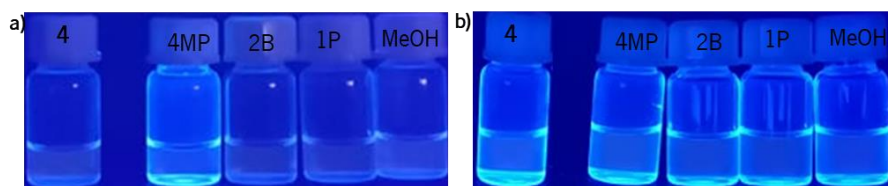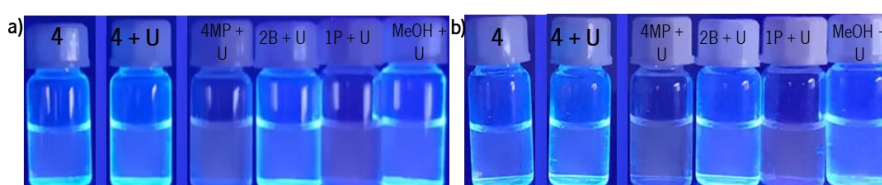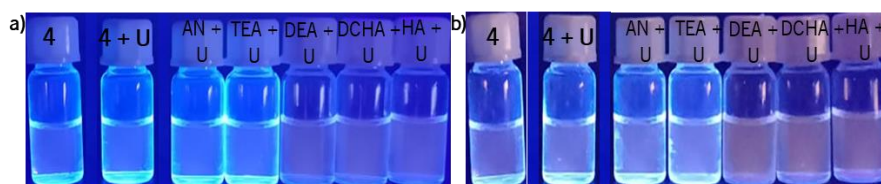

Figure A3- Fluorimetric changes of BODIPY **2** with 50 equiv of each amine and U in ACN/phosphate buffer pH 6.5 (3:1), 2 hours after addition.
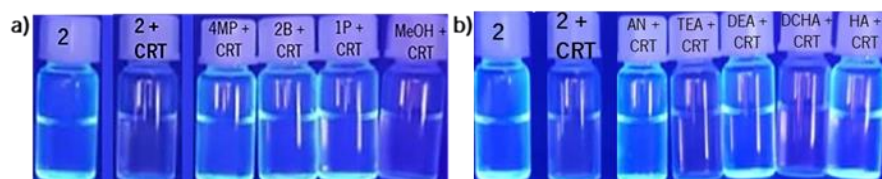
Figure A4- Fluorimetric changes of BODIPY **2** with 50 equiv of each alcohol (**a**), amine (**b**) and CRT in ACN/phosphate buffer pH 6.5 (3:1), 2 hours after addition.
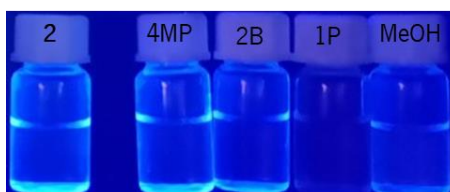
Figure A5- Fluorimetric changes of BODIPY 2 with 50 equiv of each alcohol in ACN/phosphate buffer pH 7.0 (3:1), 2 hours after addition.
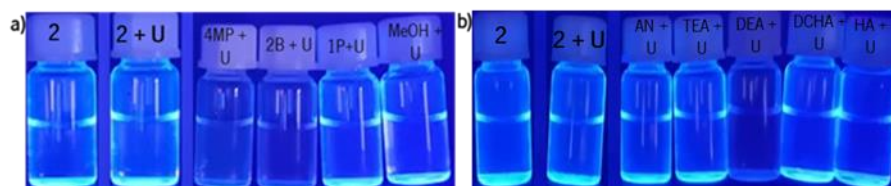
Figure A6- Fluorimetric changes of BODIPY **2** with 50 equiv of each alcohol (**a**), amine (**b**) and U in ACN/phosphate buffer pH 7.0 (3:1), 2 hours after addition.

Figure A7- Fluorimetric changes of BODIPY **2** with 50 equiv of each alcohol (**a**) and amine (**b**) and CRT in ACN/phosphate buffer pH 7.0 (3:1), 2 hours after addition.

Figure A8- Fluorimetric changes of BODIPY **2** with 50 equiv of each alcohol (**a**) and amine (**b**) in ACN/PBS pH 7.4 (3:1), 2 hours after addition.
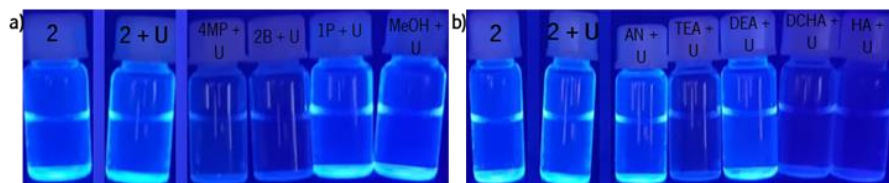
Figure A9- Fluorimetric changes of BODIPY **2** with 50 equiv of each alcohol (**a**), amine (**b**) and U in ACN/PBS pH 7.4 (3:1), 2 hours after addition.

Figure A10- Fluorimetric changes of BODIPY **2** with 50 equiv of each amine and CRT in ACN/PBS pH 7.4 (3:1), 2 hours after addition.

Figure A11- Fluorimetric changes of dicyanovinyl derivative **4** with 50 equiv of each alcohol in ACN, 2 hours (**a**) and 1 week (**b**) after addition.
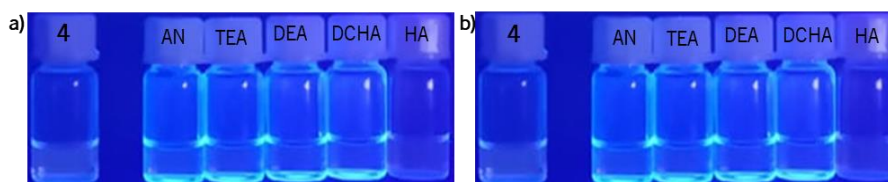
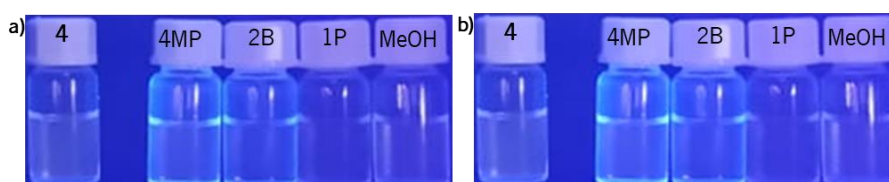**Figure A12** – Fluorimetric changes of dicyanovinyl derivative **4** with 50 equiv of each amine in ACN, 2 hours (**a**) and 1 week (**b**) after addition.
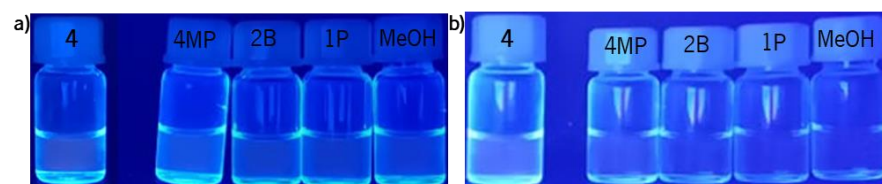
Figure A13- Fluorimetric changes of dicyanovinyl derivative **4** with 50 equiv of each alcohol in ACN/phosphate buffer pH 6.5 (3:1), 2 hours (**a**) and 1 week (**b**).
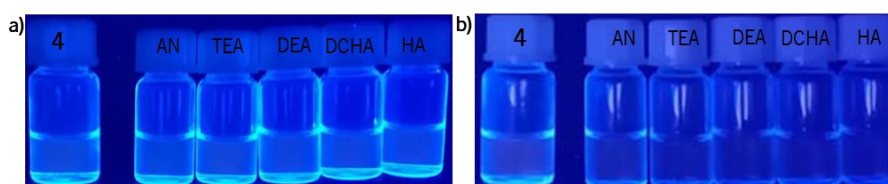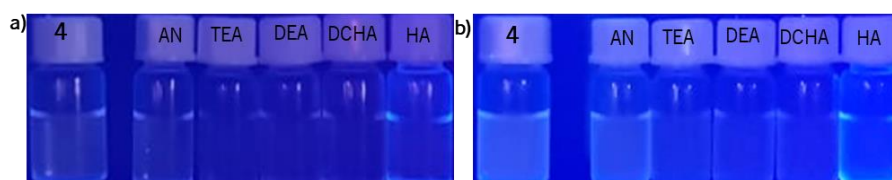

Figure A14- Fluorimetric changes of dicyanovinyl derivative **4** with 50 equiv of each amine in ACN/phosphate buffer pH 6.5 (3:1), 2 hours (**a**) and 1 week (**b**).
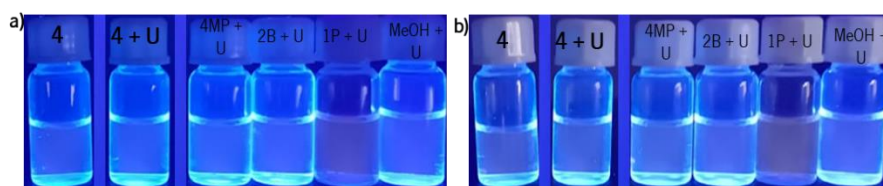

Figure A15- Fluorimetric changes of dicyanovinyl derivative **4** with 50 equiv of each alcohol and U in ACN/phosphate buffer pH 6.5 (3:1), 2 hours (**a**) and 1 week (**b**).
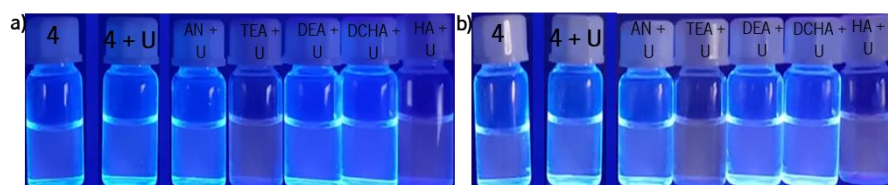
Figure A16 - Fluorimetric changes of dicyanovinyl derivative **4** with 50 equiv of each amine and U in ACN/phosphate buffer pH 6.5 (3:1), 2 hours (**a**) and 1 week (**b**).
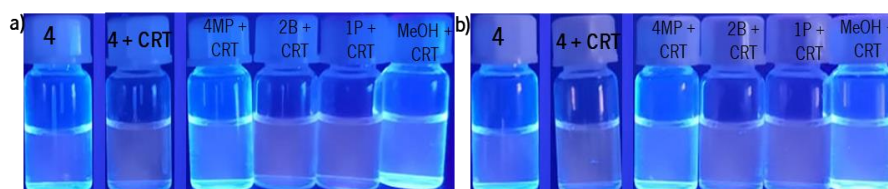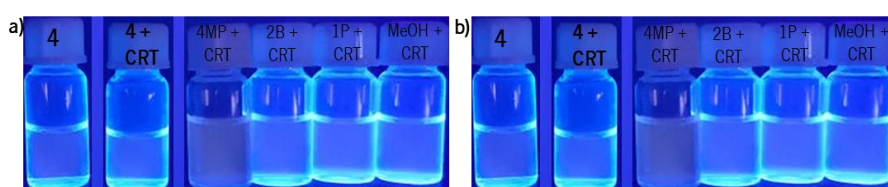

Figure A17 - Fluorimetric changes of dicyanovinyl derivative **4** with 50 equiv of each alcohol and CRT in ACN/phosphate buffer pH 6.5 (3:1), 2 hours (**a**) and 1 week (**b**).
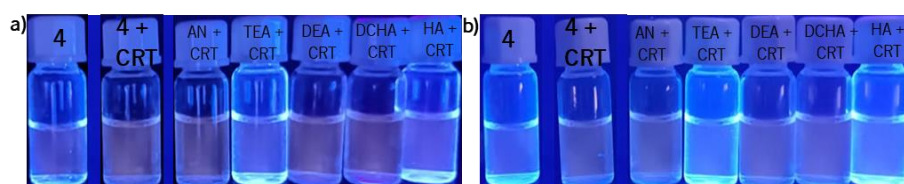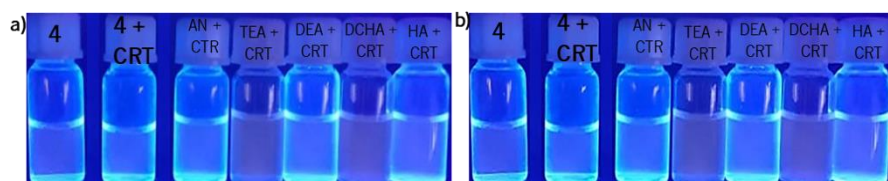

Figure A18 - Fluorimetric changes of dicyanovinyl derivative **4** with 50 equiv of each amine and CRT in ACN/phosphate buffer pH 6.5 (3:1), 2 hours (**a**) and 1 week (**b**).

Figure A19 - Fluorimetric changes of dicyanovinyl derivative **4** with 50 equiv of each alcohol ACN/PBS pH 7.0 (3:1), 2 hours (**a**) and 1 week (**b**).

Figure A20 - Fluorimetric changes of dicyanovinyl derivative **4** with 50 equiv of each amine in ACN/phosphate buffer pH 7.0 (3:1), 2 hours (**a**) and 1 week (**b**).
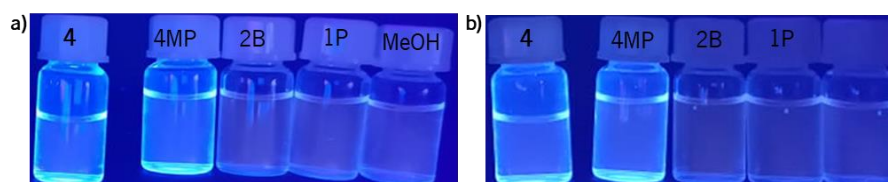
Figure A21 - Fluorimetric changes of dicyanovinyl derivative **4** with 50 equiv of each alcohol and U in ACN/phosphate buffer pH 7.0 (3:1), 2 hours (**a**) and 1 week (**b**).

Figure A22 - Fluorimetric changes of dicyanovinyl derivative **4** with 50 equiv of each amine and U in ACN/phosphate buffer pH 7.0 (3:1), 2 hours (**a**) and 1 week (**b**).

Figure A23 - Fluorimetric changes of dicyanovinyl derivative **4** with 50 equiv of each alcohol and CRT in ACN/phosphate buffer pH 7.0 (3:1), 2 hours (**a**) and 1 week (**b**).

Figure A24 - Fluorimetric changes of dicyanovinyl derivative **4** with 50 equiv of each amine and CRT in ACN/phosphate buffer pH 7.0 (3:1), 2 hours (**a**) and 1 week (**b**).

Figure A25 - Fluorimetric changes of dicyanovinyl derivative **4** with 50 equiv of each alcohol ACN/PBS pH 7.0 (3:1), 2 hours (**a**) and 1 week (**b**).
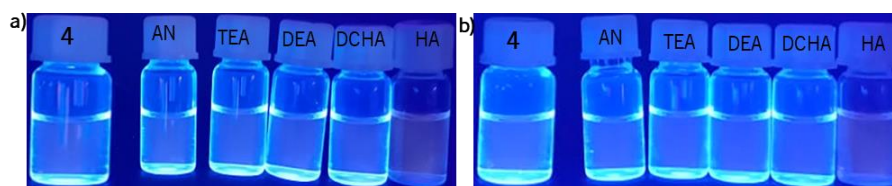
Figure A26- Fluorimetric changes of dicyanovinyl derivative **4** with 50 equiv of each amine ACN/PBS pH 7.0 (3:1), 2 hours (**a**) and 1 week (**b**).
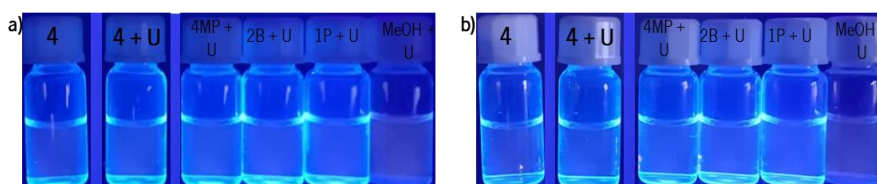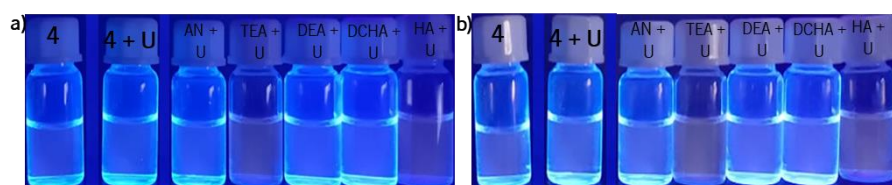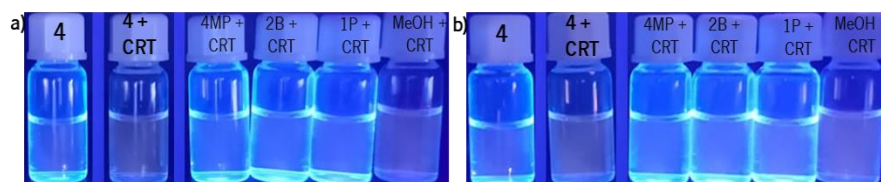

Figure A27 - Fluorimetric changes of dicyanovinyl derivative **4** with 50 equiv of each alcohol and U ACN/PBS pH 7.0 (3:1), 2 hours (**a**) and 1 week (**b**).

Figure A28- Fluorimetric changes of dicyanovinyl derivative **4** with 50 equiv of each amine and U ACN/PBS pH 7.0 (3:1), 2 hours (**a**) and 1 week (**b**).

Figure A29- Fluorimetric changes of dicyanovinyl derivative **4** with 50 equiv of each alcohol and CRT ACN/PBS pH 7.0 (3:1), 2 hours (**a**) and 1 week (**b**).
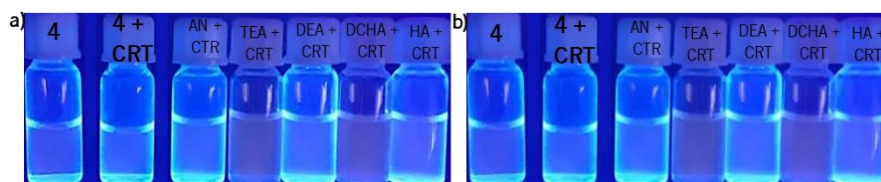

Figure A30- Fluorimetric changes of dicyanovinyl derivative **4** with 50 equiv of each amine and CRT ACN/PBS pH 7.0 (3:1), 2 hours (**a**) and 1 week (**b**).
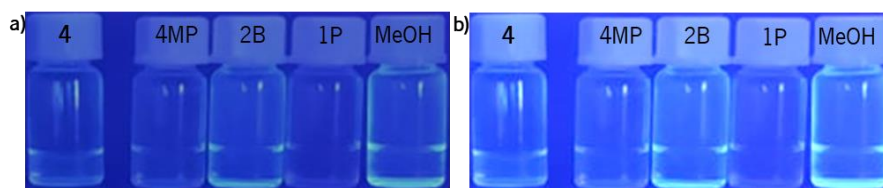
Figure A31 - Fluorimetric visualization of compound **4** DCM solution in presence of 50 equiv of each alcohol 2 hours **(a)** 1 week **(b)** after addition.
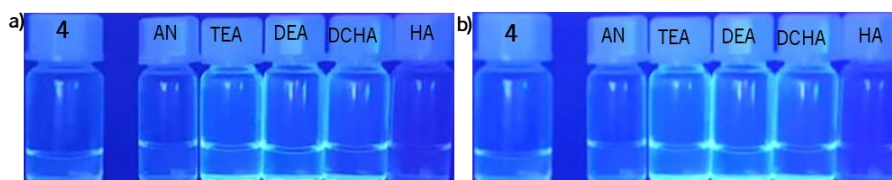

Figure A32 - Fluorimetric visualization of compound **4** DCM solution in presence of 50 equiv of each amine 2 hours **(a)** 1 week **(b)** after addition.